Title
Discovery of Selective Small Molecule Protein-Protein Interaction Modulators Utilizing Site-Directed Fragment Binding

Permalink
https://escholarship.org/uc/item/80s97364

Author
Kenanova, Dyana N

Publication Date
2023

Supplemental Material
https://escholarship.org/uc/item/80s97364#supplemental

Peer reviewed|Thesis/dissertation

Discovery of Selective Small Molecule Protein-Protein Interaction Modulators Utilizing Site-Directed Fragment Binding

by
Dyana Kenanova

DISSERTATION
Submitted in partial satisfaction of the requirements for degree of
DOCTOR OF PHILOSOPHY

in

Chemistry and Chemical Biology

in the

GRADUATE DIVISION
of the
UNIVERSITY OF CALIFORNIA, SAN FRANCISCO

Approved:

Michelle Arkin
Chair

Danica Galonic Fujimori

Kaveh Ashrafi

_____

_____
Committee Members

Dedication and Acknowledgments

I am extremely grateful to my mentor, Dr. Michelle Arkin, and the incredible team that is the

Arkin Lab in all of its iterations as an incredible place to learn and grow as a chemical biologist.

Michelle, you have been an incredible mentor through my evolution from a target-driven

(metabolism-or-death!) young student to the mass spectrometry and drug discovery technology

enthusiast I am today. Your unwavering support, illuminating insight both in and out of the

laboratory, and strong character have been paramount to my success as a graduate student. I

continue to look up to you as an inspiration as I move forward in my career outside of academia.

Additionally, I am grateful to Holly, who started this journey with me and has been a constant

source of laughter, patience, and banging beats. Thank you for building the lab culture from the

ground up with me, being there when the experiments weren't working (as well as celebrating

the few occasions when they were), and always being down to go to a concert at 10 pm on a

worknight. I am so excited to see where you will go, but I know wherever it is you will

accomplish great things! Johanna, thank you for putting all the other mentees I have had to

shame. They were good, but you really took the tethering technology and ran with it, and I am

so thrilled that you have done so much to advance 14-3-3 *in vitro* and in cells. You have also

opened up my curiosity to the Midwest and I look forward to visiting Wisconsin in the near

future. Thank you for rounding out the grad student portion of team 14-3-3 and carrying our

legacy forward (aka organizing all the parties)!

Thank you to all of the other fantastic people in the Arkin lab, past and present, who have

helped me along the way: Ziwen, Paul, Amanda, Jeff Neitz, Isabel Lee, Julia Davies, Greg Lee,

Chad, and Markella. You have all taught me so much and I really could not have gotten this far

without you. Thank you also to Kazuko Olsen and Ninwe Maraha without whom the lab would

not function. Thank you for the persimmon jam and cat pictures, Kazuko! And apologies for not

always doing my trainings on time, Ninwe. I always appreciated the reminders.

Thank you so much to Maddie Joy O'Brien, my love, my light, the absolute sun in my solar system, center of my universe. I love you so much! I love you with my whole heart! There are not enough words to express how much you mean to me. I feel like I have known you my entire life and I will never stop marveling at your bravery, perseverance, and dedication. You are an inspiration and every day that I am with you I become better in every way. Thank you for being such an incredible human being, amazing partner, and constant source of adventure. Thank you for being the sounding board for all of my talks, my thoughts, and always taking the time to work through any and every challenge that comes our way. I know that no matter where we go next, I will be the happiest person in the world because I will have you by my side. I cannot wait to continue to grow with you and I am so grateful to have met you in this incredibly exciting time. I adore your inquisitive spirit, sharp intellect, and optimism beyond all else. I am so thrilled to witness your evolution in your career and I am always here for you no matter what. And remember, if all else fails there is always chemistry! Or Carmax! Or moving to Greece, buying a hotel, and singing ABBA songs while searching for Aphrodite's Fountain! Life will always and forever be everything I want it to be as long as I am with you. I am yours, forever and always.

In the vein of people who have inspired me and supported me outside of the lab, major thanks to my incredible friends for making me laugh, building me up, and enthusiastically encouraging me to be the best person I can be. To the original pandemic workout crew– Joey, George, Steph, Maia, Kristina, Alan, and Nicole– you made 2020 the best year I could possibly have hoped for. It is amazing how I met most of you on a small computer screen doing burpees and jumping jacks in my tiny room with Joey whizzing around as a potato half of the time. I am so glad I got to meet you all in person and build this amazing community with you. Thank you also to the later Attack family additions: Ali, Pauline, and Pierre, who will always be the frenchiest of the fries; Vince, Summer, Nancy, Nui, and Emily, who are combaters but I'm placing in this category anyway; and Jonathan who I hope to one day play volleyball with again soon. You

have all been so incredible in so many ways I could never hope to write them all here. Just know that you have made such a profound impact on my life, and I love every single one of you. To my other incredible SF people: Jordan, Regan, Katie, Haley, Rachel, Yasi, Mekhala, Francesca, Nate, Anna, and everyone who I have had as part of my world these last 5 years, thank you for all of the light and joy and fun you have brought me. You have all been the best movie goers, Marvel fans, runners, track stars, music lovers, gym goers, board game champions, and overall fantastic people a girl in her mid to late 20s could ask for. Also special thanks to my LA friends, the originals, who have stayed in touch despite all the miles separating us. Thank you to Shashank, Verity, Cassidy, and Sanaya for always being the party. Also, thank you to Yolanda Li, Emily Merzinski, Hui Ding, and Carter James for being my science mentors and great friends and convincing me that grad school can be finished without losing your soul or your sense of humor. I will forever and always be "the Child."

Finally, thank you to my family who has been there since day one or close to it. I am so grateful to my mom, Ludmila (Ms. Lucky) Caldwell, for always believing in me, pushing me to follow my dreams, and sitting through more chemistry than anyone should. I love you so much! Thank you also to Carey, who has supported me and loved me as a daughter, and to Sofia and Jackson, the best siblings a moody teenager didn't ask for but is now so excited to have. You will both do great and amazing things! Thank you to my aunt, Dr. Vania Kenanova, for transporting me over from the old country, pulling me out of ponds, and inspiring my mom to tell me to get into biochemistry even though you were not a biochemist. Everything works out in the end, and I have always been in awe of everything you have accomplished while still taking the time to be the most incredible Aunt I could have possibly wished for. Благодаря и на Баба Гинка и Дядо Емил без които никога не щях да съм тука. Извинявай че продължих с химията въпреки много протест от първата химичка в семейството. Ти си най упоритата жена дето познажам, Баби. И добавих Биолохията за Дяадо, затова не се тревожи, работя с по

Contributions

1.   Kenanova, D. N.[⊥]; Visser, E. J.[⊥]; Virta, J. M.; Sijbesma, E.; Centorrino, F.; Vickery, H. R.;

Zhong, M.; Neitz, R. J.; Brunsveld, L.; Ottmann, C.; Arkin, M. R. A Systematic Approach to the

Discovery of Protein–Protein Interaction Stabilizers. *ACS Cent. Sci.* **2023**.

https://doi.org/10.1021/acscentsci.2c01449.

Discovery of Selective Small Molecule Protein-Protein Interaction Modulators Utilizing

Site-Directed Fragment Binding

Dyana Kenanova

Abstract

Protein-protein interactions (PPIs) are central to biology and commonly dysregulated in disease. Despite their importance in cell homeostasis and their therapeutic potential, PPIs have rarely been a target for drug discovery. This has been due to three major challenges PPIs present to small molecule engagement: the flatness problem, the disorder problem, and the selectivity problem. PPIs which bind with large, flat interfaces typically do not have deep pockets accessible to small molecules, leading to low ligand efficiency. Intrinsically disordered proteins, likewise, are lacking in "hot spots" for small molecule binding. Finally, most proteins which participate in PPIs have more than one partner– 20% of so-called hub proteins with multiple interactions have over 20 binding partners– thus necessitating a selective small molecule to target a specific PPI edge as opposed to a general effector which inhibits the nodular hub protein. Disulfide tethering, a subset of fragment-base drug discovery (FBDD) offers a novel approach to the rapid discovery and development of potent, selective small molecule PPI modulators. This platform facilitates rapid and robust compound discovery and validation as well as simple, accessible scaffolds for hit-to-lead development, circumventing the difficulty of natural product total synthesis and mitigating costly late-stage failures in selectivity and safety. This work showcases multiple projects utilizing disulfide tethering to discover and optimize small molecule modulators for various "undruggable" targets within oncology, neurodegeneration, metabolic disease, and infectious disease.

Table of Contents

List of Figures

List of Tables

List of Abbreviations

Abbreviation	Meaning
2*SD	two standard deviations
3*SD	three standard deviations
5-FAM	5-carboxyfluorescein
Ac	acetylated
APOBEC3A	apolipoprotein B mRNA editing enzyme, catalytic polypeptide-like 3A
BME	β-mercaptoethanol
CARD	caspase activation and recruitment domain
CN-A	Cotylenin-A
DMSO	dimethyl sulfoxide
DNA	deoxyribonucelic acid
DR_{50}	dose response 50
EC_{50}	effective concentration 50
ER	edoplasmic reticulum
ERα	estrogen receptor alpha
FA	fluorescence anisotropy
FADR	fluorescence anisotropy-based dose response
FBDD	fragment-based drug discovery
FC-A	Fusicoccin-A
FITC	fluorescein isothiocyanate
FPDR	fluorescence polarization-based dose response
Gq	guanine nucleotide binding protein
GTPγS	guanosine 5'-O-[gamma-thio]triphosphate
HFD	high fat western diet

HTS	high throughput screening
IC$_{50}$	inhibitory concentration 50
LB	leuria broth
LC/MS	liquid chromatography mass spectrometry
Leu	Leucine
MALDI	matrix-assisted laser/desorption ionization
MAPK	mitogen-activated protein kinase
MS	mass spectrometry
MSDR	mass spectrometry-based dose response
MTase nsp14	nonstructural protein 14 (N7-guanine)-methyltransferase
NAFLD	nonalcoholic fatty liver disease
NASH	nonalcoholic liver steatohepatitis
NMR	nuclear magnetic resonance
PAINS	pan-assay interference compounds
PCLβ$_3$	polycaprolactone β$_3$
PIDD	p53-inducible death domain-containing protein
PPI	Protein-protein interaction
PTM	posttranslational modifications
Q-TOF	quadrupole time-of-flight
RAIDD	RIP-associated ICH-1 homologous protein with a death domain
S-1-P	site-1-protease
SAM	S-adenosyl methionine
SAR	structure activity relationship
SCAP	SREBP cleavage-activating protein
Ser	Serine

SMDC	small molecule discovery center
SPE-MS	solid-phase extraction mass spectrometry
SPR	surface plasmon resonance
SREBP1/2	sterol regulatory element-binding proteins 1 and 2
TAMRA	Carboxytetramethylrhodamine
TB	terrific broth
Thr	Threonine
TR-FRET	time resolved fluorescence resonance energy transfer
Trp	Tryptophan
UPLC	ultra-pressure liquid chromatography
Val	Valine
WT	wildtype

List of Symbols

Symbol	Meaning
σ	sigma isoform
Å	Angstroms
Δ	change
K_D	dissociation constant

Chapter 1 Applications of Disulfide Tethering as a Versatile Tool in Fragment-Based Drug Discovery
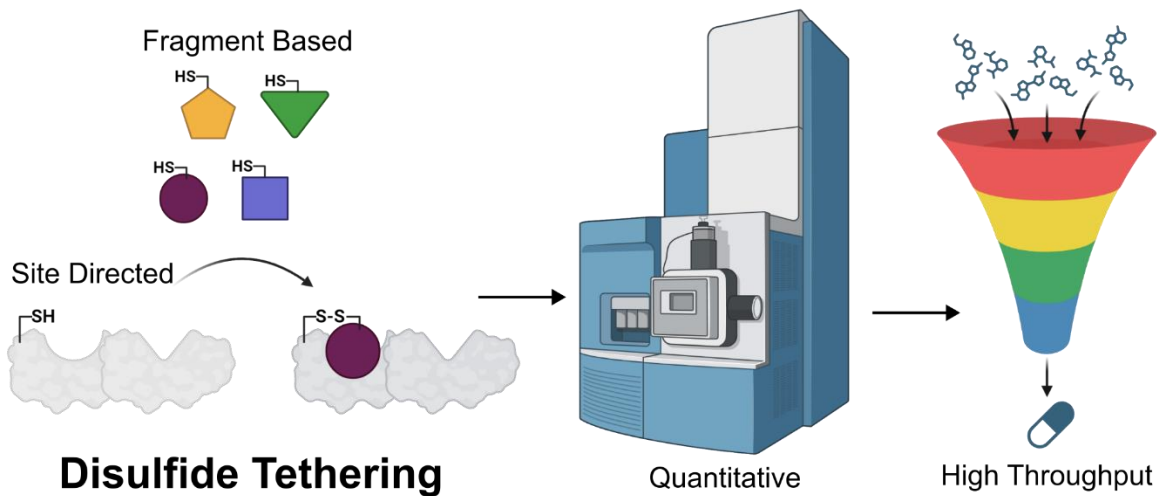
ABSTRACT: Fragment-based drug discovery has provided a novel platform for rapid and systematic development of small molecule probes and therapeutics. Disulfide tethering is a quantitative, mass spectrometry driven technology which falls under FBDD. Tethering utilizes a small, chemically diverse fragment pharmacophore attached to a thiol moiety in order to sample "hotspots" within a protein or protein-protein interaction (PPI) target of interest. The fragment forms a reversible covalent disulfide bond with a native or engineered cysteine proximal to the binding site. The abundance of fragment tethering can then be visualized and measured via a mass shift readout. The transient nature of the disulfide bond necessitates that true "hit" molecules make stronger interactions between the pharmacophore and the protein target. Due to its versatility, scalability, and applicability to high throughput screening, tethering is a robust, prospective approach to discovering and optimizing fragments in order to address challenges in drug discovery.

INTRODUCTION

Within the past 20 years, drug discovery has expanded its arsenal beyond the total synthesis of natural products and expensive medicinal chemistry campaigns for complex natural product derivatives.[1,2] Although powerful, such compounds are typically difficult to synthesize, owing to challenges such as intricate ring systems and multiple chiral centers (**Figure 1.1A**).[3–5] This makes development slow and costly, especially if leads fail late-stage in clinical trials. In order to address these limitations, fragment-based drug discovery (FBDD) has provided a novel platform for the discovery and optimization of therapeutics and biological probes.[6–8]

FBDD provides a robust, systematic way to explore chemical space for good starting points for biologically active small molecules. These fragments are typically smaller, easily synthesized, and readily merged or elaborated (**Figure 1.1B**).[9] This has initiated a new, prospective strategy for the discovery of drugs, highlighting selectivity and mechanistic understanding of underlying disease-relevant target as opposed to the serendipitous discoveries made in the past.

Disulfide tethering is a subset of FBDD which takes advantage of the quantitative nature of mass spectrometry (MS) in order to directly visualize target engagement by a fragment molecule.[7,10–12] Thiol-containing fragments are screened for binding to a native or engineered cysteine residue proximal to the desired protein 'hotspot,' making the technique extremely tunable, precise, and versatile for target selection.[10] The reversibility of the disulfide bond necessitates fragment molecular recognition of the binding interface, minimizing the risk of energetics driven binding and false positives such as pan-assay interference compounds (PAINS; **Figure 1.1C**). Additionally, the sensitivity of intact protein mass spectrometry (LC/MS) is easily scalable and readily enables high throughput screening (HTS).[13] Herein, I outline the capabilities of the disulfide tethering technology in the context of protein-protein interaction (PPI) modulation and highlight hit-to-lead strategies for novel therapeutic and probe development.
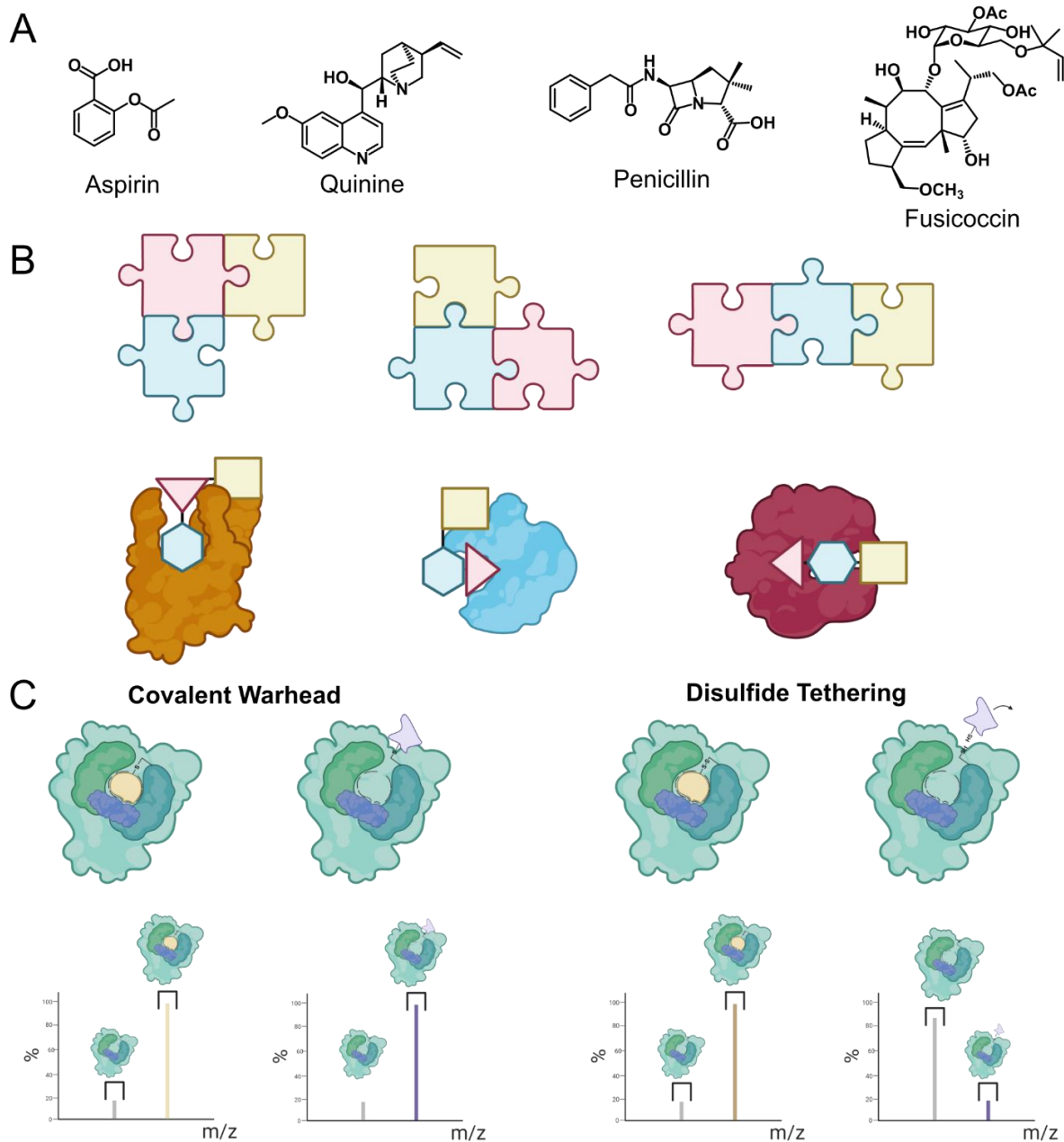
Figure 1.1 Drug discovery techniques. (A) Biologically active natural products ranging in ease of access and derivatization through total synthesis and medicinal chemistry. (B) Cartoon conceptualization of fragment based drug discovery, its customizability, and applicability to a variety of protein targets similar to assembling puzzle pieces to fit a specific binding interface. (C) Comparison of covalent warhead vs disulfide tethering detection via mass spectrometry (MS). Covalent warheads must be optimized to not be overly reactive with target cysteine. Inherent transiency of disulfide interaction ensures that only privileged scaffolds show high labeling of target.

BACKGROUND

 FBDD is emerging as a reliable technique for the discovery and development of drugs and

biological probes.[14] The emphasis on compound mechanism of action, site-directed specificity,

and structural characterization of binding has given unprecedented insight into the functionality

of small molecule bioactivity. Multiple technologies have been developed that fall within the

FBDD umbrella ranging in detail and resource requirements. X-ray crystallography currently

exemplifies the most thorough approach to fragment discovery, allowing for the visualization of

the exact binding motifs between the fragment and target. The B-RAF[V600E] therapeutic,

vemurafenib,[15] BCL-2 inhibitor venetoclax,[16] and the FGFR inhibitor, erdafitinib,[17] are powerful

examples of structure-based fragment optimization efforts that resulted in FDA approved

therapeutics within oncology. Crystallographic studies have even resulted in some PPI

stabilizers with potential as molecular glues.[18] However, x-ray crystallography is limited by the

number of proteins amenable to crystallization and is extremely resource intensive, making it

challenging for HTS in the majority of cases. Therefore, crystallography reserved for later hit-to-

lead development as opposed to hit determination. Assays such as surface plasmon resonance

(SPR)[19] and nuclear magnetic resonance (NMR)[20] are more amenable to HTS and provide

insights into the binding kinetics and specificity of the fragments but are also limited by

Table 1.1 Comparison of FBDD techniques

Technique	Application to FBDD	Resource Intensive	Scalable to HTS
X-ray Crystallography	Structural determination of important contacts between fragment and target	Yes	Target Dependent
Nuclear Magnetic Resonance	Visualization of fragment interactions with target	Yes	No
Mass Spectrometry	Direct quantification of fragment engagement to target via covalent bond	No	Yes
Surface Plasmon Resonance	Binding affinity and kinetics to target	Target Dependent	Yes
Fluorescence Anisotropy	Binding affinity to target and potential kinetics measurements for enzyme activity	No	Yes

resources and time. By contrast, MS provides a label-free method for direct detection and quantitation of compound/target binding whilst requiring minimal resources and rapid turnover time (**Table 1.1**).[7,10,12,21]

Multiple covalent FBDD campaigns have resulted in novel scaffolds for drug development.[22,23] Due to the small size and relatively weak binding of fragment molecules, the discovery, validation, and optimization of such compounds can be challenging for low-sensitivity techniques and can result in false negatives. Having a covalent handle anchor the small molecule to the target binding site allows for easier detection, especially with MS.[9,24–26] Cysteine
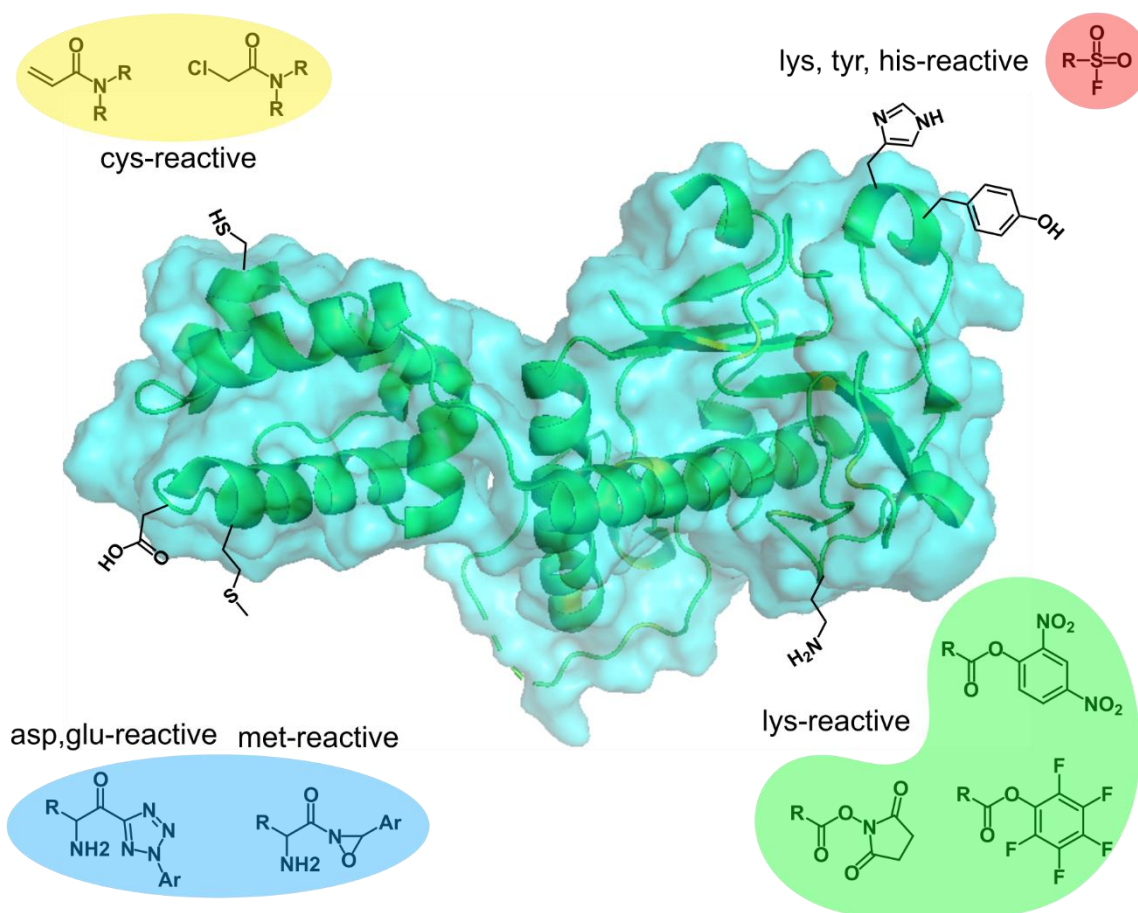
Figure 1.2 Summary of irreversible covalent warheads targeted at various amino acids. Acrylamides and chloroacetamides (yellow) target cysteine. Sulfonyl fluorides (red) are promiscuous and can label lysine, tyrosine, histidine, serine, threonine, and cysteine residues. Aspartic acid and glutamic acid reactive warheads and methionine reactive warheads are highlighted in blue. Lysine reactive warheads are highlighted in green. PDB ID 7TW7. Amino acid placements not exact or to scale.

reactive warheads predominate the covalent labeling landscape, however, recent work has expanded this to target lysine, tyrosine, histidine, aspartic and glutamic acid, methionine, serine, and threonine (**Figure 1.2**).[13] The sensitivity of intact mass spectrometry (LC/MS) is able to directly measure the degree of compound engagement in less than 3 minutes per sample in ultra-pressure liquid chromatography (UPLC) and even 20 seconds per sample with solid-phase extraction (SPE-MS) and matrix-assisted laser/desorption ionization (MALDI).[13] The more rapid methods hold some limitation as there is no chromatographic step to separate species. Thus, sample purity or robust controls are critical for such assays. The Arkin lab has developed a medium throughput screening method that is able to read samples utilizing an 84 second per sample method, UPLC separation of species, and a quadrupole time-of-flight (Q-TOF) MS instrument which has the capacity to screen 1000 compounds per day.[27]

Whilst irreversible covalent fragments useful for MS quantification, finding the right warhead can be a challenge wherein no single warhead is applicable to every protein and even small changes can have dramatic effects on fragment binding.[28] Overly reactive warheads such as chloroacetamides may result in off-target reactivity and false positives, whilst more attenuated warheads such as acrylamides require longer incubation times, reducing the high throughput capabilities of the assay and increasing the number of false negatives. Despite the potential drawbacks, promiscuous labeling has only been found in approximately 3% of cases.[28] Disulfide tethering offers another simple solution to the problems of optimization and promiscuity by employing a reversible covalent thiol which can form transient disulfide bonds with a cysteine proximal to the binding site of interest.[7,10,12,24] Within a reducing environment, the disulfide bond between protein and fragment can easily be disrupted for a nonspecific binder. The system is reliant upon the contacts made between the pharmacophores of the fragment and the target which then hold the fragment in a position favorable for longer engagement (**Figure 1.1C**). Tethering can thus utilize the disulfide as an anchor for the low affinity fragment and the

quantitative capabilities of MS while removing the disadvantage of off-target labeling in other covalent systems, making it a versatile and easily scalable technology for FBDD and therapeutic development.

DISULFIDE FRAGMENT LIBRARY DESIGN

Fragment compounds tend to be small (200-500 Da) with functionalized cores sampling a wide breadth of chemical space, a linker separating the body of the fragment and the thiol moiety, and a solubilizing cap which is later reduced in the screen. Fragments also tend to loosely follow Lipinski's rule of 5 (≤5 rotatable bonds, ≤5 hydrogen bond acceptors, ≤5 hydrogen bond donors, computed logP ≤5) or even more stringent guidelines.[9,10,20,28] Whilst useful for initial library design and synthesis, these guidelines are constantly being revised as more data is collected and are therefore useful starting points but should not be limitations on creativity. Chemical diversity and customizability of the fragment core are much more critical for a successful screening campaign.[29]

Fragment libraries tend to be relatively small, consisting of 1000-2000 compounds, as they are typically custom synthesized. However, recent advances in cleaner synthetic strategies have allowed for high throughput synthesis which can rapidly increase a library's size and diversity while decreasing the time spent in purification stages and instead directly applying the final product to the HTS assay.[7,21,30] Quality is typically determined via MS. Derivatization based on follow-up optimization strategies such as fragment linking, merging, and growing achieves a much larger diversity equivalent to if not broader than a typical druglike compound library.[20,28,31–35] Optimized compounds can always be added to the original screen and utilized for new targets, therefore consistently growing the scope of the screen. The flexible linker allows for sampling multiple binding geometries and conformations. The weak binding of the fragments and the reversibility of the thiol ensure that labeling of the target is facilitated by the fragment interactions within the binding pocket as opposed to nonspecific reactivity of the covalent

7

warhead, eliminating the need to sample a swath of nonreversible covalent moieties per target before performing the screen.[11,23,24,28,35]
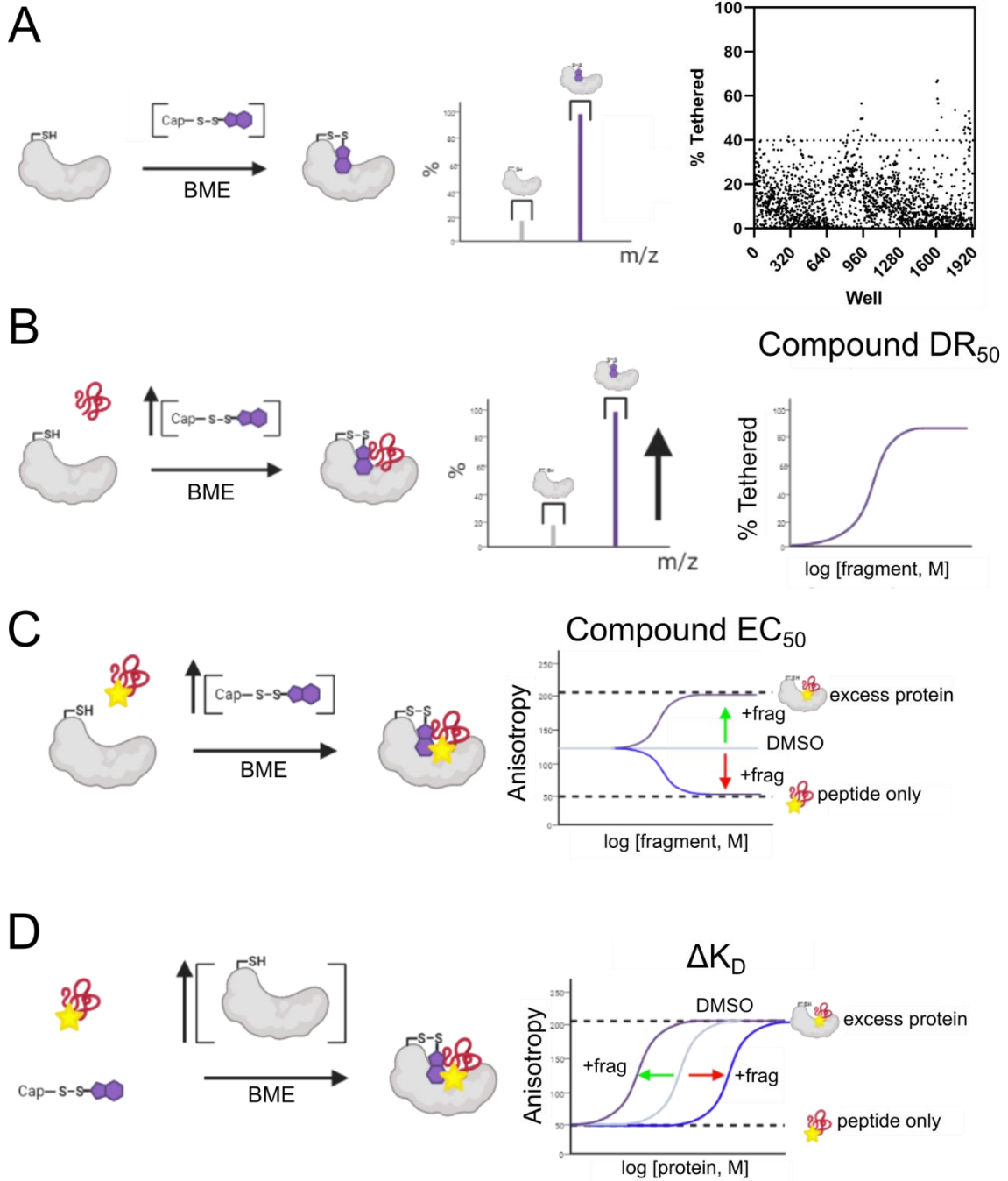
Figure 1.3 Overview of disulfide tethering screen and follow-up orthogonal validation assays. (A) Initial screen with protein target (white), single concentration of fragment (purple), and β-mercaptoethanol (BME). % tethering is measured by dividing the % of fragment labeled protein by the sum of all present species including protein alone, protein and BME, protein and solubilizing cap, and protein with fragment then multiplied by 100. Fragments that fall above 3 standard deviations from the average (dotted line in scatterplot) are considered hits. (B) MS compound dose responses (MSDR) take target (white) and titrate in fragment (purple) from high concentration to low concentration in order to determine dose dependence and fragment dose response 50 (DR_{50}) value representative of 50% of fragment tethered to protein. (C) Fluorescence anisotropy compound dose responses (FADR) show compound stabilization or inhibition of binding. Fluorescently labeled peptide (red) is added to single concentration of protein (white) and compound (purple) is titrated from high concentration to low concentration. If compound shows stabilization, anisotropy will increase (purple curve) as compared to DMSO control (grey curve). If compound is inhibiting, anisotropy will decrease (blue curve). Top dotted line indicates anisotropy at excess protein and bottom dotted line indicates anisotropy with peptide alone. These indicate the upper and lower limits of peptide binding. (D) Fluorescence anisotropy protein titrations. Fluorescently labeled peptide (red) and fragment (purple) at excess of the EC_{50} or IC_{50} determined in the FADR are incubated with titrated protein (white) from high to low concentrations. For stabilizers, protein/peptide binding affinity will shift to the left indicating a decrease in K_D (purple curve) as compared to DMSO control (grey curve). For inhibitors, binding affinity will shift to the right (blue curve).

DISULFIDE TETHERING SCREEN DESIGN

Chapters 2,3, and 5 have in depth discussions of various scenarios and applications of the disulfide tethering technology, including scope and limitations. This section will focus on the general principles for a successful screening campaign.

Disulfide tethering is a site-directed approach which can be tailored to the specific target by screening against a native or engineered cysteine within 5 to 10 Å from the site of interest.[7] For targets with large, open binding interfaces such as the hub protein 14-3-3 (Chapters 2-4), tethering is readily applicable.[10,11,26,36] For targets with deep, narrow binding sites or highly specific structure or catalytic machinery, the screen may necessitate an offshoot approach known as tethering with breakaway extenders. This approach takes advantage of a further removed cysteine that can be bound by a general "breakaway extender."[7,21,35] When cleaved, this extender positions a thiol closer to the binding site without necessitating a disruption of the binding site. Later optimization of the breakaway extender can also result in starting points for extended tethering and fragment linking.[20,35,37]

Nucleophilicity of the cysteine residue is another consideration when designing the screening conditions. Non-catalytic cysteine pKa ranges from 7.4 to 9.1 with an average of approximately 8.6 whilst catalytic cysteines can have pKa values as low as 2.8.[38] If the protein of interest has multiple cysteines, even small changes in pKa can have dramatic effects on selectivity for the target cysteine vs others. A simple diagnostic for the number of binding events on a given targets is a titration curve using nonspecific covalent modifier iodoacetamide.[39,40] Overnight incubations followed by optional LC/MS/MS can indicate with great accuracy which cysteines are most reactive and likely to be labeled. The Arkin lab disulfide tethering screen is performed at pH 8.0 to facilitate formation of the active thiol and, once fragment has been added, the disulfide bond.[10,11,36] Due to the reservable nature of the disulfide, reaction is thermodynamically driven as opposed to the more common kinetics of irreversible covalent warheads.[10,12] Previous work in the lab has shown reaction completion and saturation of the pocket at 1-3 hours of incubation, but some screens reach equilibrium in as little as 30 minutes. Subsequent assays in this work were run at the more conservative 3 hour incubation timepoint to standardize the process. Disulfide exchange can be halted by the addition of a quencher, such as hydrochloric acid, or lowered to 10°C.

Another consideration is optimization of reducing conditions. Typically, fragments are stored either as disulfide bonded symmetrical dimers or connected to a solubilizing cap (**Figure 1.3**). A reducing environment is critical for initiation of disulfide exchange, not only to free the fragment, but also to induce the nonreversible binding to the target cysteine that is central to the on-target selectivity of this FBDD method. β-mercaptoethanol (BME) is a preferred reducing reagent for a variety of reasons. It is a mild reductant that is well-tolerated by many proteins, increasing the versatility of the screen when comparing multiple constructs.[10,24,26] BME also performs disulfide exchange and can thus be visualized via MS. The Arkin lab capitalizes on this by incubating the reaction with excess amounts of BME as dictated by tolerance of the protein and fragment

concentration. BME binds to the target cysteine nonspecifically and acts as a competitive inhibitor of fragment binding unless the fragment is able to form favorable connections with the binding site, minimizing false positives and "sticky" artefacts. Multiple BME titration curves are tested prior to running a screen to determine optimal concentration– typically 250 µM or 500 µM, but as low as 125 µM for sensitive proteins and up to 1 mM for proteins containing multiple solvent exposed cysteine residues. High BME labeling in the absence of fragment and low BME labeling in the presence of fragment indicates cooperativity between the fragment pharmacophore and the protein binding interface.

Due to the high sensitivity of MS-based screening, there is a lower protein requirement than many functional screens. Even proteins with poor resolution have discernable peaks and quantifiable fragment labeling at a maximal concentration of 500 nM, however more stable proteins have shown robust signal at 100 nM.[10,11,36] When available, positive controls can be utilized as a metric for hit selection. Alternatively, the Arkin lab developed a high throughput analysis software which bins the various species into specific lots including unlabeled protein, fragment-labeled protein, BME-labeled protein, and cap-labeled protein. The signal significance of the fragment is determined as the quotient of the fragment-labeled protein over the sum of all aforementioned species, multiple by 100 to give a "% tethered." Any % tethered values three standard deviations (3*SD) above the screen average is considered to be a hit fragment (**Figure 1.3A**). Most of the screens performed in this work have resulted in an average of 30 compounds, approximately a 1-2% hit rate, with various chemical classes and engagement motifs.[10,11,36] The protocol established following the criteria summarized above has effectively discovered fragment binders for a broad range of proteins of various stabilities and ease of expression. This work exemplifies the versatility, selectivity, and applicability of disulfide tethering in determining starting points for drug discovery.

FRAGMENT TRIAGING AND VALIDATION

Once fragment hits have been found, it is incredibly important to validate them. Multiple reviews have highlighted various follow-up assay platforms. Biophysical assays which corroborate fragment binding and elucidate mechanism of action inform further steps in lead optimization. Orthogonal activity assays then further assess compound efficacy and selectivity. Other HTS techniques, including fluorescence-based and binding-based assays, readily lend themselves to expansion of the results from the initial screen. X-ray crystallography, NMR, and MS are common examples of binding assays while time resolved fluorescence resonance energy transfer (TR-FRET) and fluorescence anisotropy (FA) is the preferred fluorescence-based tool for fragment activity profiling for most of the screen targets.[41]

For our efforts, MS and x-ray crystallography are the preferred binding methods. MS compound dose responses (MSDR) expand the data from the screen beyond single data point and determine compound dose response 50 (DR_{50}) values (**Figure 1.3B**). Compounds which do not show dose dependence or inconsistent labeling are considered artefacts and not taken forward into the following validation experiments and structural studies. X-ray crystal structures provide the most concrete data on compound binding but requires large amounts of compound and protein. When structures are available, however, they determine exact points of contact between the fragment and the target of interest. Utilizing soaking techniques, our collaborators in the Eindhoven University of Technology have determined hundreds of crystal structures with 14-3-3, client, and fragment.[42–47] We have also begun efforts to crystallize the SARS-CoV-2 MTase nsp14 protein with disulfide and covalent compound engagers within the SAM binding pocket. Due to its incredible applicability and insight, crystallography remains the final point in our early drug discovery pipeline as opposed to the orthogonal activity assay directly following the MSDR.

In order to determine compound inhibitory or stabilization effects (IC_{50} and EC_{50} values respectively), we utilize anisotropy (**Figures 1.3C** and **1.3D**).[48–51] FA measures the rotational correlation time, or tumbling time, of a specific fluorescent species, typically a peptide or small molecule. Small species rotate faster, scattering the light emitted from the fluorophore and resulting in a low anisotropy value. Larger species, such as a peptide bound to a protein, tend to tumble much more slowly, increasing the anisotropy of the system. Depending on whether the screen is employed for stabilization or inhibition of an interaction, the dose-dependent increase or decrease in anisotropy determines compound efficacy respectively. Finally, FA based protein titrations with excess fragment from the IC_{50} or EC_{50} value are compared to DMSO control to determine shift in affinity between the protein and peptide client. FA is relatively inexpensive in time and resources and allows for enzyme kinetics measurements making it a versatile tool for compound biophysical property determination studies.[52–54] In PPI stabilization campaigns, it also is amenable to a tripartite system consisting of the fragment, protein, and fluorescently labeled peptide, making it extremely useful for the discovery of fragment stabilizers and molecular glues.[11,36,55]

Assay quality is extremely important for the precision and reproducibility of FA. Utilizing the appropriate corrective factor (G-factor) for each fluorophore and instrument of choice ensures normalization of signal and decreases error.[56] Alternatively, purchase of specific polarization filters per fluorophore provides this correction mechanistically with greater accuracy. The other industry standard measurement for signal quality is the Z' factor. This measurement quantifies the high and low limits of the assay as well as the error in well-to-well or plate-to-plate variance. The Z' factor is quantified as a number between 0 and 1 wherein a Z' value above 0.6 is considered significant and a Z' value above 0.4 is acceptable for screening.[2,57–60] Choosing the correct binding and orthogonal activity assay is pivotal to a successful drug discovery campaign and should therefore be carefully considered.
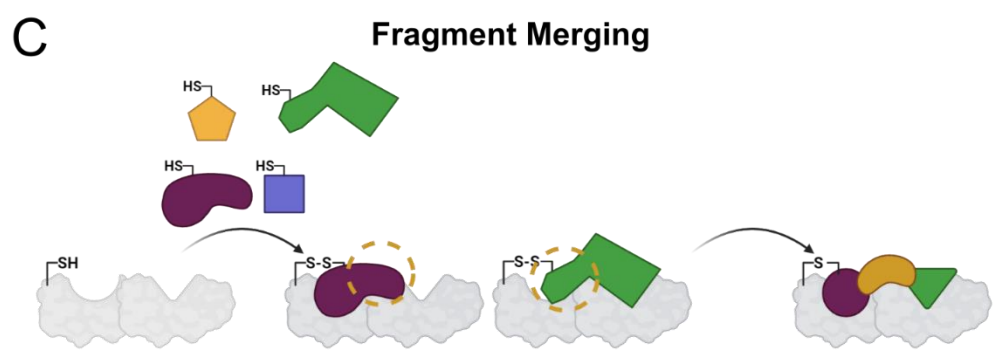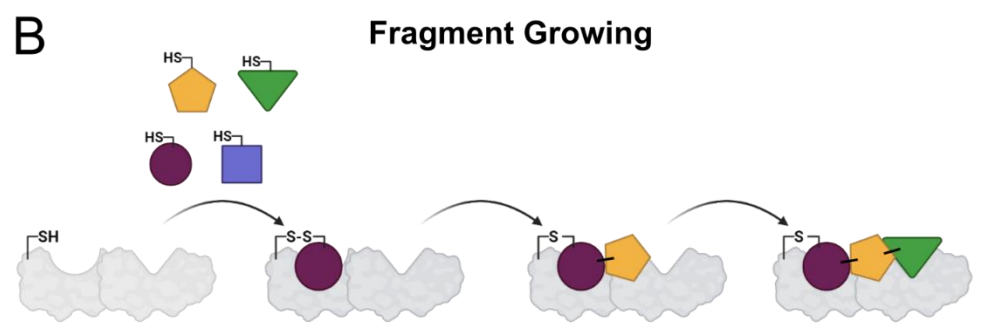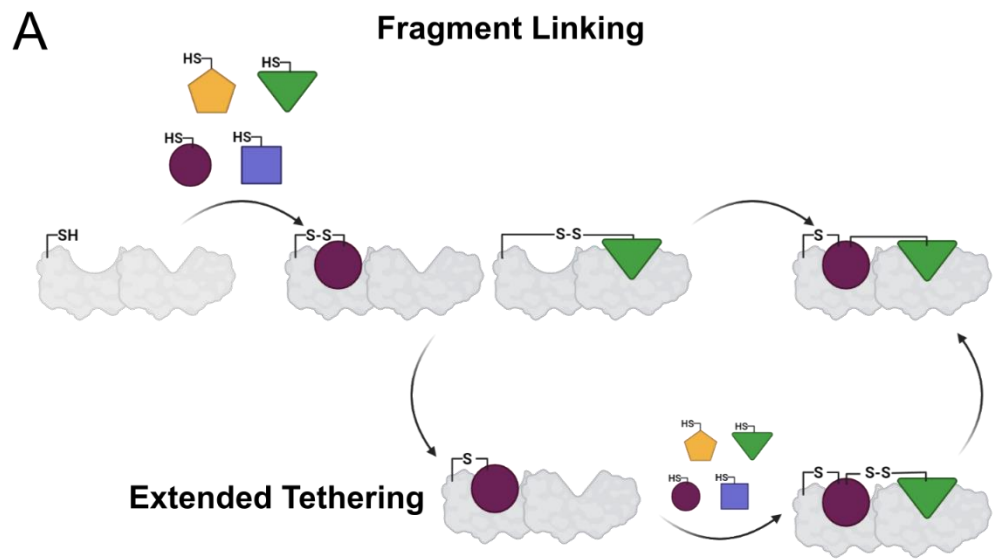
Figure 1.4 Summary of the three main approaches for fragment-to-lead optimization. (A) The fragment linking approach takes advantage of fragment hits (plum circle and green triangle) that have been found via tethering and connecting them to maximize important contacts with a protein target (white). A subset of this approach is extended tethering wherein a fragment hit from a primary screen (plum circle) is converted to a covalent compound and modified with a thiol which can then be screened against to access other potential "hotspots" in the binding site. A secondary fragment (green triangle) will then tether to the initial hit. The two fragments can then be linked to form a more druglike molecule. (B) Fragment growing utilizes a fragment hit (plum circle) as a starting point and increases ligand efficiency by installing bioactive functional groups (yellow pentagon and green triangle) in order to build more interactions with the target protein. (C) Fragment merging is a similar strategy to fragment linking, but specific to when fragment hits (plum bean and green boomerang) share overlaps in their interaction interfaces with the target (white). Shared functionalities or crystal structures can indicate points for bridging and merging fragments into a larger, more druglike compound (plum, dark yellow, green amalgam).

FRAGMENT LINKING, FRAGMENT GROWING, AND FRAGMENT MERGING

Disulfide fragments are useful starting points for the development of drugs and biological probes. However, they do require optimization before being fully applicable to a cell-based or *in vivo* assay. The thiol is promiscuous and problematic when introduced to the glutathione rich cellular environment. The fragment also requires optimization and derivatization in order to improve binding, bioavailability, and the pharmacokinetic properties necessary for it to have the desired effect. There are three main strategies that will be covered for fragment optimization and lead design: fragment linking, fragment growing, and fragment merging (**Figure 1.4**).[37] Each strategy has its benefits and drawbacks and should be considered on a case-by-case basis with regards to fragment and target.

Fragment linking utilizes multiple fragment scaffolds that each target a different pocket in the binding site of interest.[37,61,62] The fragment interactions with target protein can be visualized via crystallography and then linked together to create a larger molecule with the conserved binding motifs of the two smaller fragments (**Figure 1.4A**). If crystal structures are unavailable, extended tethering is an alternative fragment linking approach. In extended tethering, the thiol of the original fragment hit is converted to an irreversible warhead which engages the target

cysteine. The "extender" fragment then has a thiol that can be targeted by another disulfide tethering screen.[21,32,33,35,37] Once fragments are found and triaged, the thiol can be converted to another binding element with the appropriate orientation of the fragments in the binding pocket (**Figure 1.4A**).

Fragment growing is perhaps the most utilized of the three approaches and has resulted in multiple FDA approved drugs.[37,63,64] Growing relies on rational drug design wherein the fragment is optimized by the addition of novel functional groups that increase the size of the molecule and better engage the target "hotspot" interactions (**Figure 1.4B**). Geometry, substituent size, and flexibility play key roles in fragment growing. Libraries with small alterations to the fragment pharmacophores provide great insight into which moieties are exemplary (the hit fragments), which are tolerated (lower binding molecules with similar structures to the hit compounds), and which are impermissible (compounds that do not bind to target). This allows for a rudimentary structure activity relationship (SAR) series.

Fragment merging is similar in concept to fragment linking with the two fragments sharing an overlap in their binding region (**Figure 1.4C**).[37,65–67] Merging has resulted in interesting bioactive compounds, especially when paired with fragment linking as an additive approach to fragment optimization.[37] Similarly to the aforementioned approaches, x-ray crystallography is invaluable in understanding how the fragments engage the target so as best to capitalize on favorable binding interactions. If no structures are present, comparing conserved pharmacophores may give insight into compound binding and thus inform merging strategies around the shared motifs. Docking and molecular modeling campaigns can also assist in lead design.[68–70]

All three strategies share similarities in technique and output. Fragment linking and merging have similar principles but vary in how proximal the fragments are to one another in the binding site. All three focus on building out the molecule in order to facilitate greater contacts with the target binding site and improve ligand efficiency. Higher binding affinity and greater selectivity

are necessary for application of compounds in cell studies and more complex systems such as animal models. Crystallographic data offers the highest level of detail in understanding the points of contact between the fragment and target, but modeling software and docking continue to provide useful information when structural data is unavailable so long as careful follow-up activity experiments are performed on the proposed compounds. The simplicity of the fragment building blocks allows for relatively simple derivatization. Utilization of negative data as well as positive data from the screen provides invaluable insight into important pharmacophores and substituents even without structural data. The rapid, high throughput nature and diverse chemical space sampled by FBDD makes it a powerful, systematic, and customizable tool for precise and effective drug discovery.

DISULFIDE TETHERING IN PPI DRUG DISCOVERY

PPIs are central to the function of cellular processes. However, they provide certain challenges in terms of druggability. The first challenge is the flatness problem. Most PPI interfaces, unlike enzymes, are lacking in a deep binding pocket that is readily accessible to a small molecule. Instead, large, bulky molecules with low ligand efficiency take advantage of multiple small interactions and are limited in their scope as modulators.[71–75] The second issue is the disorder problem. Many proteins that participate in PPIs are intrinsically disordered until bound to their partner. This provides a potential platform for small molecule binding in the form of a "hotspot" which forms upon the binding of the two proteins.[76–81] However, it is difficult to determine such hotspots in a functional assay and even more challenging to derivatize a natural product or druglike molecule to take advantage of these transient interactions. Proteins also tend to have multiple interaction partners. It is estimated that humans may have up to 650,000 PPIs while only having approximately 20,000 protein encoding genes.[6] Certain so-called hub proteins with multiple interacting partners have 20 or more partners.

There have been many powerful examples of PPI modulators which have resulted in clinical compounds.[82–88] However, many of these molecules were found serendipitously and their mechanisms of action were elucidated after their introduction to the market. A prospective, systematic, reproducible strategy for the discovery of small molecule PPI modulators could provide a novel platform for understanding the biology underlying disease and developing selective and efficacious therapeutics with minimal impact on safety. FBDD, as well as disulfide tethering specifically, lend themselves as such a strategy.[11,36] The versatility of target selection via native or engineered cysteines, the relative simplicity of the starting molecules, the range of optimization strategies, and the inherent understanding of their impact on biology elevates FBDD as the next stage in drug development. The sensitivity, precision, quantification capabilities, and high throughput scalability of the MS technology also elevates disulfide tethering as a platform with far reaching capabilities and applications in precision medicine. The subsequent chapters showcase multiple projects in various stages of the drug discovery pipeline which have all harnessed the power of MS and disulfide tethering as a starting point for the discovery of potent and selective small molecule modulators of multiple PPIs.

REFERENCES

(1)   Butler, M. S.; Robertson, A. A. B.; Cooper, M. A. Natural Product and Natural Product Derived Drugs in Clinical Trials. *Nat. Prod. Rep.* **2014**, *31* (11), 1612–1661. https://doi.org/10.1039/C4NP00064A.

(2)   Hughes, J.; Rees, S.; Kalindjian, S.; Philpott, K. Principles of Early Drug Discovery. *Br. J. Pharmacol.* **2011**, *162* (6), 1239–1249. https://doi.org/10.1111/j.1476-5381.2010.01127.x.

(3)   Atanasov, A. G.; Zotchev, S. B.; Dirsch, V. M.; Supuran, C. T. Natural Products in Drug Discovery: Advances and Opportunities. *Nat. Rev. Drug Discov.* **2021**, *20* (3), 200–216. https://doi.org/10.1038/s41573-020-00114-z.

(4)   Zhang, M.-Q.; Wilkinson, B. Drug Discovery beyond the 'Rule-of-Five.' *Curr. Opin. Biotechnol.* **2007**, *18* (6), 478–488. https://doi.org/10.1016/j.copbio.2007.10.005.

(5)   Tiwari, P.; Bae, H. Endophytic Fungi: Key Insights, Emerging Prospects, and Challenges in Natural Product Drug Discovery. *Microorganisms* **2022**, *10* (2), 360. https://doi.org/10.3390/microorganisms10020360.

(6)   Wang, Z.-Z.; Shi, X.-X.; Huang, G.-Y.; Hao, G.-F.; Yang, G.-F. Fragment-Based Drug Discovery Supports Drugging 'Undruggable' Protein–Protein Interactions. *Trends Biochem. Sci.* **2023**, *0* (0). https://doi.org/10.1016/j.tibs.2023.01.008.

(7)   Erlanson, D. A.; Wells, J. A.; Braisted, A. C. Tethering: Fragment-Based Drug Discovery. *Annu. Rev. Biophys. Biomol. Struct.* **2004**, *33* (1), 199–223. https://doi.org/10.1146/annurev.biophys.33.110502.140409.

(8)   Mansouri, M.; Rumrill, S.; Dawson, S.; Johnson, A.; Pinson, J.-A.; Gunzburg, M. J.; Latham, C. F.; Barlow, N.; Mbogo, G. W.; Ellenberg, P.; Headey, S. J.; Sluis-Cremer, N.; Tyssen, D.; Bauman, J. D.; Ruiz, F. X.; Arnold, E.; Chalmers, D. K.; Tachedjian, G. Targeting

HIV-1 Reverse Transcriptase Using a Fragment-Based Approach. *Molecules* **2023**, *28* (7), 3103. https://doi.org/10.3390/molecules28073103.

(9)   Kirsch, P.; Hartman, A. M.; Hirsch, A. K. H.; Empting, M. Concepts and Core Principles of Fragment-Based Drug Design. *Molecules* **2019**, *24* (23), 4309. https://doi.org/10.3390/molecules24234309.

(10)   Hallenbeck, K. K.; Davies, J. L.; Merron, C.; Ogden, P.; Sijbesma, E.; Ottmann, C.; Renslo, A. R.; Wilson, C.; Arkin, M. R. A Liquid Chromatography/Mass Spectrometry Method for Screening Disulfide Tethering Fragments. *SLAS Discov. Adv. Life Sci. R D* **2018**, *23* (2), 183– 192. https://doi.org/10.1177/2472555217732072.

(11)   Sijbesma, E.; Hallenbeck, K. K.; Leysen, S.; de Vink, P. J.; Skóra, L.; Jahnke, W.; Brunsveld, L.; Arkin, M. R.; Ottmann, C. Site-Directed Fragment-Based Screening for the Discovery of Protein–Protein Interaction Stabilizers. *J. Am. Chem. Soc.* **2019**, *141* (8), 3524– 3531. https://doi.org/10.1021/jacs.8b11658.

(12)   Erlanson, D. A.; Braisted, A. C.; Raphael, D. R.; Randal, M.; Stroud, R. M.; Gordon, E. M.; Wells, J. A. Site-Directed Ligand Discovery. *Proc. Natl. Acad. Sci.* **2000**, *97* (17), 9367– 9372. https://doi.org/10.1073/pnas.97.17.9367.

(13)   Dueñas, M. E.; Peltier-Heap, R. E.; Leveridge, M.; Annan, R. S.; Büttner, F. H.; Trost, M. Advances in High-Throughput Mass Spectrometry in Drug Discovery. *EMBO Mol. Med.* **2023**, *15* (1), e14850. https://doi.org/10.15252/emmm.202114850.

(14)   Erlanson, D. A.; McDowell, R. S.; O'Brien, T. Fragment-Based Drug Discovery. *J. Med. Chem.* **2004**, *47* (14), 3463–3482. https://doi.org/10.1021/jm040031v.

(15)   Bollag, G.; Hirth, P.; Tsai, J.; Zhang, J.; Ibrahim, P. N.; Cho, H.; Spevak, W.; Zhang, C.; Zhang, Y.; Habets, G.; Burton, E. A.; Wong, B.; Tsang, G.; West, B. L.; Powell, B.; Shellooe, R.;

Marimuthu, A.; Nguyen, H.; Zhang, K. Y. J.; Artis, D. R.; Schlessinger, J.; Su, F.; Higgins, B.; Iyer, R.; D'Andrea, K.; Koehler, A.; Stumm, M.; Lin, P. S.; Lee, R. J.; Grippo, J.; Puzanov, I.; Kim, K. B.; Ribas, A.; McArthur, G. A.; Sosman, J. A.; Chapman, P. B.; Flaherty, K. T.; Xu, X.; Nathanson, K. L.; Nolop, K. Clinical Efficacy of a RAF Inhibitor Needs Broad Target Blockade in BRAF-Mutant Melanoma. *Nature* **2010**, *467* (7315), 596–599. https://doi.org/10.1038/nature09454.

(16)   Souers, A. J.; Leverson, J. D.; Boghaert, E. R.; Ackler, S. L.; Catron, N. D.; Chen, J.; Dayton, B. D.; Ding, H.; Enschede, S. H.; Fairbrother, W. J.; Huang, D. C. S.; Hymowitz, S. G.; Jin, S.; Khaw, S. L.; Kovar, P. J.; Lam, L. T.; Lee, J.; Maecker, H. L.; Marsh, K. C.; Mason, K. D.; Mitten, M. J.; Nimmer, P. M.; Oleksijew, A.; Park, C. H.; Park, C.-M.; Phillips, D. C.; Roberts, A. W.; Sampath, D.; Seymour, J. F.; Smith, M. L.; Sullivan, G. M.; Tahir, S. K.; Tse, C.; Wendt, M. D.; Xiao, Y.; Xue, J. C.; Zhang, H.; Humerickhouse, R. A.; Rosenberg, S. H.; Elmore, S. W. ABT-199, a Potent and Selective BCL-2 Inhibitor, Achieves Antitumor Activity While Sparing Platelets. *Nat. Med.* **2013**, *19* (2), 202–208. https://doi.org/10.1038/nm.3048.

(17)   Murray, C. W.; Newell, D. R.; Angibaud, P. A Successful Collaboration between Academia, Biotech and Pharma Led to Discovery of Erdafitinib, a Selective FGFR Inhibitor Recently Approved by the FDA. *MedChemComm* **2019**, *10* (9), 1509–1511. https://doi.org/10.1039/C9MD90044F.

(18)   Guillory, X.; Wolter, M.; Leysen, S.; Neves, J. F.; Kuusk, A.; Genet, S.; Somsen, B.; Morrow, J. K.; Rivers, E.; van Beek, L.; Patel, J.; Goodnow, R.; Schoenherr, H.; Fuller, N.; Cao, Q.; Doveston, R. G.; Brunsveld, L.; Arkin, M. R.; Castaldi, P.; Boyd, H.; Landrieu, I.; Chen, H.; Ottmann, C. Fragment-Based Differential Targeting of PPI Stabilizer Interfaces. *J. Med. Chem.* **2020**, *63* (13), 6694–6707. https://doi.org/10.1021/acs.jmedchem.9b01942.

(19)   Gosu, R.; Zaheer, S. M. Introduction to Surface Plasmon Resonance. In *Methods for Fragments Screening Using Surface Plasmon Resonance*; Zaheer, S. M., Gosu, R., Eds.; Springer: Singapore, 2021; pp 1–4. https://doi.org/10.1007/978-981-16-1536-8_1.

(20)   Troelsen, N. S.; Clausen, M. H. Library Design Strategies To Accelerate Fragment-Based Drug Discovery. *Chem. – Eur. J.* **2020**, *26* (50), 11391–11403. https://doi.org/10.1002/chem.202000584.

(21)   K. Hallenbeck, K.; M. Turner, D.; R. Renslo, A.; R. Arkin, M. Targeting Non-Catalytic Cysteine Residues Through Structure-Guided Drug Discovery. *Curr. Top. Med. Chem.* **2017**, *17* (1), 4–15.

(22)   Boike, L.; Henning, N. J.; Nomura, D. K. Advances in Covalent Drug Discovery. *Nat. Rev. Drug Discov.* **2022**, *21* (12), 881–898. https://doi.org/10.1038/s41573-022-00542-z.

(23)   Dalton, S. E.; Campos, S. Covalent Small Molecules as Enabling Platforms for Drug Discovery. *ChemBioChem* **2020**, *21* (8), 1080–1100. https://doi.org/10.1002/cbic.201900674.

(24)   G. Kathman, S.; V. Statsyuk, A. Covalent Tethering of Fragments for Covalent Probe Discovery. *MedChemComm* **2016**, *7* (4), 576–585. https://doi.org/10.1039/C5MD00518C.

(25)   Chan, W. C.; Sharifzadeh, S.; Buhrlage, S. J.; Marto, J. A. Chemoproteomic Methods for Covalent Drug Discovery. *Chem. Soc. Rev.* **2021**, *50* (15), 8361–8381. https://doi.org/10.1039/D1CS00231G.

(26)   Harvey, E. P.; Hauseman, Z. J.; Cohen, D. T.; Rettenmaier, T. J.; Lee, S.; Huhn, A. J.; Wales, T. E.; Seo, H.-S.; Luccarelli, J.; Newman, C. E.; Guerra, R. M.; Bird, G. H.; Dhe-Paganon, S.; Engen, J. R.; Wells, J. A.; Walensky, L. D. Identification of a Covalent Molecular Inhibitor of Anti-Apoptotic BFL-1 by Disulfide Tethering. *Cell Chem. Biol.* **2020**, *27* (6), 647-656.e6. https://doi.org/10.1016/j.chembiol.2020.04.004.

(27)   Hallenbeck, K. K.; Davies, J. L.; Merron, C.; Ogden, P.; Sijbesma, E.; Ottmann, C.; Renslo, A. R.; Wilson, C.; Arkin, M. R. A Liquid Chromatography/Mass Spectrometry Method for Screening Disulfide Tethering Fragments. *SLAS Discov. Adv. Life Sci. R D* **2018**, *23* (2), 183–192. https://doi.org/10.1177/2472555217732072.

(28)   Keeley, A.; Petri, L.; Ábrányi-Balogh, P.; Keserű, G. M. Covalent Fragment Libraries in Drug Discovery. *Drug Discov. Today* **2020**, *25* (6), 983–996. https://doi.org/10.1016/j.drudis.2020.03.016.

(29)   Konteatis, Z. What Makes a Good Fragment in Fragment-Based Drug Discovery? *Expert Opin. Drug Discov.* **2021**, *16* (7), 723–726. https://doi.org/10.1080/17460441.2021.1905629.

(30)   Gao, K.; Shaabani, S.; Xu, R.; Zarganes-Tzitzikas, T.; Gao, L.; Ahmadianmoghaddam, M.; R. Groves, M.; Dömling, A. Nanoscale, Automated, High Throughput Synthesis and Screening for the Accelerated Discovery of Protein Modifiers. *RSC Med. Chem.* **2021**, *12* (5), 809–818. https://doi.org/10.1039/D1MD00087J.

(31)   Shi, Y.; von Itzstein, M. How Size Matters: Diversity for Fragment Library Design. *Molecules* **2019**, *24* (15), 2838. https://doi.org/10.3390/molecules24152838.

(32)   Erlanson, D. A.; Davis, B. J.; Jahnke, W. Fragment-Based Drug Discovery: Advancing Fragments in the Absence of Crystal Structures. *Cell Chem. Biol.* **2019**, *26* (1), 9–15. https://doi.org/10.1016/j.chembiol.2018.10.001.

(33)   Lu, W.; Kostic, M.; Zhang, T.; Che, J.; P. Patricelli, M.; H. Jones, L.; T. Chouchani, E.; S. Gray, N. Fragment-Based Covalent Ligand Discovery. *RSC Chem. Biol.* **2021**, *2* (2), 354–367. https://doi.org/10.1039/D0CB00222D.

(34)   Dalton, S. E.; Campos, S. Covalent Small Molecules as Enabling Platforms for Drug Discovery. *ChemBioChem* **2020**, *21* (8), 1080–1100. https://doi.org/10.1002/cbic.201900674.

(35)   Erlanson, D. A.; Lam, J. W.; Wiesmann, C.; Luong, T. N.; Simmons, R. L.; DeLano, W. L.; Choong, I. C.; Burdett, M. T.; Flanagan, W. M.; Lee, D.; Gordon, E. M.; O'Brien, T. In Situ Assembly of Enzyme Inhibitors Using Extended Tethering. *Nat. Biotechnol.* **2003**, *21* (3), 308–314. https://doi.org/10.1038/nbt786.

(36)   Kenanova, D. N.; Visser, E. J.; Virta, J. M.; Sijbesma, E.; Centorrino, F.; Vickery, H. R.; Zhong, M.; Neitz, R. J.; Brunsveld, L.; Ottmann, C.; Arkin, M. R. A Systematic Approach to the Discovery of Protein–Protein Interaction Stabilizers. *ACS Cent. Sci.* **2023**. https://doi.org/10.1021/acscentsci.2c01449.

(37)   Bancet, A.; Raingeval, C.; Lomberget, T.; Le Borgne, M.; Guichou, J.-F.; Krimm, I. Fragment Linking Strategies for Structure-Based Drug Design. *J. Med. Chem.* **2020**, *63* (20), 11420–11435. https://doi.org/10.1021/acs.jmedchem.0c00242.

(38)   Awoonor-Williams, E.; Rowley, C. N. Evaluation of Methods for the Calculation of the PKa of Cysteine Residues in Proteins. *J. Chem. Theory Comput.* **2016**, *12* (9), 4662–4673. https://doi.org/10.1021/acs.jctc.6b00631.

(39)   Abo, M.; Li, C.; Weerapana, E. Isotopically-Labeled Iodoacetamide-Alkyne Probes for Quantitative Cysteine-Reactivity Profiling. *Mol. Pharm.* **2018**, *15* (3), 743–749. https://doi.org/10.1021/acs.molpharmaceut.7b00832.

(40)   Nelson, K. J.; Day, A. E.; Zeng, B.-B.; King, S. B.; Poole, L. B. Isotope-Coded, Iodoacetamide-Based Reagent to Determine Individual Cysteine PKa Values by Matrix-Assisted Laser Desorption/Ionization Time-of-Flight Mass Spectrometry. *Anal. Biochem.* **2008**, *375* (2), 187–195. https://doi.org/10.1016/j.ab.2007.12.004.

(41)   Blay, V.; Tolani, B.; Ho, S. P.; Arkin, M. R. High-Throughput Screening: Today's Biochemical and Cell-Based Approaches. *Drug Discov. Today* **2020**, S1359644620303056. https://doi.org/10.1016/j.drudis.2020.07.024.

(42)   Gardino, A. K.; Smerdon, S. J.; Yaffe, M. B. Structural Determinants of 14-3-3 Binding

Specificities and Regulation of Subcellular Localization of 14-3-3-Ligand Complexes: A

Comparison of the X-Ray Crystal Structures of All Human 14-3-3 Isoforms. *Semin. Cancer Biol.*

2006, *16* (3), 173–182. https://doi.org/10.1016/j.semcancer.2006.03.007.

(43)   Iralde-Lorente, L.; Tassone, G.; Clementi, L.; Franci, L.; Munier, C. C.; Cau, Y.; Mori, M.;

Chiariello, M.; Angelucci, A.; Perry, M. W. D.; Pozzi, C.; Mangani, S.; Botta, M. Identification of

Phosphate-Containing Compounds as New Inhibitors of 14-3-3/c-Abl Protein–Protein

Interaction. *ACS Chem. Biol.* **2020**. https://doi.org/10.1021/acschembio.0c00039.

(44)   Pennington, K. L.; Chan, T. Y.; Torres, M. P.; Andersen, J. L. The Dynamic and Stress-

Adaptive Signaling Hub of 14-3-3: Emerging Mechanisms of Regulation and Context-Dependent

Protein–Protein Interactions. *Oncogene* **2018**, *37* (42), 5587. https://doi.org/10.1038/s41388-

018-0348-3.

(45)   Ballone, A.; Lau, R. A.; Zweipfenning, F. P. A.; Ottmann, C. A New Soaking Procedure

for X-Ray Crystallographic Structural Determination of Protein–Peptide Complexes. *Acta

Crystallogr. Sect. F Struct. Biol. Commun.* **2020**, *76* (Pt 10), 501–507.

https://doi.org/10.1107/S2053230X2001122X.

(46)   Centorrino, F.; Ballone, A.; Wolter, M.; Ottmann, C. Biophysical and Structural Insight

into the USP8/14-3-3 Interaction. *FEBS Lett.* **2018**, *592* (7), 1211–1220.

https://doi.org/10.1002/1873-3468.13017.

(47)   Stevers, L. M.; Sijbesma, E.; Botta, M.; MacKintosh, C.; Obsil, T.; Landrieu, I.; Cau, Y.;

Wilson, A. J.; Karawajczyk, A.; Eickhoff, J.; Davis, J.; Hann, M.; O'Mahony, G.; Doveston, R. G.;

Brunsveld, L.; Ottmann, C. Modulators of 14-3-3 Protein–Protein Interactions. *J. Med. Chem.*

2018, *61* (9), 3755–3778. https://doi.org/10.1021/acs.jmedchem.7b00574.

(48)   Hesterkamp, T.; Barker, J.; Davenport, A.; Whittaker, M. Fragment Based Drug Discovery Using Fluorescence Correlation Spectroscopy Techniques: Challenges and Solutions. *Curr. Top. Med. Chem.* **2007**, *7* (16), 1582–1591.

(49)   Schmidt, M. F.; Rademann, J. Dynamic Template-Assisted Strategies in Fragment-Based Drug Discovery. *Trends Biotechnol.* **2009**, *27* (9), 512–521. https://doi.org/10.1016/j.tibtech.2009.06.001.

(50)   Chessari, G.; Buck, I. M.; Day, J. E. H.; Day, P. J.; Iqbal, A.; Johnson, C. N.; Lewis, E. J.; Martins, V.; Miller, D.; Reader, M.; Rees, D. C.; Rich, S. J.; Tamanini, E.; Vitorino, M.; Ward, G. A.; Williams, P. A.; Williams, G.; Wilsher, N. E.; Woolford, A. J.-A. Fragment-Based Drug Discovery Targeting Inhibitor of Apoptosis Proteins: Discovery of a Non-Alanine Lead Series with Dual Activity Against CIAP1 and XIAP. *J. Med. Chem.* **2015**, *58* (16), 6574–6588. https://doi.org/10.1021/acs.jmedchem.5b00706.

(51)   Valkov, E.; Sharpe, T.; Marsh, M.; Greive, S.; Hyvönen, M. Targeting Protein–Protein Interactions and Fragment-Based Drug Discovery. In *Fragment-Based Drug Discovery and X-Ray Crystallography*; Davies, T. G., Hyvönen, M., Eds.; Topics in Current Chemistry; Springer: Berlin, Heidelberg, 2012; pp 145–179. https://doi.org/10.1007/128_2011_265.

(52)   Kieffer, C.; Jourdan, J. P.; Jouanne, M.; Voisin-Chiret, A. S. Noncellular Screening for the Discovery of Protein–Protein Interaction Modulators. *Drug Discov. Today* **2020**, *25* (9), 1592–1603. https://doi.org/10.1016/j.drudis.2020.07.012.

(53)   Centorrino, F.; Andlovic, B.; Cossar, P.; Brunsveld, L.; Ottmann, C. Fragment-Based Exploration of the 14-3-3/Amot-P130 Interface. *Curr. Res. Struct. Biol.* **2022**, *4*, 21–28. https://doi.org/10.1016/j.crstbi.2021.12.003.

(54)   Valenti, D.; Hristeva, S.; Tzalis, D.; Ottmann, C. Clinical Candidates Modulating Protein-Protein Interactions: The Fragment-Based Experience. *Eur. J. Med. Chem.* **2019**, *167*, 76–95. https://doi.org/10.1016/j.ejmech.2019.01.084.

(55)   Sijbesma, E.; Somsen, B. A.; Miley, G. P.; Leijten-van de Gevel, I. A.; Brunsveld, L.; Arkin, M. R.; Ottmann, C. Fluorescence Anisotropy-Based Tethering for Discovery of Protein–Protein Interaction Stabilizers. *ACS Chem. Biol.* **2020**, *15* (12), 3143–3148. https://doi.org/10.1021/acschembio.0c00646.

(56)   Kitchner, E.; Seung, M.; Chavez, J.; Ceresa, L.; Kimball, J.; Gryczynski, I.; Gryczynski, Z. Fluorescence Measurements: Importance of G-Factor Correction, Magic Angle, and Observation Wavelengths. *Methods Appl. Fluoresc.* **2022**, *10* (4), 043001. https://doi.org/10.1088/2050-6120/ac92c5.

(57)   Jameson, D. M.; Ross, J. A. Fluorescence Polarization/Anisotropy in Diagnostics and Imaging. *Chem. Rev.* **2010**, *110* (5), 2685–2708. https://doi.org/10.1021/cr900267p.

(58)   Kimple, A. J.; Yasgar, A.; Hughes, M.; Jadhav, A.; Willard, F. S.; Muller, R. E.; Austin, C. P.; Inglese, J.; Ibeanu, G. C.; Siderovski, D. P.; Simeonov, A. A High Throughput Fluorescence Polarization Assay for Inhibitors of the GoLoco Motif/G-Alpha Interaction. *Comb. Chem. High Throughput Screen.* **2008**, *11* (5), 396–409. https://doi.org/10.2174/138620708784534770.

(59)   Zhang, H.; Nimmer, P.; Rosenberg, S. H.; Ng, S.-C.; Joseph, M. Development of a High-Throughput Fluorescence Polarization Assay for Bcl-XL. *Anal. Biochem.* **2002**, *307* (1), 70–75. https://doi.org/10.1016/S0003-2697(02)00028-3.

(60)   Burke, T. J.; Loniello, K. R.; Beebe, J. A.; Ervin, K. M. Development and Application of Fluorescence Polarization Assays in Drug Discovery. *Comb. Chem. High Throughput Screen.* **2003**, *6* (3), 183–194. https://doi.org/10.2174/138620703106298365.

(61)   Frank, A. O.; Feldkamp, M. D.; Kennedy, J. P.; Waterson, A. G.; Pelz, N. F.; Patrone, J. D.; Vangamudi, B.; Camper, D. V.; Rossanese, O. W.; Chazin, W. J.; Fesik, S. W. Discovery of a Potent Inhibitor of Replication Protein A Protein–Protein Interactions Using a Fragment-Linking Approach. *J. Med. Chem.* **2013**, *56* (22), 9242–9250. https://doi.org/10.1021/jm401333u.

(62)   Möbitz, H.; Machauer, R.; Holzer, P.; Vaupel, A.; Stauffer, F.; Ragot, C.; Caravatti, G.; Scheufler, C.; Fernandez, C.; Hommel, U.; Tiedt, R.; Beyer, K. S.; Chen, C.; Zhu, H.; Gaul, C. Discovery of Potent, Selective, and Structurally Novel Dot1L Inhibitors by a Fragment Linking Approach. *ACS Med. Chem. Lett.* **2017**, *8* (3), 338–343. https://doi.org/10.1021/acsmedchemlett.6b00519.

(63)   Hung, A. W.; Silvestre, H. L.; Wen, S.; Ciulli, A.; Blundell, T. L.; Abell, C. Application of Fragment Growing and Fragment Linking to the Discovery of Inhibitors of Mycobacterium Tuberculosis Pantothenate Synthetase. *Angew. Chem. Int. Ed.* **2009**, *48* (45), 8452–8456. https://doi.org/10.1002/anie.200903821.

(64)   C. Miller, D.; P. Martin, M.; Adhikari, S.; Brennan, A.; A. Endicott, J.; T. Golding, B.; R. Hardcastle, I.; Heptinstall, A.; Hobson, S.; Jennings, C.; Molyneux, L.; Ng, Y.; R. Wedge, S.; M. Noble, M. E.; Cano, C. Identification of a Novel Ligand for the ATAD2 Bromodomain with Selectivity over BRD4 through a Fragment Growing Approach. *Org. Biomol. Chem.* **2018**, *16* (11), 1843–1850. https://doi.org/10.1039/C8OB00099A.

(65)   O. Nikiforov, P.; Surade, S.; Blaszczyk, M.; Delorme, V.; Brodin, P.; R. Baulard, A.; L. Blundell, T.; Abell, C. A Fragment Merging Approach towards the Development of Small Molecule Inhibitors of Mycobacterium Tuberculosis EthR for Use as Ethionamide Boosters. *Org. Biomol. Chem.* **2016**, *14* (7), 2318–2326. https://doi.org/10.1039/C5OB02630J.

(66)   Prakash, M.; Itoh, Y.; Fujiwara, Y.; Takahashi, Y.; Takada, Y.; Mellini, P.; Elboray, E. E.; Terao, M.; Yamashita, Y.; Yamamoto, C.; Yamaguchi, T.; Kotoku, M.; Kitao, Y.; Singh, R.; Roy, R.; Obika, S.; Oba, M.; Wang, D. O.; Suzuki, T. Identification of Potent and Selective Inhibitors of Fat Mass Obesity-Associated Protein Using a Fragment-Merging Approach. *J. Med. Chem.* **2021**, *64* (21), 15810–15824. https://doi.org/10.1021/acs.jmedchem.1c01107.

(67)   Scott, D. E.; Coyne, A. G.; Hudson, S. A.; Abell, C. Fragment-Based Approaches in Drug Discovery and Chemical Biology. *Biochemistry* **2012**, *51* (25), 4990–5003. https://doi.org/10.1021/bi3005126.

(68)   de Souza Neto, L. R.; Moreira-Filho, J. T.; Neves, B. J.; Maidana, R. L. B. R.; Guimarães, A. C. R.; Furnham, N.; Andrade, C. H.; Silva, F. P. In Silico Strategies to Support Fragment-to-Lead Optimization in Drug Discovery. *Front. Chem.* **2020**, *8*.

(69)   Crisman, T. J.; Bender, A.; Milik, M.; Jenkins, J. L.; Scheiber, J.; Sukuru, S. C. K.; Fejzo, J.; Hommel, U.; Davies, J. W.; Glick, M. "Virtual Fragment Linking": An Approach To Identify Potent Binders from Low Affinity Fragment Hits. *J. Med. Chem.* **2008**, *51* (8), 2481–2491. https://doi.org/10.1021/jm701314u.

(70)   Tan, Y.; Dai, L.; Huang, W.; Guo, Y.; Zheng, S.; Lei, J.; Chen, H.; Yang, Y. DRlinker: Deep Reinforcement Learning for Optimization in Fragment Linking Design. *J. Chem. Inf. Model.* **2022**, *62* (23), 5907–5917. https://doi.org/10.1021/acs.jcim.2c00982.

(71)   Arkin, M. R.; Wells, J. A. Small-Molecule Inhibitors of Protein–Protein Interactions: Progressing towards the Dream. *Nat. Rev. Drug Discov.* **2004**, *3* (4), 301–317. https://doi.org/10.1038/nrd1343.

(72)   Bakail, M.; Ochsenbein, F. Targeting Protein–Protein Interactions, a Wide Open Field for Drug Design. *Comptes Rendus Chim.* **2016**, *19* (1), 19–27. https://doi.org/10.1016/j.crci.2015.12.004.

(73)   Buchwald, P. Small-Molecule Protein–Protein Interaction Inhibitors: Therapeutic Potential in Light of Molecular Size, Chemical Space, and Ligand Binding Efficiency Considerations. *IUBMB Life* **2010**, *62* (10), 724–731. https://doi.org/10.1002/iub.383.

(74)   Wells, J. A.; McClendon, C. L. Reaching for High-Hanging Fruit in Drug Discovery at Protein–Protein Interfaces. *Nature* **2007**, *450* (7172), 1001–1009. https://doi.org/10.1038/nature06526.

(75)   Gonzalez-Ruiz, D.; Gohlke, H. Targeting Protein-Protein Interactions with Small Molecules: Challenges and Perspectives for Omputational Binding Epitope Detection and Ligand Finding. *Curr. Med. Chem.* **2006**, *13* (22), 2607–2625. https://doi.org/10.2174/092986706778201530.

(76)   Biesaga, M.; Frigolé-Vivas, M.; Salvatella, X. Intrinsically Disordered Proteins and Biomolecular Condensates as Drug Targets. *Curr. Opin. Chem. Biol.* **2021**, *62*, 90–100. https://doi.org/10.1016/j.cbpa.2021.02.009.

(77)   Tsafou, K.; Tiwari, P. B.; Forman-Kay, J. D.; Metallo, S. J.; Toretsky, J. A. Targeting Intrinsically Disordered Transcription Factors: Changing the Paradigm. *J. Mol. Biol.* **2018**, *430* (16), 2321–2341. https://doi.org/10.1016/j.jmb.2018.04.008.

(78)   Dunker, A. K.; Oldfield, C. J.; Meng, J.; Romero, P.; Yang, J. Y.; Chen, J. W.; Vacic, V.; Obradovic, Z.; Uversky, V. N. The Unfoldomics Decade: An Update on Intrinsically Disordered Proteins. *BMC Genomics* **2008**, *9* (2), S1. https://doi.org/10.1186/1471-2164-9-S2-S1.

(79)   Tompa, P.; Schad, E.; Tantos, A.; Kalmar, L. Intrinsically Disordered Proteins: Emerging Interaction Specialists. *Curr. Opin. Struct. Biol.* **2015**, *35*, 49–59. https://doi.org/10.1016/j.sbi.2015.08.009.

(80)   Uversky, V. N. Chapter Four - Intrinsic Disorder, Protein–Protein Interactions, and Disease. In *Advances in Protein Chemistry and Structural Biology*; Donev, R., Ed.; Protein-Protein Interactions in Human Disease, Part A; Academic Press, 2018; Vol. 110, pp 85–121. https://doi.org/10.1016/bs.apcsb.2017.06.005.

(81)   Marín, M.; Thallmair, V.; Ott, T. The Intrinsically Disordered N-Terminal Region of AtREM1.3 Remorin Protein Mediates Protein-Protein Interactions *. *J. Biol. Chem.* **2012**, *287* (47), 39982–39991. https://doi.org/10.1074/jbc.M112.414292.

(82)   Ershov, P. V.; Mezentsev, Y. V.; Ivanov, A. S. Interfacial Peptides as Affinity Modulating Agents of Protein-Protein Interactions. *Biomolecules* **2022**, *12* (1), 106. https://doi.org/10.3390/biom12010106.

(83)   Ni, D.; Liu, N.; Sheng, C. Allosteric Modulators of Protein–Protein Interactions (PPIs). In *Protein Allostery in Drug Discovery*; Zhang, J., Nussinov, R., Eds.; Advances in Experimental Medicine and Biology; Springer: Singapore, 2019; pp 313–334. https://doi.org/10.1007/978-981-13-8719-7_13.

(84)   Yan, J.; Zheng, X.; You, W.; He, W.; Xu, G.-K. A Bionic-Homodimerization Strategy for Optimizing Modulators of Protein–Protein Interactions: From Statistical Mechanics Theory to Potential Clinical Translation. *Adv. Sci.* **2022**, *9* (11), 2105179. https://doi.org/10.1002/advs.202105179.

(85)   Milroy, L.-G.; Grossmann, T. N.; Hennig, S.; Brunsveld, L.; Ottmann, C. Modulators of Protein–Protein Interactions. *Chem. Rev.* **2014**, *114* (9), 4695–4748. https://doi.org/10.1021/cr400698c.

(86)   Stone, T. A.; Deber, C. M. Therapeutic Design of Peptide Modulators of Protein-Protein Interactions in Membranes. *Biochim. Biophys. Acta BBA - Biomembr.* **2017**, *1859* (4), 577–585. https://doi.org/10.1016/j.bbamem.2016.08.013.

(87)   Łączkowski, K. Z.; Baranowska-Łączkowska, A. Recent Studies on the Thalidomide and Its Derivatives. *Future Med. Chem.* **2018**, *10* (18), 2133–2136. https://doi.org/10.4155/fmc-2018-0217.

(88)   Bartlett, J. B.; Dredge, K.; Dalgleish, A. G. The Evolution of Thalidomide and Its IMiD Derivatives as Anticancer Agents. *Nat. Rev. Cancer* **2004**, *4* (4), 314–322. https://doi.org/10.1038/nrc1323.

Chapter 2 Caspase-2: An Introduction to Biological Target Validation
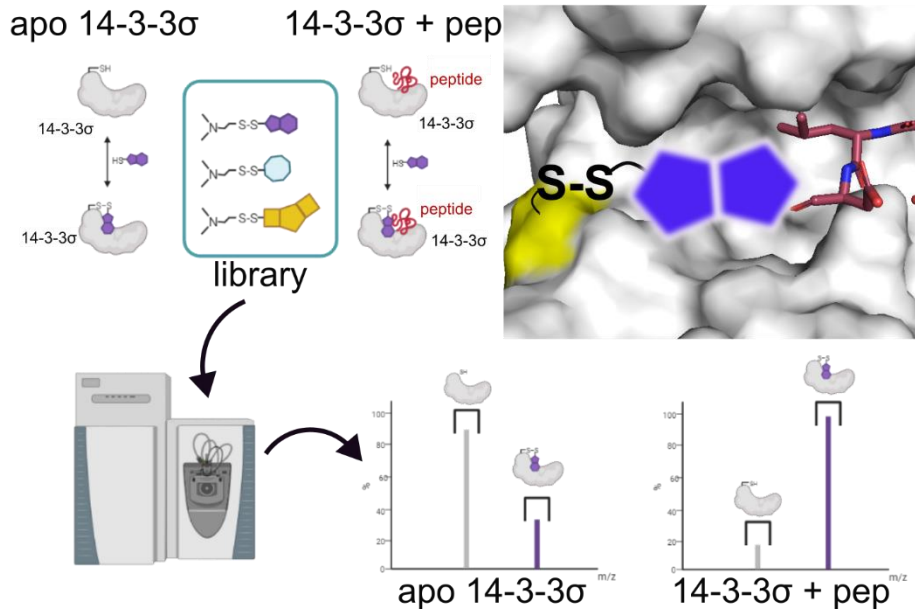
ABSTRACT: Nonalcoholic fatty liver disease (NAFLD) and its progression to the more severe nonalcoholic liver steatohepatitis (NASH) have no current treatments beyond a dramatic shift in lifestyle, presenting an opportunity for the development of novel therapeutics. Caspase-2, a protease more commonly known in the context of apoptosis, has a unique role in metabolic signaling which may be central to the activation of SREB1 and SSREB2, the primary transcription factors associated with NAFLD and NASH. Thus, targeting and inhibiting caspase-2 selectively in the liver provides an alternative path to preventing, and even reversing, liver damage. However, caspase-2 has been difficult to drug selectively via traditional screening for inhibitory small molecules. We decided to address the "undruggability" of caspase-2 by instead screening for selective small molecule stabilizers of the protein-protein interaction (PPI) between the inactive zymogen, procaspase-2, and its negative regulator, the hub protein 14-3-3. We also wanted to validate that 14-3-3 acted as a negative regulator of caspase-2 activity in the

context of metabolism as well as the canonical apoptotic pathway. The disulfide tethering screen resulted in a small number of compounds which successfully showed binding in the mass spectrometry dose response assays. However, the compounds showed no activity in the stabilization and cooperativity follow-up experiments and the subcellular localization assays were unable to produce definitive results due to the nonselective binding of the antibody to both active caspase-2 and inactive zymogen. This study highlighted the importance of biological target selection and validation prior to screening and drug discovery efforts and informed the approach to novel biological systems that will be discussed in subsequent chapters.

INTRODUCTION

Nonalcoholic fatty liver disease (NAFLD) and its potential progression into the more severe, chronic ailment nonalcoholic liver steatohepatitis (NASH) are growing global health concerns.[1,2] NAFLD is caused by the buildup of excess fat within the liver and is reversible through decreased food intake and regular exercise, however NASH is markedly more difficult to treat and results in irreversible liver damage as well as liver cirrhosis and hepatocellular carcinoma.[3] Currently, beyond a drastic lifestyle shift in both diet and exercise, there are no therapeutics for NASH or NAFLD which presents an opportunity to develop novel, effective drugs to address these metabolic syndromes.[4–6] One of the key enzymes involved in NAFLD progression, caspase-2, was of primary interest to the Arkin lab due to its involvement in a plethora of cellular pathways, classification as an "undruggable" protein, involvement in exciting protein-protein interactions (PPIs), and potential as a drug target for NAFLD and NASH in order to mitigate and even reverse liver damage and decrease overall body fat.[7–9]

Caspase-2 is the most evolutionarily conserved member of the cysteine aspartate specific proteases (caspase) family and uniquely exhibits properties characteristic of both an initiator and an effector caspase.[7,10,11] Similar to other initiator caspases, caspase-2 exists as an inactive zymogen, termed procaspase-2, distinguished by an extended N-terminal caspase activation
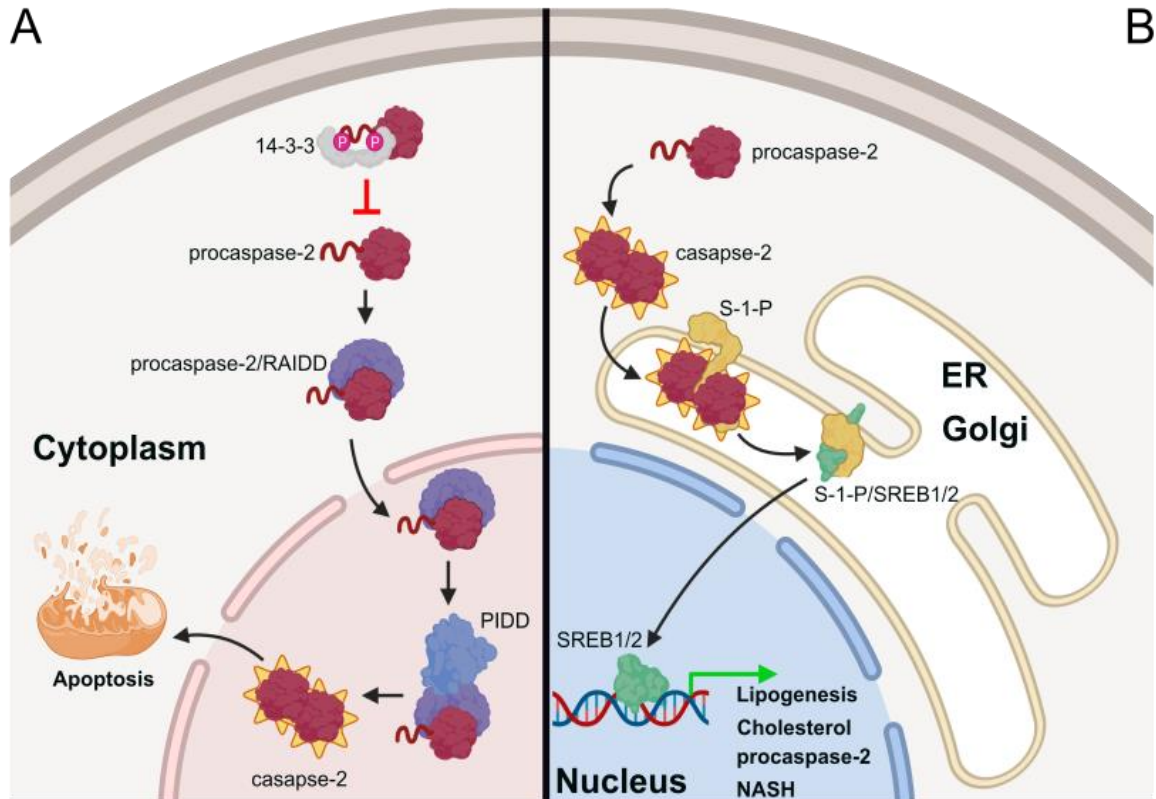
Figure 2.1. Caspase-2 apoptotic and non-apoptotic signaling pathways. (A) Mechanistic diagram of 14-3-3 regulation of caspase-2 apoptotic pathway. 14-3-3 protein (grey) binds to inactive procaspase-2 (maroon) N-terminal CARD domain via binding recognition site containing phosphorylated S139 and S164 residues (pink). This interaction sterically occludes binding of RAIDD complex (purple) which prevents nuclear import and activation of caspase-2 by PIDD (blue). The caspase-2 dimer (maroon with yellow outline) is responsible for initiation of apoptosis via activation of key proteins which induce mitochondrial permeabilization. (B) Mechanistic diagram of caspase-2 non-apoptotic pathway in liver. Procaspase-2 (maroon) dimerizes and self-cleaves the CARD domain in order to form active dimer (maroon with yellow outline). Activated caspase-2 cleaves S-1-P (yellow) which is then free to cleave SREB1 and 2 (green) within the ER and Golgi. SREB1/2 are transcription factors which activate genes associated with lipogenesis, increased cholesterol production, increased procaspase-2, and progression of NAFLD to NASH.

and recruitment domain (CARD) that must be cleaved in order to allow for activation of the enzyme. Once the CARD is cleaved, caspase-2 forms an activated homodimer with substrate specificity similar to the effector caspases (**Figure 2.1A**).[7]

As with most caspases, caspase-2 has an established role as an initiator of apoptosis under various cellular stress conditions.[7,12–14] However, it also plays a role in liver cells under endoplasmic reticulum (ER) stress that does not result in cell death, but instead drives increased *de novo* lipogenesis and cholesterol synthesis.[15–17] Caspase-2 liver-specific knockout

35

mice fed high fat western diets (HFD) or exhibiting NASH phenotype showed decreased overall body fat and NASH symptoms, respectively.[9,18] Mechanistically, caspase-2 is responsible for the activation of site-1-protease (S-1-P) which then activates the transcription factors sterol regulatory element-binding protein 1 and 2 (SREBP1/2).[19,20] S-1-P cleavage releases the N-terminus of SREBP1/2 into the cytoplasm allowing localization into the nucleus, subsequent dimerization, and activation of *de novo* lipogenesis in context of SREBP1 and cholesterol synthesis and increased caspase-2 expression in context of SREBP2 (**Figure 2.1B**).[15] SREBP2 has been implicated as the switch between NAFLD and the development of NASH.[21] Interestingly, caspase-2 activation of SREBP1/2 is independent of the canonical SREBP cleavage-activating protein (SCAP) pathway.[8,22,23] While SCAP-dependent activation of SREBP1/2 is regulated via negative feedback, caspase-2 has no established negative regulator within this nonapoptotic pathway.

The scaffolding protein 14-3-3 is a known negative regulator of caspase-2 activity within the apoptotic pathway.[16] 14-3- 3 recognizes and binds to two specific phosphorylated serine residues, pS139 and pS164, in the linker between the CARD domain and the p19 domain of the procaspase-2 zymogen (**Figures 2.2A** and **2.2B**) and acts to sterically hinder binding of RIP-associated ICH-1 homologous protein with a death domain (RAIDD).[24,25] This in turn prevents procaspase-2 cleavage and activation by the p53-inducible death domain-containing protein (PIDD).[12,22] Previous work in the Arkin lab to establish a caspase-2 inhibitor had yielded no hit molecules, however, stabilization of the 14-3-3/procaspase-2 complex is a novel approach to inhibiting caspase-2 activation. Utilizing the Arkin lab disulfide fragment library and a quantitative, mass spectrometry-based tethering screen, we attempted to discover small molecule scaffolds for the discovery and development of molecular glues between the 14-3-3/procaspase-2 PPI in order to determine the regulatory role of 14-3-3 in the nonapoptotic pathway of caspase-2 and validate the potential of using 14-3-3/procaspase-2 stabilization as a
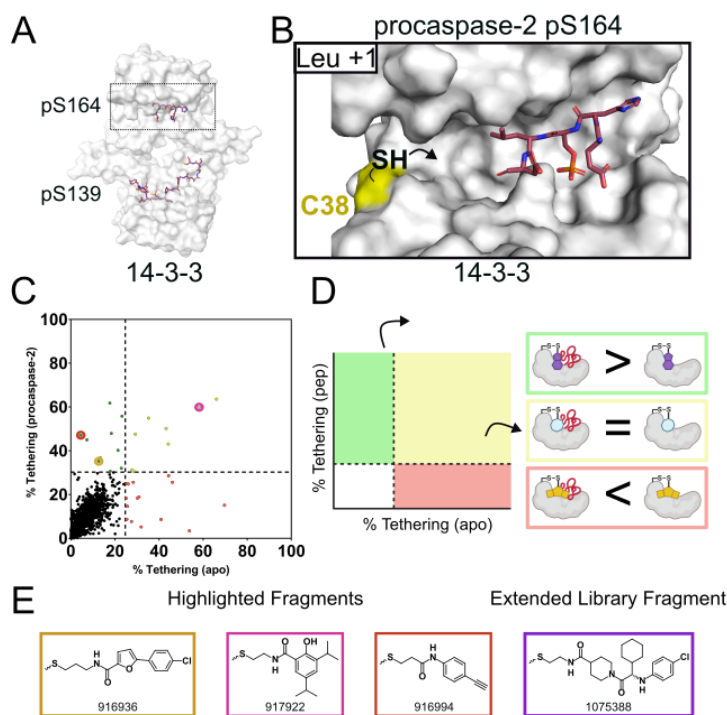
Figure 2.2. 14-3-3/procaspase-2 stabilization initial screen. (A) Crystallographic structure of 14-3-3γ dimer (white) bound to procaspase-2 phospho-peptide with residues pS139 (bottom red) and pS164 (top red in box, PDB ID: 6SAD). (B) Overlay of procaspase-2 pS164 phospho-peptide (maroon) with +1 leucine (Leu) and 14-3-3σ (white, PDB 7OBY). Target cysteine (C38) highlighted in yellow. (C) Tethering screen scatterplot. Compound **916936**, **917922**, and **916994** identified in yellow, pink, and red circles respectively. (D) Schematic of screen scatterplot. Quadrants are outlined by dotted lines signifying 3*SD above average %tethering. Green quadrant indicates increased binding to 14-3-3 in presence of procaspase-2 peptide, yellow shows neutral binding, and red indicates reduced binding in presence of peptide. (E) Chemical structures of highlighted fragment hits **916936**, **917922**, and **916944** and extended fragment hit **1075388**.

therapeutic strategy for NASH.[26–28] The initial screen resulted in 20 hit compounds (**Figure 2.2C**), 4 of which showed stabilization in the preliminary fluorescence anisotropy-based activity assay (**Figures 2.2E, 2.3, 2.4,** and **2.5**). However, none of the compounds validated in the final cooperativity assay and difficulties with in-cell imaging resulted in a project shift towards a more technology driven approach to 14-3-3/client selection for stabilization as discussed in Chapter 3.

RESULTS AND DISCUSSION

Primary Screen for 14-3-3/Caspase-2 Stabilizers. The σ isoform of 14-3-3, one of seven isoforms constitutively expressed in mammalian cells, contains a solvent-exposed cysteine, C38, proximal to the 14-3-3/client binding groove (**Figure 2.2B**). This cysteine was the target of reversible covalent engagement via the disulfide fragment thiol moiety. Phospho-peptide mimetic 14-3-3σ binding affinities of procaspase-2 pS139, pS164, and bivalent pS139 and
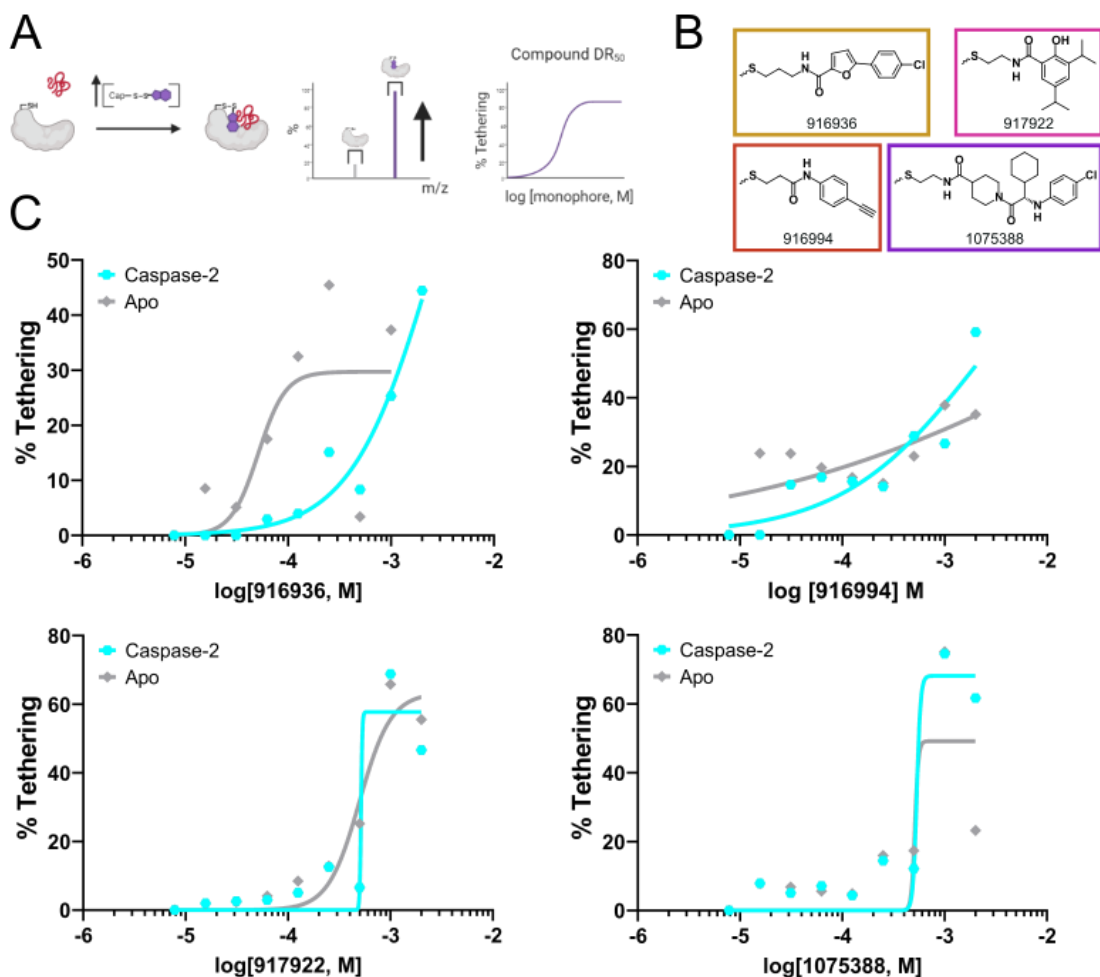
Figure 2.3. Overview of MSDR for highlighted fragments. (A) Outline of MSDR process. 14-3-3 (white) is incubated with procaspase-2 phospho-peptide (red) and increasing concentration of fragment (purple). Engagement of fragment to 14-3-3 is expected to increase in dose dependent manner. % Tethering curve gives compound DR$_{50}$ value. (B) Chemical structures of highlighted hit fragments. (C) MSDR curves for highlighted hit fragments **916936** (top left), **916994** (top right), **917922** (bottom left), and **1075388** (bottom right). Cyan line indicates %Tethering for fragments in the presence of procaspase-2 pS164 phospho-peptide and grey indicates *apo* 14-3-3 control.

pS164 were assessed via fluorescence anisotropy with the bivalent peptide having an acceptably tight K$_D$ of 12 μM. The screen was performed using 100 nM 14-3-3σ, bivalent procaspase-2 peptide at twice its K$_D$ value, 200 μM disulfide fragment, and 250 μM β-mercaptoethanol (BME). Excess phospho-peptide ensured that the 14-3-3σ/procaspase-2 complex was the primary species interacting with the disulfide fragments for consistency when comparing the engagement of the 14-3-3σ/procaspase-2 screen hit compounds to the negative control screen of 14-3-3σ alone (14-3-3σ *apo*). BME induced disulfide exchange, unclipping the

disulfide fragment and its solubility cap, but also acted as a control for nonselective binders by outcompeting such transient interactions for C38 binding. After a 3 hour incubation period, samples were measured via intact-protein LC/MS.

The % tethering – a metric defined as the quotient of the % labeling of fragment to 14-3-3σ over the summation of the % labeling of all 14-3-3σ moieties then multiplied by 100 – threshold for hit selection was three standard deviations (3*SD) above average % tethering for the particular screening condition. Fragments which bound above the % tethering threshold in the 14-3-3σ/procaspe-2 screen but bound below the % tethering threshold of the *apo* screen were considered potential stabilizers and taken forward into the validation assays. The procaspase-2 screen yielded 20 hit compounds, 11 of which were potential stabilizers, which engaged 14-3-3σ above the 30% tethering threshold (**Figures 2.2C** and **2.2D**).

Hit Fragment Validation and Activity Assays. The 20 highest tethering fragment hits and 12 other hit compounds from an additional extension to the library were taken forward into a mass spectrometry-based compound dose response (MSDR) in order to quantify dose-dependent fragment engagement of protein (compound DR_{50}; **Figure 2.3A**) and select against false positives or artifacts from the initial screen. Assays conditions were kept consistent to the original procaspase-2 disulfide screen, but with a 3-fold fragment titration series from 2 mM to 900 nM. Of the best compounds, **917922** and **1075388** had DR_{50} values of approximately 250 µM and compounds **916936** and **916994** had DR_{50} values of approximately 300 µM (**Figures 2.3B and 2.3C**). These high µM DR_{50} values indicated less than optimal compound engagement of 14-3-3σ and showed no selectivity over *apo* 14-3-3, but due to the simplicity of the molecules there was potential room for derivatization at later stages of the drug discovery process. Of the 32 compounds tested in the MSDR, 10 compounds showed enough promise and had enough material to be taken forward into the fluorescence anisotropy-based fragment dose response
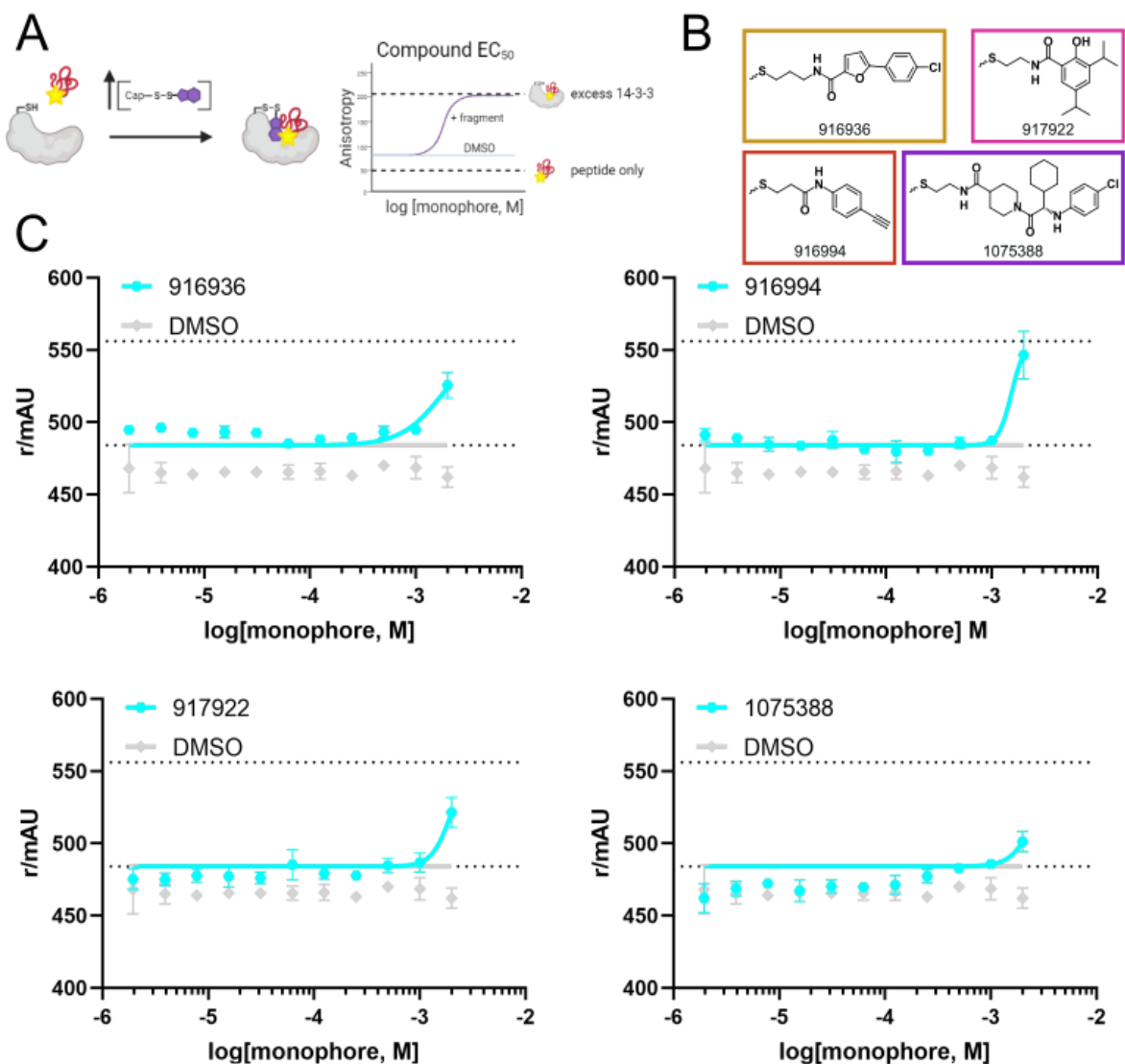
Figure 2.4. Overview of FADR for highlighted fragments. (A) Outline of FADR process. Fluorescently labeled procaspase-2 (red) is incubated with set concentration of 14-3-3 at approximately ½ K_D and increasing concentration of fragment. Increase in anisotropy is indicative of stabilization of the 14-3-3/procaspase-2 interaction. Bottom dashed line indicates lower limit, defined by peptide only. Top dashed line demarcates maximum peptide bound and is peptide with excess 14-3-3. (B) Chemical structures of highlighted hit fragments. (C) FADR curves of highlighted fragments **916936** (top left), **916994** (top right), **917922** (bottom left), and **1075388** (bottom right). Cyan line indicates treatment with compound. Grey line shows DMSO control. Bottom dash is peptide only. Top dash is peptide plus excess 14-3-3.

assay (FADR) in order to determine compound efficacy (compound EC$_{50}$; **Figure 2.4A**). Of

these 10 MSDR hits, four compounds showed some stabilization at high compound

concentrations (**Figures 2.4B** and **2.4C**). The EC$_{50}$ values were well over the measurable value

in the FADR (**Table 2.1**). Thus, the subsequent fluorescence anisotropy-based protein titration

experiments were performed at 2 mM — the highest compound concentration measured in the

FADR — in order to saturate as much of the 14-3-3σ natural product binding pocket as possible.

14-3-3σ was titrated in a 2-fold dilution series and the binding affinity of the procaspase-2

bivalent phospho-peptide was determined in the presence of compound (K_{D_app}) and with a

DMSO control (K_{D_DMSO}). A shift to the left in binding affinity is indicative of stabilization of the

14-3-3σ/procaspase-2 complex and cooperativity between the fragment, protein, and phospho-

peptide. No such shift was observed for any of the four FADR compound hits (**Figure 2.5**; **Table**

2.1).

Table 2.1 Properties of highlighted fragments

	MSDR (250 µM BME)	FADR (250 µM BME)	Protein Titrations (250 µM)		
Cmpnd	DR_{50} (µM)	EC_{50} (µM)	K_{D_app}	K_{D_DMSO}*	Fold Stab.
916936	>2000	1811	36	47	1.3
916994	>2000	1535	—	47	—
917922	515	1969	275	46	—
1075388	534	>2000	123	47	—

*K_D for peptide is accurate within 3-fold range. These values are shown on the same
plate as protein titrations with compound.

CONCLUSIONS

14-3-3 regulation of caspase-2 in apoptosis has been relatively well studied, however the role

this PPI plays in metabolic regulation, NAFLD, and NASH is less defined. The goal of the

disulfide screen and subsequent assays was to discover small molecule fragments which could

be used as scaffolds for the development of selective, potent stabilizers with which to probe the

interaction. Such a tunable foundation had great potential for optimization and lead development

for eventual cell studies of 14-3-3, caspase-2, S-1-P, SREB1/2 interactions and signaling under

disease conditions.

Unfortunately, the screen produced a low number of hit compounds, none of which were able to

show cooperativity in the final protein titration assay (**Figure 2.5C**). A cysteine located within the

peptide could be partially responsible for low fragment engagement of 14-3-3σ C38 and steric
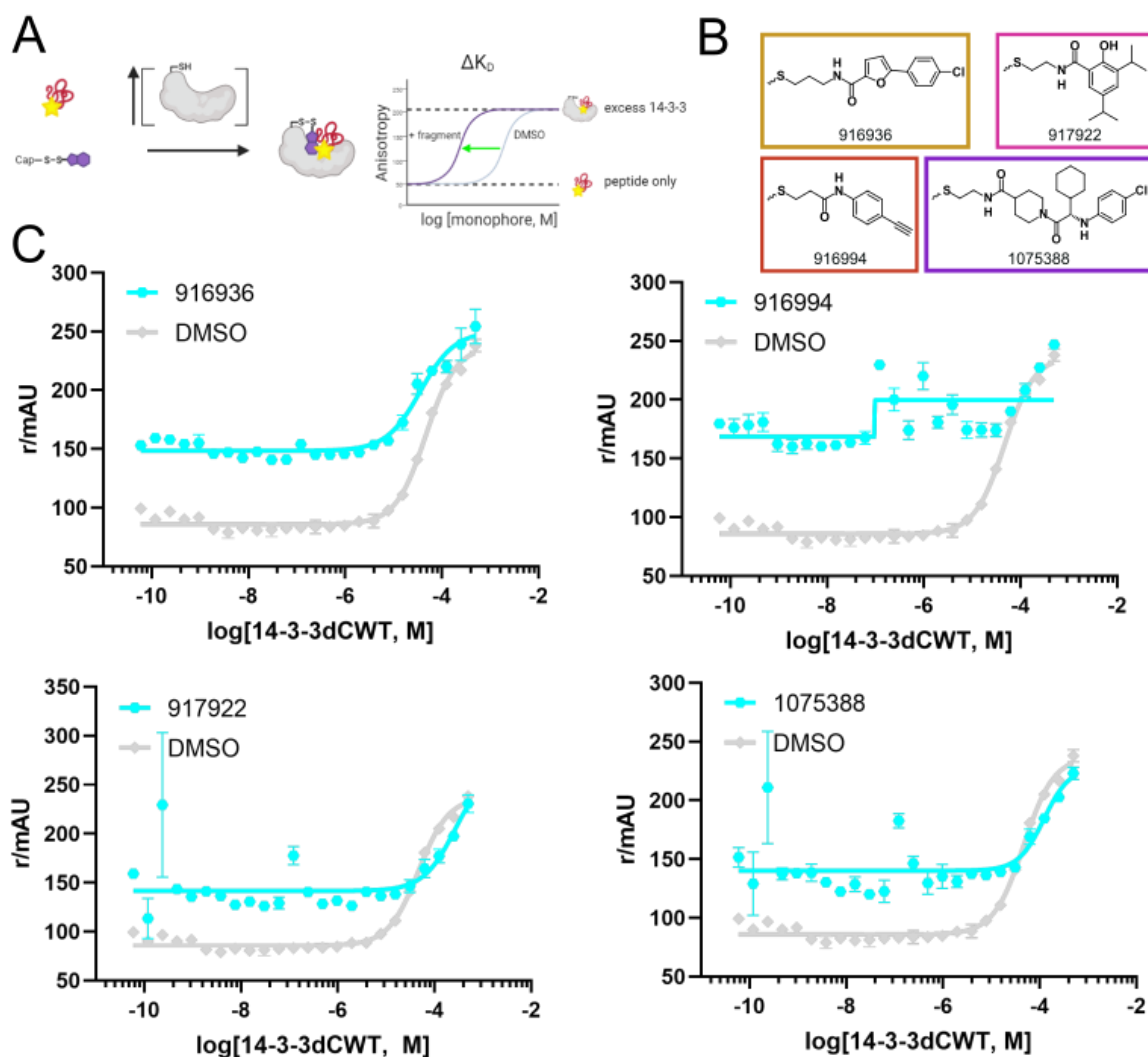
Figure 2.5. Overview of protein titration experiments. (A) Outline of protein titration process. 2 mM fragment is incubated with fluorescently labeled procaspase-2 phospho-peptide and 14-3-3σ is titrated from high concentration to low concentration. If the compound is a stabilizer, a shift in K_D to the left of the DMSO control indicates cooperativity between the fragment, protein, and phospho-peptide. (B) Chemical structures of the four highlighted compounds. (C) Protein titration curves of **916936** (top left), **916994** (top right), **917922** (bottom left), and **1075388** (bottom right). Cyan curves indicate incubation with 2 mM fragment. Grey curves are DMSO controls.

clash between a covalently labeled procaspase-2 peptide and the 14-3-3σ binding groove.

However, this may not be the only challenge as a monophosphorylated peptide of the

procaspase-2 S164 residue which did not contain the cysteine also showed no stabilization.

More likely, there is some characteristic of the 14-3-3σ/procaspase-2 phospho-peptide

composite interface which is not amenable to fragment engagement from the chemical moieties

present in the disulfide library. This phenomenon has been seen in other phospho-peptide

14-3-3 clients such as B-RAF and USP8 and SOS1, the latter two which are discussed in

Chapter 3.

Another approach to engaging the 14-3-3σ/procaspase-2 complex would be to optimize the

protein titration conditions for the four hit fragments which showed some activity in the FADR

studies. The EC_{50} values of the fragments were all well above the maximum dosage used in the

protein titrations (2 mM) and thus might still have some stabilizing effects at either a lower BME

concentration or a higher dosage of compound. Similar optimization efforts for the C-RAF, ERα,

USP8 non-selective hit fragment **917949** (denoted compound **1** in Chapter 3) showed an

increased stabilization profile in both the FADR and protein titration experiments. Once optimal

conditions have been determined, structural classification of important binding interactions

between the 14-3-3σ/procaspase-2/fragment complex could inspire novel lead compounds with

greater potency and efficacy. However, the lack of an antibody for the procaspase-2 zymogen

makes cell studies and immunoblotting difficult so further discussion of model systems beyond

in vitro hit validation would be necessary to determine the full extent of compound activity in

cells.

REFERENCES

(1)   Estes, C.; Razavi, H.; Loomba, R.; Younossi, Z.; Sanyal, A. J. Modeling the Epidemic of Nonalcoholic Fatty Liver Disease Demonstrates an Exponential Increase in Burden of Disease. *Hepatol. Baltim. Md* **2018**, *67* (1), 123–133. https://doi.org/10.1002/hep.29466.

(2)   Younossi, Z. M.; Golabi, P.; de Avila, L.; Paik, J. M.; Srishord, M.; Fukui, N.; Qiu, Y.; Burns, L.; Afendy, A.; Nader, F. The Global Epidemiology of NAFLD and NASH in Patients with Type 2 Diabetes: A Systematic Review and Meta-Analysis. *J. Hepatol.* **2019**, *71* (4), 793–801. https://doi.org/10.1016/j.jhep.2019.06.021.

(3)   Bjørndal, B.; Burri, L.; Staalesen, V.; Skorve, J.; Berge, R. K. Different Adipose Depots: Their Role in the Development of Metabolic Syndrome and Mitochondrial Response to Hypolipidemic Agents. *J. Obes.* **2011**, *2011*, 1–15. https://doi.org/10.1155/2011/490650.

(4)   Zhao, P.; Saltiel, A. R. From Overnutrition to Liver Injury: AMP-Activated Protein Kinase in Nonalcoholic Fatty Liver Diseases. *J. Biol. Chem.* **2020**, jbc.REV120.011356. https://doi.org/10.1074/jbc.REV120.011356.

(5)   Zhang, C.; Yang, M. Current Options and Future Directions for NAFLD and NASH Treatment. *Int. J. Mol. Sci.* **2021**, *22* (14), 7571. https://doi.org/10.3390/ijms22147571.

(6)   Raza, S.; Rajak, S.; Upadhyay, A.; Tewari, A.; Sinha, R. A. Current Treatment Paradigms and Emerging Therapies for NAFLD/NASH. *Front. Biosci. Landmark Ed.* **2021**, *26*, 206–237.

(7)   Fava, L. L.; Bock, F. J.; Geley, S.; Villunger, A. Caspase-2 at a Glance. *J. Cell Sci.* **2012**, *125* (24), 5911–5915. https://doi.org/10.1242/jcs.115105.

(8)   Logette, E.; Le Jossic-Corcos, C.; Masson, D.; Solier, S.; Sequeira-Legrand, A.; Dugail, I.; Lemaire-Ewing, S.; Desoche, L.; Solary, E.; Corcos, L. Caspase-2, a Novel Lipid Sensor

under the Control of Sterol Regulatory Element Binding Protein 2. *Mol. Cell. Biol.* **2005**, *25* (21), 9621–9631. https://doi.org/10.1128/MCB.25.21.9621-9631.2005.

(9)   Machado, M. V.; Michelotti, G. A.; Jewell, M. L.; Pereira, T. A.; Xie, G.; Premont, R. T.; Diehl, A. M. Caspase-2 Promotes Obesity, the Metabolic Syndrome and Nonalcoholic Fatty Liver Disease. *Cell Death Dis.* **2016**, *7* (2), e2096–e2096. https://doi.org/10.1038/cddis.2016.19.

(10)   Schweizer, A.; Briand, C.; Grütter, M. G. Crystal Structure of Caspase-2, Apical Initiator of the Intrinsic Apoptotic Pathway. *J. Biol. Chem.* **2003**, *278* (43), 42441–42447. https://doi.org/10.1074/jbc.M304895200.

(11)   Krumschnabel, G.; Sohm, B.; Bock, F.; Manzl, C.; Villunger, A. The Enigma of Caspase-2: The Laymen's View. *Cell Death Differ.* **2009**, *16* (2), 195–207. https://doi.org/10.1038/cdd.2008.170.

(12)   Bouchier-Hayes, L.; Oberst, A.; McStay, G. P.; Connell, S.; Tait, S. W. G.; Dillon, C. P.; Flanagan, J. M.; Beere, H. M.; Green, D. R. Characterization of Cytoplasmic Caspase-2 Activation by Induced Proximity. *Mol. Cell* **2009**, *35* (6), 830–840. https://doi.org/10.1016/j.molcel.2009.07.023.

(13)   Cheung, H. H.; Lynn Kelly, N.; Liston, P.; Korneluk, R. G. Involvement of Caspase-2 and Caspase-9 in Endoplasmic Reticulum Stress-Induced Apoptosis: A Role for the IAPs. *Exp. Cell Res.* **2006**, *312* (12), 2347–2357. https://doi.org/10.1016/j.yexcr.2006.03.027.

(14)   Colussi, P. A.; Harvey, N. L.; Kumar, S. Prodomain-Dependent Nuclear Localization of the Caspase-2 (Nedd2) Precursor A NOVEL FUNCTION FOR A CASPASE PRODOMAIN. *J. Biol. Chem.* **1998**, *273* (38), 24535–24542. https://doi.org/10.1074/jbc.273.38.24535.

(15)   Kim, J. Y.; Garcia-Carbonell, R.; Yamachika, S.; Zhao, P.; Dhar, D.; Loomba, R.; Kaufman, R. J.; Saltiel, A. R.; Karin, M. ER Stress Drives Lipogenesis and Steatohepatitis via

Caspase-2 Activation of S1P. *Cell* **2018**, *175* (1), 133-145.e15.

https://doi.org/10.1016/j.cell.2018.08.020.

(16)   Buchakjian, M. R. Metabolic Regulation of Caspase-2. **2011**.

(17)   Johnson, E. S.; Lindblom, K. R.; Robeson, A.; Stevens, R. D.; Ilkayeva, O. R.; Newgard,

C. B.; Kornbluth, S.; Andersen, J. L. Metabolomic Profiling Reveals a Role for Caspase-2 in

Lipoapoptosis. *J. Biol. Chem.* **2013**, *288* (20), 14463–14475.

https://doi.org/10.1074/jbc.M112.437210.

(18)   Wilson, C. H.; Nikolic, A.; Kentish, S. J.; Keller, M.; Hatzinikolas, G.; Dorstyn, L.; Page,

A. J.; Kumar, S. Caspase-2 Deficiency Enhances Whole-Body Carbohydrate Utilisation and

Prevents High-Fat Diet-Induced Obesity. *Cell Death Dis.* **2017**, *8* (10), e3136–e3136.

https://doi.org/10.1038/cddis.2017.518.

(19)   Pham, D. D.; Bruelle, C.; Thi Do, H.; Pajanoja, C.; Jin, C.; Srinivasan, V.; Olkkonen, V.

M.; Eriksson, O.; Jauhiainen, M.; Lalowski, M.; Lindholm, D. Caspase-2 and P75 Neurotrophin

Receptor (P75NTR) Are Involved in the Regulation of SREBP and Lipid Genes in Hepatocyte

Cells. *Cell Death Dis.* **2019**, *10* (7), 537. https://doi.org/10.1038/s41419-019-1758-z.

(20)   Reibe, S.; Febbraio, M. A. Relieving ER Stress to Target NASH-Driven Hepatocellular

Carcinoma. *Nat. Rev. Endocrinol.* **2019**, *15* (2), 73–74. https://doi.org/10.1038/s41574-018-

0145-7.

(21)   Horton, J. D.; Goldstein, J. L.; Brown, M. S. SREBPs: Activators of the Complete

Program of Cholesterol and Fatty Acid Synthesis in the Liver. *J. Clin. Invest.* **2002**, *109* (9),

1125–1131. https://doi.org/10.1172/JCI15593.

(22)   Sladky, V. C.; Villunger, A. Uncovering the PIDDosome and Caspase-2 as Regulators of Organogenesis and Cellular Differentiation. *Cell Death Differ.* **2020**, *27* (7), 2037–2047. https://doi.org/10.1038/s41418-020-0556-6.

(23)   Kim, J. Y.; Wang, L. Q.; Sladky, V. C.; Oh, T. G.; Liu, J.; Trinh, K.; Eichin, F.; Downes, M.; Hosseini, M.; Jacotot, E. D.; Evans, R. M.; Villunger, A.; Karin, M. PIDDosome-SCAP Crosstalk Controls High-Fructose-Diet-Dependent Transition from Simple Steatosis to Steatohepatitis. *Cell Metab.* **2022**, *34* (10), 1548-1560.e6. https://doi.org/10.1016/j.cmet.2022.08.005.

(24)   Kalabova, D.; Filandr, F.; Alblova, M.; Petrvalska, O.; Horvath, M.; Man, P.; Obsil, T.; Obsilova, V. 14-3-3 Protein Binding Blocks the Dimerization Interface of Caspase-2. *FEBS J. n/a* (n/a). https://doi.org/10.1111/febs.15215.

(25)   Smidova, A.; Alblova, M.; Kalabova, D.; Psenakova, K.; Rosulek, M.; Herman, P.; Obsil, T.; Obsilova, V. 14-3-3 Protein Masks the Nuclear Localization Sequence of Caspase-2. *FEBS J.* **2018**, *285* (22), 4196–4213. https://doi.org/10.1111/febs.14670.

(26)   Hallenbeck, K. K.; Davies, J. L.; Merron, C.; Ogden, P.; Sijbesma, E.; Ottmann, C.; Renslo, A. R.; Wilson, C.; Arkin, M. R. A Liquid Chromatography/Mass Spectrometry Method for Screening Disulfide Tethering Fragments. *SLAS Discov. Adv. Life Sci. R D* **2018**, *23* (2), 183–192. https://doi.org/10.1177/2472555217732072.

(27)   Kenanova, D. N.; Visser, E. J.; Virta, J. M.; Sijbesma, E.; Centorrino, F.; Vickery, H. R.; Zhong, M.; Neitz, R. J.; Brunsveld, L.; Ottmann, C.; Arkin, M. R. A Systematic Approach to the Discovery of Protein–Protein Interaction Stabilizers. *ACS Cent. Sci.* **2023**. https://doi.org/10.1021/acscentsci.2c01449.

(28)   Sijbesma, E.; Hallenbeck, K. K.; Leysen, S.; de Vink, P. J.; Skóra, L.; Jahnke, W.; Brunsveld, L.; Arkin, M. R.; Ottmann, C. Site-Directed Fragment-Based Screening for the

Discovery of Protein–Protein Interaction Stabilizers. *J. Am. Chem. Soc.* **2019**, *141* (8), 3524–3531. https://doi.org/10.1021/jacs.8b11658.

(29)   Sijbesma, E.; Hallenbeck, K. K.; Leysen, S.; de Vink, P. J.; Skóra, L.; Jahnke, W.; Brunsveld, L.; Arkin, M. R.; Ottmann, C. Site-Directed Fragment-Based Screening for the Discovery of Protein–Protein Interaction Stabilizers. *J. Am. Chem. Soc.* **2019**, *141* (8), 3524–3531. https://doi.org/10.1021/jacs.8b11658.

Chapter 3: A Systematic Approach to the Discovery of Protein-Protein Interaction Stabilizers
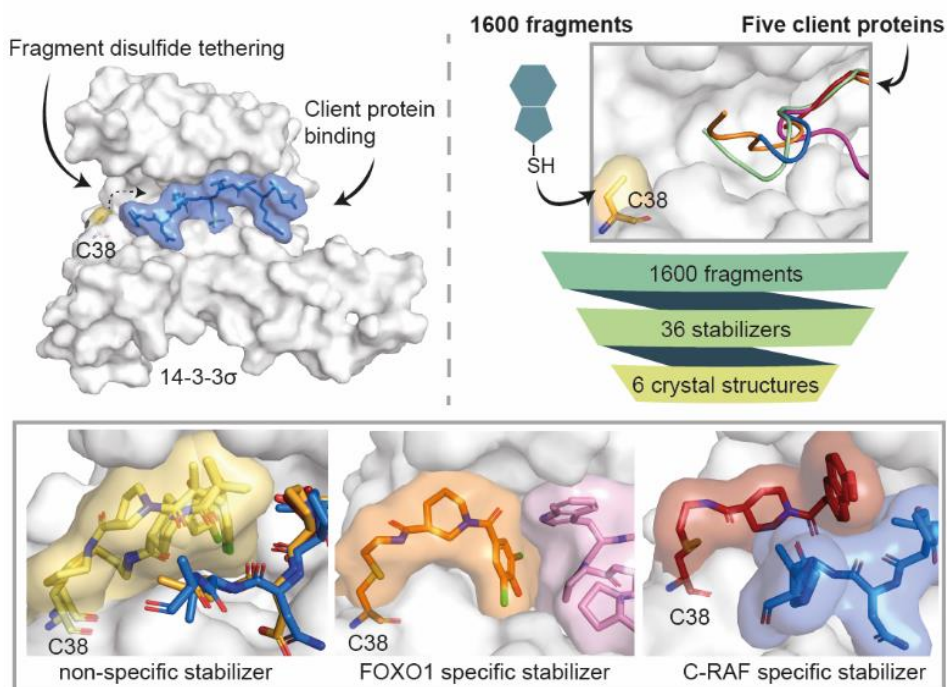
ABSTRACT: Protein-protein interactions (PPIs) are responsible for the proper function of biological processes and, when dysregulated, commonly lead to disease. PPI stabilization has only recently been systematically explored for drug discovery despite being a powerful approach to selectively target intrinsically disordered proteins and hub proteins, like 14-3-3, with multiple interaction partners. Disulfide tethering is a site-directed fragment-based drug discovery (FBDD) methodology for screening small molecules in a quantitative, high-throughput manner. We explore the scope of the disulfide tethering technology for the discovery of selective fragments as starting points for the development of potent small molecule PPI stabilizers and molecular glues using the hub protein 14-3-3σ. The complexes with 5 biologically and structurally diverse phospho-peptides, derived from the 14-3-3 client proteins ERα, FOXO1, C-RAF, USP8, and SOS1, were screened for hit identification. Stabilizing fragments could be found for 4/5 client complexes with a diversified hit-rate and stabilizing efficacy for the different 14-3-3/client phospho-peptides. Extensive structural elucidation revealed the ability and adaptivity of the peptide to make productive interactions with the tethered fragments as key criterion for cooperative complex formation. We validated eight fragment stabilizers, six of which showed selectivity for one phospho-peptide client, and structurally characterized two nonselective hits and four fragments that selectively stabilized C-RAF or FOXO1. The most efficacious of these fragments increased 14-3-3σ/C-RAF phospho-peptide affinity by 430-fold. Disulfide tethering to the wildtype C38 in 14-3-3σ provided diverse structures for future optimization of 14-3-3/client stabilizers and highlighted a systematic method to discover molecular glues.

INTRODUCTION

Protein-protein interactions (PPIs) are essential to biology and their dysregulation is central to many diseases including cancer and neurodegeneration.[1–4] Many of these important PPIs include "hub proteins" that interact with a large number of protein partners, ranging from a few dozen to a few thousand.[5] Small molecules that inhibit or stabilize individual PPIs within these networks would be powerful tools to understand the effect of a single PPI on cellular function. Although PPIs were historically considered "undruggable", there has been much progress in developing small molecule PPI inhibitors as biological probes and therapeutics.[6–10] By contrast, PPI stabilization has remained largely underexplored, despite its potential to be a selective method for the manipulation of a single interaction within a protein network.[11,12] Stabilization also has the potential to target unstructured, difficult to drug proteins via composite PPI binding pockets.[13,14] Molecular glue degraders and natural products have demonstrated the therapeutic value of stabilizing native or non-native (neomorphic) PPIs.[15–17] However, there are few robust, generalizable strategies to discover PPI stabilizers prospectively.[11,18] Here, we describe a robust and instructive approach, using site-directed fragment based drug discovery (FBDD) to systematically discover molecular glues.

FBDD is a well-established method for the discovery of small molecules towards challenging targets.[19,20] Fragments are simple chemical building blocks that – owing to their small number of atoms – sample chemical space efficiently. FBDD involves screening for weakly binding fragments that target subsites within a binding site, followed by fragment optimization via linking two fragments or elaborating a fragment-sized core. Disulfide tethering is a method of FBDD that capitalizes on a native or engineered cysteine residue proximal to an envisaged ligand binding site.[21–24] In the context of orthosteric PPI stabilization, this binding site is composed of both members of the protein complex (the composite PPI interface). Fragments that bind to this site with the correct positioning to form a protein-fragment disulfide bond are detected by intact

50
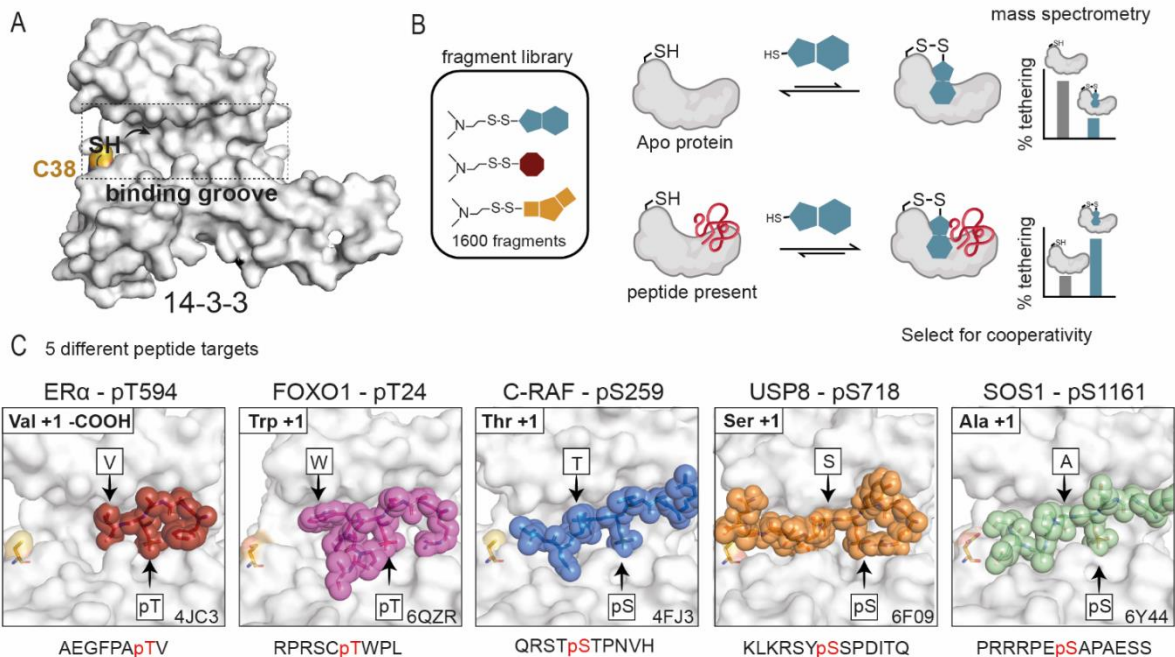
Figure 3.1 14-3-3/client stabilizer approach. (A) The client protein binding groove of a 14-3-3σ monomer (white surface) highlighting the native cysteine (C38; yellow surface) and target thiol. (B) General schematic of the primary disulfide tethering screen. Fragments were incubated with *apo* 14-3-3σ (white) without any phospho-peptide (top) and 14-3-3σ with the phospho-peptide client present (bottom). Fragments were assessed for their covalent engagement of C38 via mass spectrometry, termed "% tethering". Fragments that bind 14-3-3σ with a higher % tethering in the presence of phospho-peptide than in the *apo* screen are selected for further analysis of cooperativity. (C) Crystallographic structures of the 5 phospho-peptide clients bound in the 14-3-3σ (white surface) binding pocket showing proximity to C38 (yellow surface). ERα (red sticks) has a C-terminal motif with phospho-threonine (pT) in the penultimate position and C-terminal valine (V) in the +1 position. FOXO1 (pink sticks) has a curved motif with tryptophan (W) in +1 position. C-RAF (blue sticks), USP8 (orange sticks), and SOS1 (green sticks) extend to various degrees into the 14-3-3 binding groove, with threonine (T), serine (S), and alanine (A) residues in the +1 position, respectively. PDB left to right: 4JC3, 6QZR, 4FJ3, 6F09, 6Y44.

protein mass spectrometry (MS) in a high-throughput screen.[25] We utilize a library of approximately 1600 disulfide molecules with diverse fragments and linkers between the fragment and the disulfide.[26] To test the efficacy of this technology to discover PPI stabilizers, we have selected the hub protein 14-3-3 and a set of its diverse partner proteins.

14-3-3 is ubiquitously expressed in mammals and plays multiple roles within the cell, including phosphorylation protection, conformational changes, subcellular trafficking, and in-duction or disruption of other PPIs.[13,27–29] 14-3-3 typically binds to a phosphorylated serine/threonine of intrinsically disordered regions of its clients.[30] With several hundred known interacting partners,

the 14-3-3-binding proteome pro-vides diverse PPI interfaces with which to test the scope and limitations of our screening technology. Furthermore, 14-3-3/client stabilization could lead to therapeutics in a variety of disease fields including oncology, neurodegeneration, inflammation, and metabolic disease.[29,31] Previous studies using natural products such as Fusicoccin (FC-A) and Cotylenin-A (CN-A) have shown that stabilizing 14-3-3/client interactions regulates the activity of important cell signaling pathways including estrogen receptor α (ERα) and C-RAF, respectively.[14,32]

We recently demonstrated the utility of disulfide tethering to identify molecular glues of the 14-3-3/ERα PPI. We dis-covered a series of disulfide fragments that stabilized the complex when bound to an engineered cysteine residue in the binding groove of 14-3-3, enhancing binding of the ERα C-terminal phosphopeptide up to 40-fold.[25] We now focus on targeting the native cysteine found in the 14-3-3 sigma isoform (14-3-3σ), which offers greater translatability for covalent molecules. Of the 7 isoforms found in mammalian cells, 14-3-3σ is the only one that harbors a cysteine residue proximal to the client binding groove, providing an additional degree of isoform specificity (**Figure 3.1A**).[30] The Protein Data Bank contains dozens of crystallographic structures of 14-3-3 with bound phospho-peptides derived from many of its binding partners, as well as a few examples of CryoEM structures of full length proteins.[13,33–35] This wealth of structural information allows for direct visualization of the various 14-3-3/client binding interfaces which could be capitalized on for the discovery of selective fragment stabilizers and the development of potent lead compounds through structure-guided chemical optimization. For our screens, we utilized the phospho-peptide mimetics of 14-3-3 PPI partners which bind 14-3-3 in a similar fashion to the unstructured regions of the full-length proteins but offer greater synthetic flexibility and simplified crystallography.[13,34]
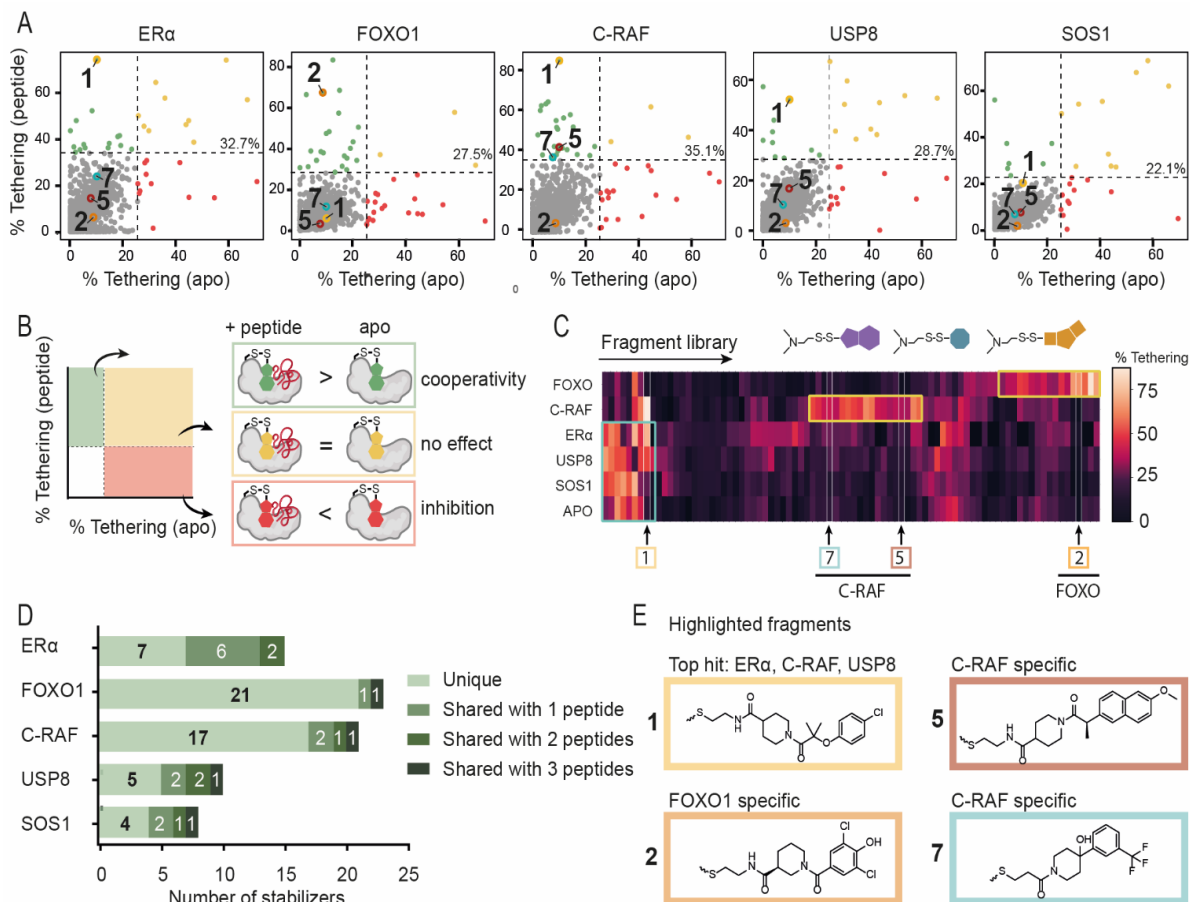
Figure 3.2 Primary tethering screen results. (A) Scatterplot data illustrating the correlation of % tethering of fragments to 14-3-3σ in the presence of the phospho-peptide (y-axis) as compared to *apo* 14-3-3σ (x-axis). Hit selection threshold (mean + 3*SD) in each screen is indicated by a black dashed line. Compounds **1**, **2**, **5** and **7** are indicated as yellow, orange, red and cyan circles, respectively. (B) Schematic of compound scatterplots. Quadrants are outlined by dotted lines signifying 3*SD above average % tethering for compounds in the presence of phospho-peptide (horizontal line) and *apo* 14-3-3σ (vertical line). Compounds in green quadrant showed increased binding to 14-3-3σ in the presence of phospho-peptide, yellow quadrant showed neutral binding to 14-3-3σ, and red quadrant showed a reduced binding in presence of phospho-peptide. (C) Heat map of hit fragments across all 5 phospho-peptide screens and *apo* 14-3-3σ screen. Compounds clustered based on % tethering in each screen. Compounds **1**, **2**, **5** and **7** were of primary interest as non-selective and selective stabilizers. (D) Number of stabilizers of each peptide that were: unique, shared with one other peptide, shared with two other peptides, or shared with three other peptides (green bars with the darker color shared with more peptides). (E) Chemical structures of highlighted fragment hits **1**, **2**, **5**, and **7**.

Here, we used the disulfide tethering technology to systematically achieve selective PPI

stabilization of 14-3-3 client phospho-peptides with diverse sequences and structures. The

selected clients are also modulated by 14-3-3 in a way that could be therapeutically useful in

cancer, metabolic disease, and/or rare disease.[14,36–39] For four of the five targets, effective PPI

stabilizers were identified. Crystallographic and functional data highlight the molecular recognition of fragments for the distinctive composite PPI interfaces formed by 14-3-3 bound to client phospho-peptides. In particular, the C-RAF- and FOXO1-based peptide-protein interactions with 14-3-3 yielded fragments with high selectivity and/or stabilization factors. The diversity of sequences and conformations found in 14 3 3/client complexes make the 14-3-3 interactome particularly promising for small-molecule PPI stabilization; furthermore, the disulfide tethering approach is remarkably effective at selecting chemical starting points for further design of potent and selective PPI stabilizers.

RESULTS AND DISCUSSION

Primary Screen for 14-3-3/Client Stabilizers. The disulfide tethering screen targeted C38, a native cysteine on 14-3-3σ located proximal to the natural product binding pocket within the phospho-peptide recognition groove (**Figure 3.1A, Figure S3.1**). The cysteine forms a reversible covalent bond with the fragment thiol through disulfide exchange; the amount of bound fragment is measured by MS. A fragment stabilizer is expected to show a higher "% tethering" in the presence of the 14-3-3σ/client phospho-peptide complex than 14-3-3σ alone due to cooperativity between the fragment and the peptide (**Figure 3.1B**). The screening was performed on five different peptide targets displaying three conceptually distinct 14-3-3 interaction motifs (**Figure 3.1C**): truncated (ERα),[14,40] turned (FOXO1),[37] and linear (C-RAF, USP8, SOS1).[32,35,38,41]

14-3-3σ (100 nM) was screened in complex with the 5 client phospho-peptides at a concentration twice their respective K_D values (**Figure S3.2**). This condition provided a consistent presence of the 14-3-3σ/phospho-peptide composite interface that the fragments would engage. The 14-3-3σ/phospho-peptide complex was incubated with a single concentration of fragment (200 μM) under reducing conditions (250 μM β-mercaptoethanol) for 3 hours before samples were measured by intact-protein LC/MS. The % tethering threshold for
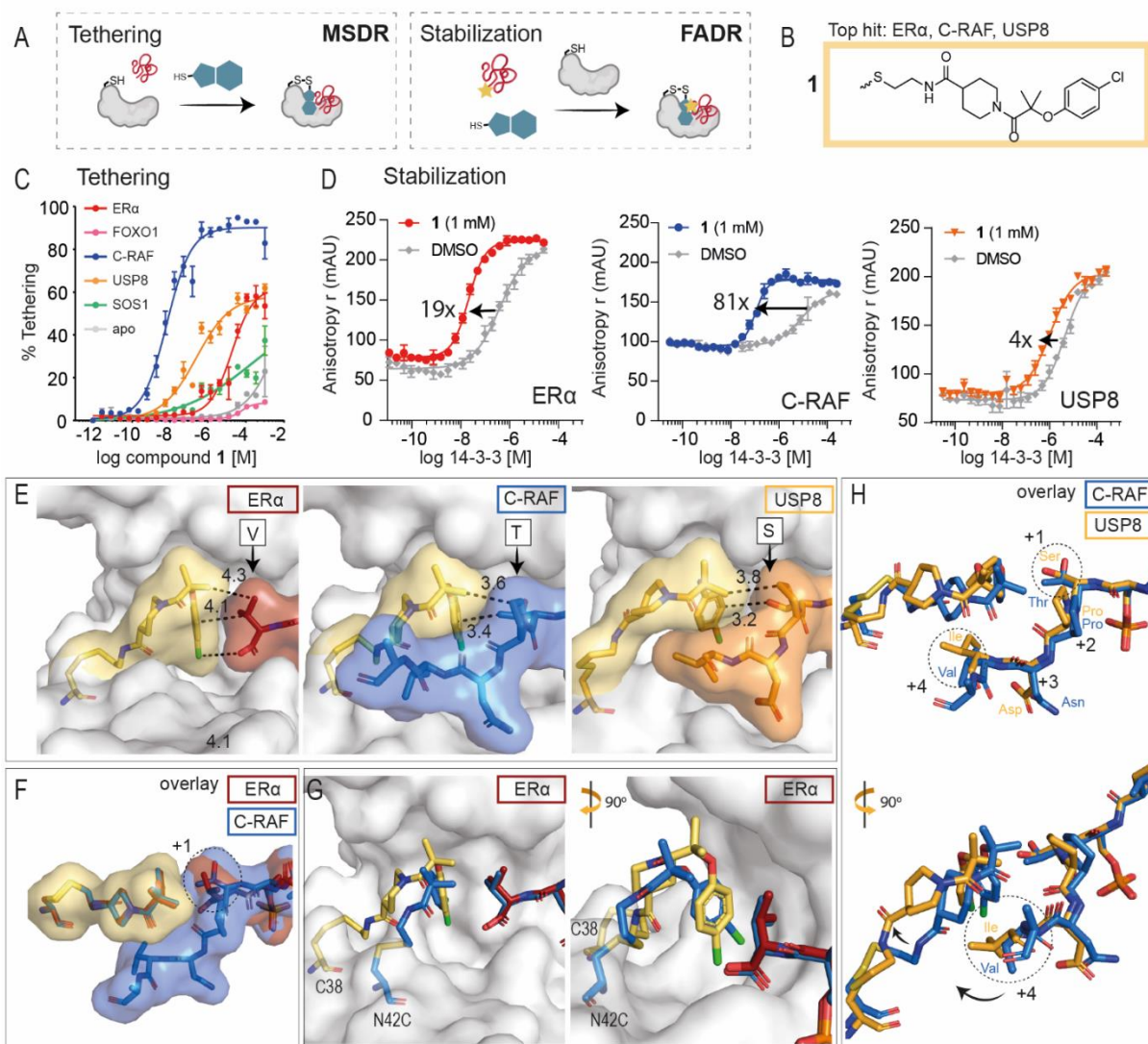
Figure 3.3 Overview of biochemical and structural properties of non-selective stabilizer **1**. (A) In mass spec dose response (MSDR), the focus was on compound binding to 14-3-3σ, measured by % tethering; fluorescence anisotropy dose response (FADR) experiments determined degree of stabilization, measured by phospho-peptide binding to 14-3-3σ in presence of compound. (B) Chemical structure of stabilizer **1**. (C) MSDR curves for **1** showing percentage of fragment/protein conjugate formation with 14-3-3σ *apo*, or in the presence of ERα, FOXO1, C-RAF, USP8 or SOS1 peptide. (D) 14-3-3σ titrations to fluorescein-labeled ERα, C-RAF or USP8 in the presence of DMSO or **1** (1 mM), reporting a 19-, 81-, and 4-fold increase of the 14-3-3σ/peptide binding interface, respectively. (E) Crystal structure of **1** bound to 14-3-3σ C38 in complex with (from left to right) ERα peptide, C-RAF peptide, and USP8 peptide. Distances are indicated (Å, black dashes). (F) Overlay of **1's** conformations when interacting with ERα and C-RAF. (G) Overlay of **1** (yellow) bound to 14-3-3σ C38 and previously reported stabilizer (blue) bound to 14-3-3σ mutant N42C (PDB ID: 6HMT) interacting with ERα phospho-peptides. (H) Overlay of **1** bound to 14-3-3σ C38 interacting with C-RAF and USP8.

hit selection was three standard deviations (3*SD) above the average % tethering for that

condition (**Figure 3.2A**). In the quadrant of highest interest, potential stabilizing fragments

showed % tethering above the tethering threshold in the peptide screen and % tethering below the tethering threshold in the *apo* screen (**Figure 3.2B**, green quadrant). Neutral compounds showed significant % tethering for both 14-3-3σ/phospho-peptide and *apo* (**Figure 3.2B**, yellow quadrant). Potential inhibitory fragments showed significant % tethering above the tethering threshold in the *apo* screen but not in the presence of peptide (**Figure 3.2B**, red quadrant). Compounds were clustered in a heat map based on % tethering in each of the five peptide screens and *apo* 14-3-3 screen (**Figure 3.2C**). An overlapping fragment hit cluster was identified for ERα, USP8, and SOS1 (**Figure 3.2C**, green box), whereas a cluster of unique hit fragments was identified for both C-RAF and FOXO1 (**Figure 3.2C**, yellow boxes), indicating a difference in the abundance of selective stabilizers from the primary screens.

Each 14-3-3σ/phospho-peptide screen yielded potential stabilizing fragments, but the number and binding efficiency varied (**Figure 3.2A**, **3.2C**, **3.2D**, and **Tables S3.1-S3.5**). The initial screen for ERα yielded 15 hit fragments including 7 unique stabilizers and a 33% tethering threshold. The FOXO1 screen yielded 23 hit fragments including 21 unique stabilizers and a 28% tethering threshold. The C-RAF screen yielded 21 fragments including 16 unique stabilizers and a 35% tethering threshold. The USP8 screen yielded 10 hit fragments including 5 unique stabilizers and a 29% tethering threshold. The SOS1 screen yielded 8 hit fragments including 4 unique stabilizers and a 22% tethering threshold (**Figures 3.2A** and **3.2D**). Figure 2E depicts representative chemical structures for each target.

Non-Selective Stabilizing Compound 1. In the initial screen, compound **1** was identified as top hit for ERα, C-RAF and USP8 (**Figure 3.2**). **1** was further characterized by three dose-response experiments. Mass spectrometry (MSDR, analyzing fragment binding to protein, quantified by DR_{50} values) and fluorescent anisotropy (FADR, analyzing peptide binding to protein in the presence of compound, quantified by EC_{50} values) defined the binding affinity for the fragment and its effective concentration, respectively (**Figure 3.3B**). The compound's effect

Table 3.1. Tethering and stabilization of 14-3-3σ/clients by compound 1

Peptide	MSDR (250 µM BME) DR_{50} (μM)	FADR (50 µM BME) EC_{50} (μM)	Protein Titrations (50 µM BME) K_{D_app}	K_{D_DMSO}	Fold Stab.
CRAF	0.007	0.922	106 nM	8.5 µM	81
ERα	18.1	1.31	21 nM	360 nM	19
USP8	0.024	3.38	1.1 µM	4.5 µM	4
SOS1	>2 mM	>2 mM	N/A	N/A	N/A
FOXO1	>2 mM	>2 mM	N/A	N/A	N/A
apo	>2 mM	>2 mM	N/A	N/A	N/A

on the 14-3-3/client PPI was then determined by titrating 14-3-3 in a fluorescence anisotropy assay at constant peptide and compound concentrations (quantified by K_{D_app}). In all three validation assays, **1** displayed a strong preference for C-RAF, followed by ERα and USP8, and had no activity with FOXO1 or SOS1. Compound **1** showed DR_{50} values of 7 nM for C-RAF, 18.1 µM for ERα, and 24 nM for USP8 (**Figure 3.3C**) as well as EC_{50} values of 922 nM for C-RAF, 1.31 µM for ERα, and 3.38µM for USP8 (**Figure S3.3**). In the protein titrations, **1** increased peptide affinity for 14-3-3σ by 81-fold in the C-RAF complex, 19-fold for 14-3-3σ/ERα, and 4-fold for 14-3-3σ/USP8 (**Figure 3.3D** and **Table 3.1**).

Crystal structures for compound **1** were obtained by co-crystallizing with ERα, C-RAF, or USP8 bound to 14-3-3σ (**Figure 3.3E**), with clear density for both **1** and the peptides (**Figure S3.4**). Comparing the three co-crystal structures, the strongest electron density and ligand occupancy for **1** was observed in the co-crystal structure with ERα. For ERα, the phenyl ring of **1** stacked against the +1 Val with a distance of ~4 Å (**Figure 3.3E**). Compound **1** showed an identical binding mode in the presence of C-RAF (**Figure 3.3F**), for which the +1 Thr was 3.5 Å from the phenyl ring, while the remainder of the C-RAF peptide wrapped around the fragment. These additional hydrophobic interactions could explain the higher fold stabilization with the C-RAF peptide compared to ERα (**Figure 3.3D**, **3.3F**). Interestingly, **1** shared the binding moiety with N42C-tethered stabilizers that were discovered previously for ERα (**Figure 3.3G**).25 Whereas compound **1**'s chloro-group was not positioned identically, the longer linker of **1** bridged the larger distance from C38 compared to N42C. In the presence of the USP8 peptide, the phenyl ring of **1** was turned, thereby shifting the fragment up and back into the 14-3-3σ pocket (**Figure**

Figure 3.4 Overview of selective stabilizers for FOXO1. (A) Chemical structures of highlighted FOXO1 selective stabilizers **2-4**. (B) MSDR curves for **2** showing percentage of fragment/protein conjugate formation with 14-3-3σ *apo*, or in the presence of ERα, FOXO1, C-RAF, USP8 or SOS1 peptide. (C) 14-3-3σ titrations to fluorescein-labeled FOXO1 in the presence of DMSO or **2** (1 mM), reporting a 5-fold increase in 14-3-3σ/FOXO1 binding. (D) Crystal structure of **2** (orange) bound to 14-3-3σ (white) C38 in complex with FOXO1 phospho-peptide (pink). (E) Overlay of FOXO1 peptide in the apo-structure (white) with the FOXO peptide (pink) in presence of **2** (orange).

3.3E). This conformational change seemed necessary because the USP8 peptide allowed for less space (**Figure 3.3H**). While the +1 Ser of UPS8 did not show any specific interaction with **1**, its +4 Ile pushed the fragment towards 14-3-3σ, which was not an ideal position for this fragment as was reflected by the weak electron density and the minimal stabilization for USP8. By contrast, the +4 Val of C-RAF allowed for more space, thereby positioning **1** in a preferred conformation. It is noteworthy that **1** did not stabilize FOXO1 or SOS1 to 14-3-3σ. A crystallographic overlay of **1** with the FOXO1 peptide showed a steric clash with the +1 Trp of FOXO1, explaining its lack of stabilization (**Figure S3.5A**). In contrast, the +1 Ala residue of SOS1 would not contact the phenyl ring of **1**, perhaps explaining why no stabilization was observed (**Figure S3.5B**).

FOXO1 Selective Stabilizers. The FOXO1 peptide showed the highest number of stabilizing hits in our initial screen. For FOXO1, of the 23 initial stabilizers, 21 showed selectivity for the 14-3-3σ/FOXO1 phospho-peptide complex over *apo* 14-3-3σ and the other phospho-peptide

clients in the initial screen (**Figure 3.2D**). Interestingly, the unique 21 FOXO-stabilizers had a highly conserved scaffold, with the phenyl ring engaging FOXO1 often decorated with halogens or a triazole moiety (**Figure S3.6**). Eight of these compounds were validated in the MSDR (**Figure S3.7**). Of the eight compounds, five compounds had enough material to retest and were active in the FADR assays (**Figure 3.4A**, **Figure S3.8**, and **Table S3.2**). The binding affinity of compound **2** to 14-3-3σ was >10,000-fold better in the presence of the FOXO1 phospho-peptide than *apo* 14-3-3σ and all other phospho-peptide clients (DR_{50} = 360 nM vs. >2 mM; **Figure 3.4B** and **Table 3.2**). Compounds **3** and **4** had DR_{50} values >450-fold and >2,000-fold better, respectively (**Table 3.2** and **Figure S3.7**). Compounds **2**, **3**, and **4** showed the greatest fold-stabilization in the protein titrations decreasing 14-3-3σ/FOXO1 K_D values 5-fold, 4-fold, and 12-fold (**Figure 3.4C**, **Table 3.2**, and **Figure S3.9**). It should be noted that while a high % tethering was observed for the FOXO1 stabilizers, the protein titrations only showed a modest shift in stabilization. This is likely due to the tight binding of the FOXO1 phospho-peptide, with a K_D value of 50 nM, already close to the limit of detection of this assay. A co-crystal structure for FOXO1/**2**/14-3-3σ was obtained, with clear density for both **2** and the FOXO1 peptide (**Figure S3.10A**). The phenyl ring of **2** stacked against the front of the FOXO1 peptide consisting of the +1 Trp and the +2 Pro residues (**Figure 3.4D**). Strikingly, in the presence of **2**, the Trp of FOXO1 underwent a conformational change to form a hydrogen bond with its NH and the amide carbonyl of **2** (**Figure 3.4E**). Moreover, the hydroxyl on the phenyl ring of **2** made a hydrogen bond with the S45 of 14-3-3σ, explaining the benefit of a hydrogen donor or, potentially, acceptor at that position. Compound **3** was also co-crystallized with FOXO1 (**Figure S3.10B**), showing a highly similar binding mode, but a lack of the hydrogen bonding with S45 of

Table 3.2 Properties of selective FOXO1 stabilizers

Cmpnd	MSDR (250 μM BME) DR_{50} (μM)	FADR (50 μM BME) EC_{50} (μM)	Protein Titrations (50 μM BME) K_{D_app}	K_{D_DMSO}[*]	Fold Stab.
2	0.36	5.10	7.7 nM	39 nM	5
3	2.2	N/A	10.6 nM	42 nM	4
4	143	N/A	9.7 nM	111 nM	12

[*]K_D for peptide is accurate within 3-fold range. These values are shown on the same plate as protein titrations with compound.
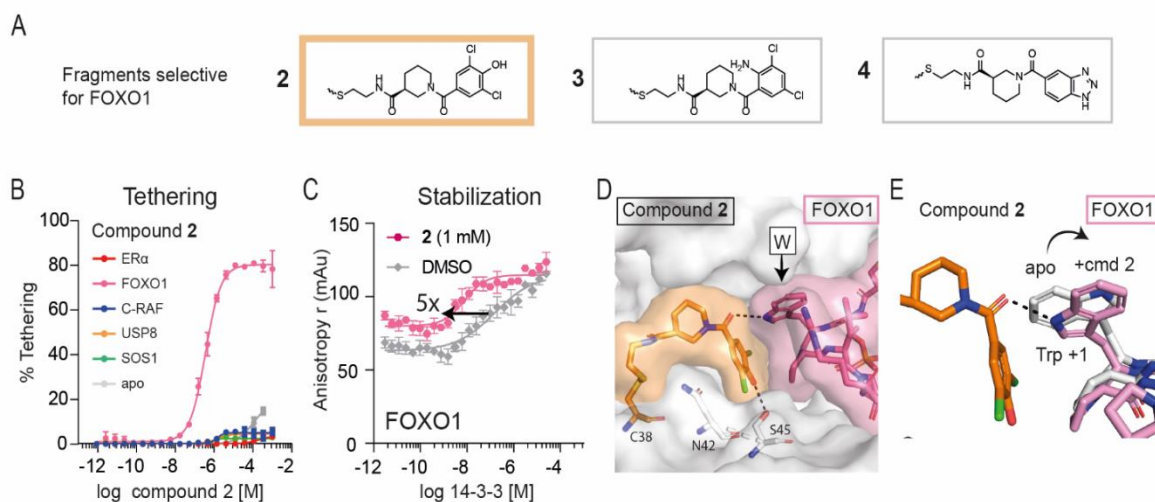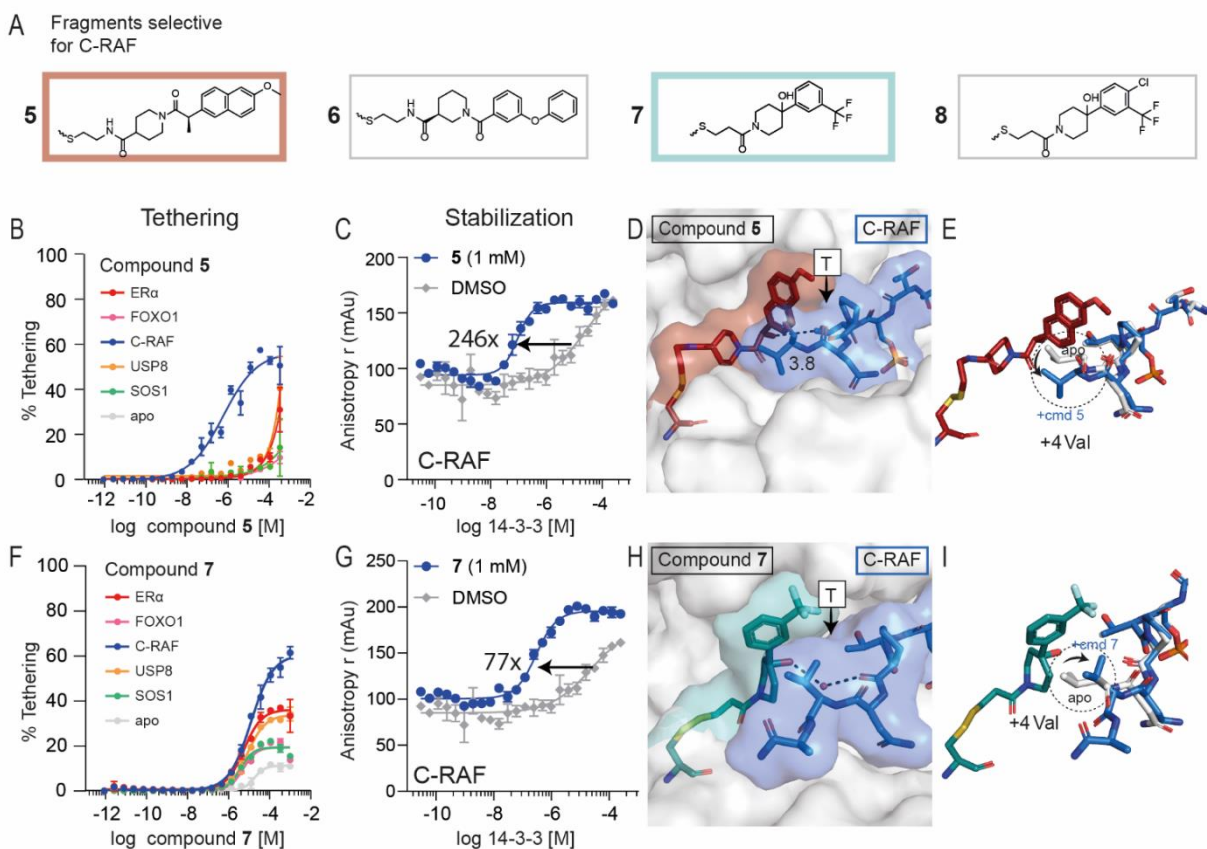
Figure 3.5 Overview of selective stabilizers for C-RAF. (A) Chemical structures of highlighted C-RAF selective stabilizers **5-8.** (B) MSDR curves for **5** showing percentage of fragment/protein conjugate formation with 14-3-3σ *apo*, or in the presence of ERα, FOXO1, C-RAF, USP8 or SOS1 peptide. (C) 14-3-3σ titration to fluorescein-labeled C-RAF in the presence of DMSO or **5** (1 mM), reporting a 246-fold increase of 14-3-3σ/C-RAF binding. (D) Crystal structure of **5** (red) bound to 14-3-3σ (white) in complex with C-RAF phospho-peptide (blue). (E) Overlay of C-RAF peptide in the apo-structure (white) with the C-RAF peptide (blue) in presence of **5** (red). (F) MSDR curves for **7** showing percentage of fragment/protein conjugate formation with 14-3-3σ *apo*, or in the presence of ERα, FOXO1, C-RAF, USP8 or SOS1 peptide. (G) 14-3-3σ titration to fluorescein-labeled C-RAF in the presence of DMSO or **7** (1 mM), reporting a 77-fold increase of 14-3-3σ/C-RAF binding (H) Crystal structure of **7** (teal) bound to 14-3-3σ (white) in complex with C-RAF phospho-peptide (blue). (I) Overlay of C-RAF peptide in the apo-structure (white) with the C-RAF peptide (blue) in presence of **7** (teal).

14-3-3σ (**Figure S3.10C**). An overlay of **2** with the other peptides revealed that **2** could not

reach the smaller +1 residues in the other client peptides or that the peptides sterically clashed

(**Figure S3.11**), potentially explaining its selectivity for FOXO1 over the other peptides. Previous

work discovered imine-based stabilizers for the 14-3-3/Pin-1 complex which, similar to FOXO1,

has a +1 Trp.[42] In that work, the Trp engaged in π-π stacking interactions with an aromatic ring

of the stabilizers. By contrast, the +2 Pro of FOXO1 locked the conformation of the +1 Trp and

thereby prevented such a π-π stacking interaction with **2**, while the +2 Arg of Pin-1 allowed π-π

stacking to take place. Thus, while the compound **2/3** scaffold emphasized the chemical moieties necessary for stabilizing FOXO1, crystal structures also expose a lack of flexibility of the FOXO1 peptide.

C-RAF Selective Stabilizers. Following FOXO1, C-RAF had the highest number of stabilizers. Of the 21 initial C-RAF stabilizers, 16 compounds showed selectivity for the 14 3 3σ/C-RAF phospho-peptide complex over *apo* 14-3-3σ and the other phospho-peptide clients in the primary screen (**Figure 3.2D**). Eleven compounds showed a similar scaffold which was remarkably analogous to the conserved scaffold for the FOXO1 stabilizers (**Figure S3.12**). However, the linker element of these compounds was often longer in the case for C-RAF, and the phenyl ring was decorated with large cyclic groups while for FOXO1 only smaller halogen groups were tolerated. This is likely due to the smaller +1 residue of C-RAF (Thr for C-RAF, Trp for FOXO1), thereby leaving more space for the compound. Furthermore, two C-RAF stabilizers were shared with ERα, both of which have a similar size in +1 residue (Val for ERα, Thr for C-RAF). Nine of the 16 selective compounds were validated for potency and selectivity in the MSDR (**Figure S3.13**). Four of the nine compounds (compounds **5-8**; **Figure 3.5A**) showed activity in FADR (Figure S14 and Table S3) and stabilization in the protein titrations (**Table 3.3** and **Figure S3.15**).

Compounds **5** and **6** were the most effective stabilizers. Compound **5** had a DR_{50} value >3,000-fold lower in the presence of the C-RAF peptide compared to 14-3-3σ alone (**Figure 3.5B**) and showed a 246-fold stabilization of the 14-3-3σ/C-RAF phospho-peptide complex (K_D = 23 μm to 92 nM; **Figure 3.5C**). Compound **6** had a DR_{50} value 230-fold lower in the presence of C-RAF

Table 3.3 Properties of selective C-RAF stabilizers

Cmpnd	MSDR (250 μM BME) DR_{50} (μM)	FADR (50 μM BME) EC_{50} (μM)	Protein Titrations (50 μM BME) K_{D_app}	Protein Titrations (50 μM BME) K_{D_DMSO}*	Fold Stab.
5	0.58	0.22	92 nM	23 μM	246
6	8.78	1.33	100 nM	42 μM	426
7	12.2	3.18	294 nM	23 μM	77
8	3.71	13.5	207 nM	23 μM	110

*K_D for peptide is accurate within 3-fold range. These values are shown on the same plate as protein titrations with compound.

compared to *apo* 14-3-3σ and a 426-fold stabilization of the 14-3-3σ/C-RAF complex (**Table 3.3**, **Figure S3.13** and **S3.15**).

The crystal structure of **5** with C-RAF and 14-3-3σ revealed a contact between the naphthalene ring of **5** and the +1 Thr residue of C-RAF. The methyl group of **5** also seems important for hydrophic interactions with the +1 Thr residue of C-RAF, at a distance of 3.8 Å (**Figure 3.5D**, **Figure S3.16A**). An overlay of the C-RAF peptide in the presence of **5** with the *apo* C-RAF peptide showed no change in conformation of the +1 Thr residue. In contrast, the +4 Val residue of the C-RAF peptide changed conformation to make space for **5** (**Figure 3.5E**).

We also crystallized compound **7** as a representative of the other structural class of the selective C-RAF stabilizers (**Figure S3.16B**). Compound **7** had a DR_{50} value >228-fold lower in the presence of the C-RAF peptide than *apo* 14-3-3σ (**Figure 3.5F**) and was less selective for C-RAF compared to **5** in the MSDR (**Figure S3.13**). However, compound **7** showed no stabilization of any of the peptides other than C-RAF in the FADR (**Figure S3.14C**), reflecting the selectivity shown in the primary screen. The weaker 14-3-3σ binding of **7** (12.2 µM DR_{50}) was reflected in a somewhat lower stabilization of the 14-3-3σ/C-RAF complex compared to the other chemotype of **5** and **6** (77-fold vs 246- and 426-fold, respectively; **Figure 3.5G**, **Figure S3.15**). Co-crystallization of **7** with C-RAF and 14-3-3σ revealed a novel orientation of its phenyl ring towards the roof of 14-3-3σ, positioning its trifluoromethyl group above the C-RAF peptide (**Figure 3.5H**). While the conformations of **5** and **7** were quite different, an overlay of the two structures shows that the trifluoromethyl group of **7** occupied the same cavity as the naphthalene ring of **5** (**Figure S3.16C**). Furthermore, an overlay of the C-RAF peptide in the presence of **7** with the *apo* C-RAF peptide revealed a conformational change of the +4 Val of C-RAF, which stacked against the compound, pushing it towards 14-3-3σ. Additionally, a water-mediated hydrogen bond was formed between **7** and the backbone of C-RAF peptide (**Figure 3.5I**). The lower specificity for C-RAF of **7** in the MSDR could be due to its small size, leaving

room for alternative +1 residues to have a cooperative effect on 14-3-3σ engagement. Stabilizer 8 had an almost identical structure to **7**, differing only in a chloro-group in the para-position of the phenyl ring, and showed similar binding modes to **7** in its structure with C-RAF (**Figure S3.16D** and **E**).

Next to these C-RAF selective stabilizers, the non-selective stabilizer compound **1** also showed a large fold-stabilization towards the C-RAF peptide (**Figure 3.3**). A crystallographic overlay of these three scaffolds revealed remarkable differences in conformation of the C-RAF/compound interactions (**Figure S3.16F**). These changes highlight the flexibility of the C-RAF peptide, perhaps leading to its facility for stabilization, especially in the case of the stabilizers' phenyl ring, which can occupy a wide range of positions and conformations in combination with the C-RAF client phospho-peptide.

CONCLUSIONS

Systematic methods to discover small-molecule stabilizers of PPI would enable chemical biologists to probe challenging biological systems with potency and precision. By trapping proteins in complexes, stabilization can target proteins with intrinsically disordered regions and allow manipulation of a specific PPI from among related hub protein complexes within a network. Disulfide tethering, a powerful FBDD technique, is readily tunable to a specific site on a protein of interest, amenable to HTS, and provides a direct quantitative measurement of fragment binding.

Here, we explored the scope of the disulfide tethering technology using the hub protein 14-3-3σ and 5 biologically and structurally diverse phospho-peptides derived from the 14-3-3 client proteins ERα, FOXO1, C-RAF, USP8, and SOS1. Of the 1600 fragments in the disulfide library, 62 showed activity as stabilizers for one or more phospho-peptides and were assessed by MSDR. 36 of the 62 compounds were taken forward into the FADR assays to determine

stabilization of a 14-3-3 client phospho-peptide. Finally, eight compounds showed cooperativity with the 14-3-3σ/phospho-peptide complex via 14-3-3σ protein titrations, and six were structurally characterized for their contacts with 14-3-3σ and the client phospho-peptide via x-ray crystallography (**Figure S3.17A**). Thus, the disulfide tethering strategy systematically discovered stabilizers for a range of peptide sequences, conformations, and affinities.

Of the 5 peptide targets selected, we discovered stabilizers for four clients, two of which also had selective stabilizers. Fragments increased binding affinity of the 14-3-3σ/phospho-peptide complex as much as 430-fold in the case of **6** and 250-fold for our best structurally characterized hit, **5**. Selective stabilizers distinguished between phospho-peptide clients due to the unique composite binding surface created by the phospho-peptide/14-3-3σ interface (**Figures 3.4** and **3.5**). The non-selective stabilizers also showed varying degrees of efficacy in stabilizing different clients. Compound **1** facilitated a greater than 80-fold shift in affinity for C-RAF, a 19-fold shift for ERα, a more modest 4-fold shift for USP8, but had no effect on SOS1 and FOXO1 (**Figure 3.3**).

The individual phospho-peptide binding motifs and C-terminal residues following the phosphorylation site create a distinct environment around the 14-3-3σ C38 fragment binding pocket, dictating what chemical moieties effectively facilitated cooperativity between 14-3-3σ, the phospho-peptide client, and the fragments. The stabilizers for FOXO1 had a highly conserved scaffold, consistent with the rigidity of this peptide (**Figure S3.17B**). In contrast, the stabilizers of C-RAF were larger and showed more chemical diversity in their scaffold, emphasizing the flexibility of the C-RAF peptide. The short ERα peptide resulted in limited selectivity, sharing many stabilizers with C-RAF. Lastly, USP8 and SOS1 were the hardest to target, likely due to the proximity of the peptide C-terminus to C38 of 14-3-3σ, which was also reflected in the small scaffold of the discovered stabilizers from the primary screen (**Figure S3.17B**). Alternative cysteine tethering mutations could sample different sub-pockets to stabilize

peptides which occupy more of the 14-3-3 binding groove. Taken together, the intrinsic diversity of the 14 3 3/phospho-peptide composite binding interface allowed for selectivity and precision when targeting a specific 14-3-3/client PPI.

While the focus of the screen was the discovery of fragment stabilizers, the screen also identified selective inhibitors, non-selective inhibitors, and neutral compounds for each client peptide and 14-3-3 (**Figure S3.18**). Therefore, disulfide tethering is a versatile tool that can be expanded to meet a wide range of conditions and results in hits that disrupt or stabilize PPIs. 14-3-3 provides an exciting proof of concept due to its large roster of clients, involvement in many biological processes, therapeutic potential, and extensive structural data, but the applicability of FBDD reaches beyond targeting a singular protein. It is due to this ease of access and applicability that disulfide tethering lends itself to the discovery of biological probes for PPIs and novel therapeutics for previously inaccessible biological challenges and diseases related to intrinsically disordered proteins.

REFERENCES

(1)   Garlick, J. M.; Mapp, A. K. Selective Modulation of Dynamic Protein Complexes. Cell Chem. Biol. 2020, 27 (8), 986–997. https://doi.org/10.1016/j.chembiol.2020.07.019.

(2)   Ivanov, A. A.; Revennaugh, B.; Rusnak, L.; Gonzalez-Pecchi, V.; Mo, X.; Johns, M. A.; Du, Y.; Cooper, L. A. D.; Moreno, C. S.; Khuri, F. R.; Fu, H. The OncoPPi Portal: An Integrative Resource to Explore and Prioritize Protein-Protein Interactions for Cancer Target Discovery. Bioinforma. Oxf. Engl. 2018, 34 (7), 1183–1191. https://doi.org/10.1093/bioinformatics/btx743.

(3)   Kim, M.; Park, J.; Bouhaddou, M.; Kim, K.; Rojc, A.; Modak, M.; Soucheray, M.; McGregor, M. J.; O'Leary, P.; Wolf, D.; Stevenson, E.; Foo, T. K.; Mitchell, D.; Herrington, K. A.; Muñoz, D. P.; Tutuncuoglu, B.; Chen, K. H.; Zheng, F.; Kreisberg, J. F.; Diolaiti, M. E.; Gordan, J. D.; Coppé, J. P.; Swaney, D. L.; Xia, B.; Veer, L. van 't; Ashworth, A.; Ideker, T.; Krogan, N. J. A Protein Interaction Landscape of Breast Cancer. Science 2021, 374 (6563), abf3066. https://doi.org/10.1126/science.abf3066.

(4)   Wright, M. T.; Plate, L. Revealing Functional Insights into ER Proteostasis through Proteomics and Interactomics. Exp. Cell Res. 2021, 399 (1), 112417. https://doi.org/10.1016/j.yexcr.2020.112417.

(5)   Hu, G.; Wu, Z.; Uversky, V. N.; Kurgan, L. Functional Analysis of Human Hub Proteins and Their Interactors Involved in the Intrinsic Disorder-Enriched Interactions. Int. J. Mol. Sci. 2017, 18 (12), E2761. https://doi.org/10.3390/ijms18122761.

(6)   Arkin, M. R.; Tang, Y.; Wells, J. A. Small-Molecule Inhibitors of Protein-Protein Interactions: Progressing toward the Reality. Chem. Biol. 2014, 21 (9), 1102–1114. https://doi.org/10.1016/j.chembiol.2014.09.001.

(7)   Celis, S.; Hobor, F.; James, T.; Bartlett, G. J.; Ibarra, A. A.; Shoemark, D. K.; Hegedüs, Z.; Hetherington, K.; Woolfson, D. N.; Sessions, R. B.; Edwards, T. A.; Andrews, D. M.; Nelson, A.; Wilson, A. J. Query-Guided Protein-Protein Interaction Inhibitor Discovery. Chem. Sci. 2021, 12 (13), 4753–4762. https://doi.org/10.1039/d1sc00023c.

(8)   Linhares, B. M.; Grembecka, J.; Cierpicki, T. Targeting Epigenetic Protein-Protein Interactions with Small Molecule Inhibitors. Future Med. Chem. 2020, 12 (14), 1305–1326. https://doi.org/10.4155/fmc-2020-0082.

(9)   Modell, A. E.; Blosser, S. L.; Arora, P. S. Systematic Targeting of Protein-Protein Interactions. Trends Pharmacol. Sci. 2016, 37 (8), 702–713. https://doi.org/10.1016/j.tips.2016.05.008.

(10)   Zhong, M.; Lee, G. M.; Sijbesma, E.; Ottmann, C.; Arkin, M. R. Modulating Protein-Protein Interaction Networks in Protein Homeostasis. Curr. Opin. Chem. Biol. 2019, 50, 55–65. https://doi.org/10.1016/j.cbpa.2019.02.012.

(11)   Andrei, S. A.; Sijbesma, E.; Hann, M.; Davis, J.; O'Mahony, G.; Perry, M. W. D.; Karawajczyk, A.; Eickhoff, J.; Brunsveld, L.; Doveston, R. G.; Milroy, L.G.; Ottmann, C. Stabilization of Protein-Protein Interactions in Drug Discovery. Expert Opin. Drug Discov. 2017, 12 (9), 925–940. https://doi.org/10.1080/17460441.2017.1346608.

(12)   Tang, C.; Mo, X.; Niu, Q.; Wahafu, A.; Yang, X.; Qui, M.; Ivanov, A. A.; Du, Y.; Fu, H. Hypomorph Mutation Directed Small Molecule Protein-Protein Interaction Inducers to Restore Mutant SMAD4 Suppressed TGF-β Signaling. Cell Chem. Biol. 2021, 28 (5), 636-647.e5. https://doi.org/10.1016/j.chembiol.2020.11.010.

(13)   Stevers, L. M.; Sijbesma, E.; Botta, M.; MacKintosh, C.; Obsil, T.; Landrieu, I.; Cau, Y.; Wilson, A. J.; Karawajczyk, A.; Eickhoff, J.; Davis, J.; Hann, M.; O'Mahony, G.; Doveston, R. G.;

Brunsveld, L.; Ottmann, C. Modulators of 14-3-3 Protein–Protein Interactions. J. Med. Chem. 2018, 61 (9), 3755–3778. https://doi.org/10.1021/acs.jmedchem.7b00574.

(14)   De Vries van Leeuwen, I. J.; da Costa Pereira, D.; Flach, K. D.; Piersma, S. R.; Haase, C.; Bier, D.; Yalcin, Z.; Michalides, R.; Feenstra, K. A.; Jiménez, C. R.; de Greef, T. F. A.; Brunsveld, L.; Ottmann, C.; Zwart, W.; de Boer, A. H. Interaction of 14-3-3 Proteins with the Estrogen Receptor Alpha F Domain Provides a Drug Target Inter-face. Proc. Natl. Acad. Sci. U. S. A. 2013, 110 (22), 8894–8899. https://doi.org/10.1073/pnas.1220809110.

(15)   Mayor-Ruiz, C.; Bauer, S.; Brand, M.; Kozicka, Z.; Si-klos, M.; Imrichova, H.; Kaltheuner, I. H.; Hahn, E.; Seiler, K.; Koren, A.; Petzold, G.; Fellner, M.; Bock, C.; Müller, A. C.; Zuber, J.; Geyer, M.; Thomä, N. H.; Kubicek, S.; Winter, G. E. Rational Discovery of Molecular Glue Degraders via Scalable Chemical Profiling. Nat. Chem. Biol. 2020, 16 (11), 1199–1207. https://doi.org/10.1038/s41589-020-0594-x.

(16)   Chamberlain, P. P.; Cathers, B. E. Cereblon Modulators: Low Molecular Weight Inducers of Protein Degradation. Drug Discov. Today Technol. 2019, 31, 29–34. https://doi.org/10.1016/j.ddtec.2019.02.004.

(17)   Słabicki, M.; Kozicka, Z.; Petzold, G.; Li, Y.-D.; Manojkumar, M.; Bunker, R. D.; Donovan, K. A.; Siev-ers, Q. L.; Koeppel, J.; Suchyta, D.; Sperling, A. S.; Fink, E. C.; Gasser, J. A.; Wang, L. R.; Corsello, S. M.; Sellar, R. S.; Jan, M.; Gillingham, D.; Scholl, C.; Fröhling, S.; Golub, T. R.; Fischer, E. S.; Thomä, N. H.; Ebert, B. L. The CDK Inhibitor CR8 Acts as a Molecular Glue Degrader That Depletes Cyclin K. Nature 2020, 585 (7824), 293–297. https://doi.org/10.1038/s41586-020-2374-x.

(18)   Hartman, A. M.; Elgaher, W. A. M.; Hertrich, N.; Andrei, S. A.; Ottmann, C.; Hirsch, A. K. H. Discovery of Small Molecule Stabilizers of 14-3-3 Protein-Protein Interactions via Dynamic

Combinatorial Chemistry. ACS Med. Chem. Lett. 2020, 11 (5), 1041–1046.
https://doi.org/10.1021/acsmedchemlett.9b00541.

(19)   Pfaff, S. J.; Chimenti, M. S.; Kelly, M. J. S.; Arkin, M. R. Biophysical Methods for
Identifying Fragment-Based Inhibitors of Protein-Protein Interactions. In Protein-Protein
Interactions: Methods and Applications; Meyerkord, C. L., Fu, H., Eds.; Methods in Molecular
Biology; Springer: New York, NY, 2015; pp 587–613. https://doi.org/10.1007/978-1-4939-2425-
7_39.

(20)   Erlanson, D. A.; Arndt, J. W.; Cancilla, M. T.; Cao, K.; Elling, R. A.; English, N.;
Friedman, J.; Hansen, S. K.; Hession, C.; Joseph, I.; Kumaravel, G.; Lee, W.-C.; Lind, K. E.;
McDowell, R. S.; Miatkowski, K.; Nguyen, C.; Nguyen, T. B.; Park, S.; Pathan, N.; Penny, D. M.;
Ro-manowski, M. J.; Scott, D.; Silvian, L.; Simmons, R. L.; Tangonan, B. T.; Yang, W.; Sun, L.
Discovery of a Potent and Highly Selective PDK1 Inhibitor via Fragment-Based Drug Discovery.
Bioorg. Med. Chem. Lett. 2011, 21 (10), 3078–3083. https://doi.org/10.1016/j.bmcl.2011.03.032.

(21)   Hallenbeck, K. K.; Davies, J. L.; Merron, C.; Ogden, P.; Sijbesma, E.; Ottmann, C.;
Renslo, A. R.; Wilson, C.; Arkin, M. R. A Liquid Chromatography/Mass Spectrometry Method for
Screening Disulfide Tethering Fragments. SLAS Discov. Adv. Life Sci. R D 2018, 23 (2), 183–
192. https://doi.org/10.1177/2472555217732072.

(22)   Raimundo, B. C.; Oslob, J. D.; Braisted, A. C.; Hyde, J.; McDowell, R. S.; Randal, M.;
Waal, N. D.; Wilkinson, J.; Yu, C. H.; Arkin, M. R. Integrating Fragment Assembly and
Biophysical Methods in the Chemical Advancement of Small-Molecule Antagonists of IL-2: An
Approach for Inhibiting Protein-Protein Interactions. J. Med. Chem. 2004, 47 (12), 3111–3130.
https://doi.org/10.1021/jm049967u.

(23)   Lodge, J. M.; Rettenmaier, T. J.; Wells, J. A.; Pomerantz, W. C.; Mapp, A. K. FP Tethering: A Screening Technique to Rapidly Identify Compounds That Disrupt Protein-Protein Interactions. MedChemComm 2014, 5, 370–375. https://doi.org/10.1039/C3MD00356F.

(24)   Sadowsky, J. D.; Burlingame, M. A.; Wolan, D. W.; McClendon, C. L.; Jacobson, M. P.; Wells, J. A. Turning a Protein Kinase on or off from a Single Allosteric Site via Disulfide Trapping. Proc. Natl. Acad. Sci. U. S. A. 2011, 108 (15), 6056–6061. https://doi.org/10.1073/pnas.1102376108.

(25)   Sijbesma, E.; Hallenbeck, K. K.; Leysen, S.; de Vink, P. J.; Skóra, L.; Jahnke, W.; Brunsveld, L.; Arkin, M. R.; Ottmann, C. Site-Directed Fragment-Based Screening for the Discovery of Protein–Protein Interaction Stabilizers. J. Am. Chem. Soc. 2019, 141 (8), 3524–3531. https://doi.org/10.1021/jacs.8b11658.

(26)   Burlingame, M. A.; Tom, C. T. M. B.; Renslo, A. R. Simple One-Pot Synthesis of Disulfide Fragments for Use in Disulfide Exchange Screening. ACS Comb. Sci. 2011, 13 (3), 205–208. https://doi.org/10.1021/co200038g.

(27)   Morrison, D. K. The 14-3-3 Proteins: Integrators of Diverse Signaling Cues That Impact Cell Fate and Cancer Development. Trends Cell Biol. 2009, 19 (1), 16–23. https://doi.org/10.1016/j.tcb.2008.10.003.

(28)   Obsilova, V.; Obsil, T. The 14-3-3 Proteins as Important Allosteric Regulators of Protein Kinases. Int. J. Mol. Sci. 2020, 21 (22), E8824. https://doi.org/10.3390/ijms21228824.

(29)   Aghazadeh, Y.; Papadopoulos, V. The Role of the 14-3-3 Protein Family in Health, Disease, and Drug Development. Drug Discov. Today 2016, 21 (2), 278–287. https://doi.org/10.1016/j.drudis.2015.09.012.

(30)   Gardino, A. K.; Smerdon, S. J.; Yaffe, M. B. Structural Determinants of 14-3-3 Binding
Specificities and Regulation of Subcellular Localization of 14-3-3-Ligand Complexes: A
Comparison of the X-Ray Crystal Structures of All Human 14-3-3 Isoforms. Semin. Cancer Bi-ol.
2006, 16 (3), 173–182. https://doi.org/10.1016/j.semcancer.2006.03.007.

(31)   Zhao, J.; Meyerkord, C. L.; Du, Y.; Khuri, F. R.; Fu, H. 14-3-3 Proteins as Potential
Therapeutic Targets. Semin. Cell Dev. Biol. 2011, 22 (7), 705–712.
https://doi.org/10.1016/j.semcdb.2011.09.012.

(32)   Molzan, M.; Kasper, S.; Röglin, L.; Skwarczynska, M.; Sassa, T.; Inoue, T.;
Breitenbuecher, F.; Ohkanda, J.; Kato, N.; Schuler, M.; Ottmann, C. Stabilization of Physical
RAF/14-3-3 Interaction by Cotylenin A as Treatment Strategy for RAS Mutant Cancers. ACS
Chem. Biol. 2013, 8 (9), 1869–1875. https://doi.org/10.1021/cb4003464.

(33)   Bank, R. P. D. RCSB PDB: Homepage. https://www.rcsb.org/ (accessed 2022-06-21).

(34)   Liau, N. P. D.; Wendorff, T. J.; Quinn, J. G.; Steffek, M.; Phung, W.; Liu, P.; Tang, J.;
Irudayanathan, F. J.; Izadi, S.; Shaw, A. S.; Malek, S.; Hymowitz, S. G.; Sudhamsu, J. Negative
Regulation of RAF Kinase Activity by ATP Is Overcome by 14-3-3 Induced Dimerization. Nat.
Struct. Mol. Biol. 2020, 27 (2), 134–141. https://doi.org/10.1038/s41594-019-0365-0.

(35)   Ballone, A.; Lau, R. A.; Zweipfenning, F. P. A.; Ottmann, C. A New Soaking Procedure
for X-Ray Crystallographic Structural Determination of Protein-Peptide Complexes. Acta
Crystallogr. Sect. F Struct. Biol. Com-mun. 2020, 76 (Pt 10), 501–507.
https://doi.org/10.1107/S2053230X2001122X.

(36)   Saha, M.; Carriere, A.; Cheerathodi, M.; Zhang, X.; La-voie, G.; Rush, J.; Roux, P. P.;
Ballif, B. A. RSK Phosphorylates SOS1 Creating 14-3-3 Docking Sites and Negatively
Regulating MAPK Activation. Biochem. J. 2012, 447 (1), 159–166.
https://doi.org/10.1042/BJ20120938.

(37)   Saline, M.; Badertscher, L.; Wolter, M.; Lau, R.; Gunnarsson, A.; Jacso, T.; Norris, T.; Ottmann, C.; Snijder, A. AMPK and AKT Protein Kinases Hierarchically Phosphorylate the N-Terminus of the FOXO1 Transcription Factor, Modulating Interactions with 14-3-3 Proteins. J. Biol. Chem. 2019, 294 (35), 13106–13116. https://doi.org/10.1074/jbc.RA119.008649.

(38)   Centorrino, F.; Ballone, A.; Wolter, M.; Ottmann, C. Biophysical and Structural Insight into the USP8/14-3-3 Interaction. FEBS Lett. 2018, 592 (7), 1211–1220. https://doi.org/10.1002/1873-3468.13017.

(39)   Molzan, M.; Schumacher, B.; Ottmann, C.; Baljuls, A.; Polzien, L.; Weyand, M.; Thiel, P.; Rose, R.; Rose, M.; Kuhenne, P.; Kaiser, M.; Rapp, U. R.; Kuhlmann, J.; Ottmann, C. Impaired Binding of 14-3-3 to C-RAF in Noonan Syndrome Suggests New Approaches in Diseases with Increased Ras Signaling. Mol. Cell. Biol. 2010, 30 (19), 4698–4711. https://doi.org/10.1128/MCB.01636-09.

(40)   Falcicchio, M.; Ward, J. A.; Chothia, S. Y.; Basran, J.; Mohindra, A.; Macip, S.; Roversi, P.; Doveston, R. G. Cooperative Stabilisation of 14-3-3σ Protein–Protein In-teractions via Covalent Protein Modification. Chem. Sci. 2021. https://doi.org/10.1039/D1SC02120F.

(41)   Molzan, M.; Ottmann, C. Synergistic Binding of the Phosphorylated S233- and S259-Binding Sites of C-RAF to One 14-3-3ζ Dimer. J. Mol. Biol. 2012, 423 (4), 486–495. https://doi.org/10.1016/j.jmb.2012.08.009.

(42)   Cossar, P. J.; Wolter, M.; van Dijck, L.; Valenti, D.; Levy, L. M.; Ottmann, C.; Brunsveld, L. Reversible Covalent Imine-Tethering for Selective Stabilization of 14-3-3 Hub Protein Interactions. J. Am. Chem. Soc. 2021, 143 (22), 8454–8464. https://doi.org/10.1021/jacs.1c03035.

Chapter 4 Hit-to-Lead Optimization of Selective 14-3-3/FOXO1 and 14-3-3/C-RAF Stabilizers
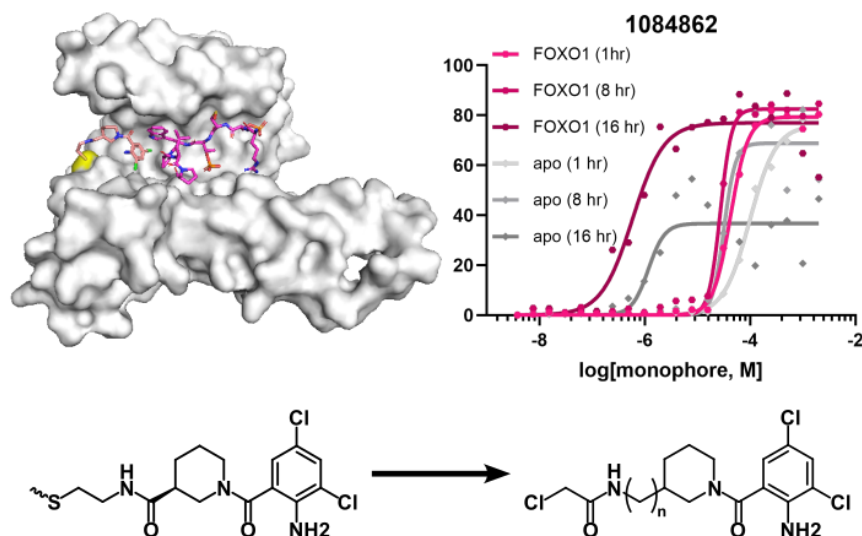
ABSTRACT: Disulfide tethering, a subset of fragment-based drug discovery (FBDD), is a versatile tool for the discovery of simple small molecule building blocks for the engagement of a plethora of protein targets. While disulfide tethering has been validated for a number of protein-protein interaction (PPI) inhibitors, the technology is vastly underutilized in the development of PPI stabilizers. PPIs are critical to the regulation and function of cellular pathways and offer novel "hotspots" for compound engagement. A prior study, discussed in Chapter 3, discovered eight selective disulfide stabilizers for two phospho-peptide mimetics of clients of the hub protein 14-3-3σ (five stabilizers for the 14-3-3σ/FOXO1 interaction and 3 stabilizers for the 14-3-3σ/C-RAF interaction), six of which were validated biochemically and four which provided structural data of the tricomplex binding and interaction interface. Utilizing these compounds as a framework, we designed and synthesized a series of covalent compounds in order to increase the selectivity, bioavailability, and pharmacokinetic properties of the molecules in an effort to develop biological probes and potential drug-like molecules for cell studies. Variation of

warhead, linker length, compound symmetry, diastereomer selectivity, as well as functionalization of the piperidine and phenyl rings provides valuable insight into the importance of the contacts between the compounds, 14-3-3σ, and the phospho-peptide clients, enabling prioritization for future hit-to-lead optimization efforts. Although the covalent compounds showed attenuated C38 engagement and stabilization activity as compared to their disulfide counterparts, the trends that have been established via this limited SAR series have interesting implications for the next generation of 14-3-3σ/client stabilizers.

INTRODUCTION

The cellular "interactome" is a diverse, highly connected network comprised of a variety of proteins including "hub" proteins with dozens to hundreds of binding partners. It is estimated that there are several hundred such hub proteins in mammalian cells which, due to their broad range of interactions, subcellular localizations, and functions, are crucial to a plethora of cellular processes.[1–4] The hub protein 14-3-3 has been of primary interest to the Arkin lab due to hundreds of known protein binding partners, an expansive breadth of functionalities including phosphorylation protection, subcellular localization, induction and/or disruption of other PPIs, and accessibility to structural characterization.[5–16] 14-3-3 also has a proclivity for binding to intrinsically disordered regions of proteins creating novel, ordered "hotspots" for small molecule engagement on otherwise "undruggable" protein targets.[17–20] These features position 14-3-3 not only as a fascinating tool within basic biology research, but also a potential target for drug discovery. The discovery and development of potent, selective small molecule probes of 14-3-3 PPI networks could provide valuable insight into the role 14-3-3 plays in cell signaling and produce a platform for the development of therapeutics.[21–23] This chapter focuses on the selective stabilization of two 14-3-3 client proteins, the transcription factor FOXO1 and the kinase C-RAF, with disease relevance in metabolic disease, developmental disorders, and cancer.
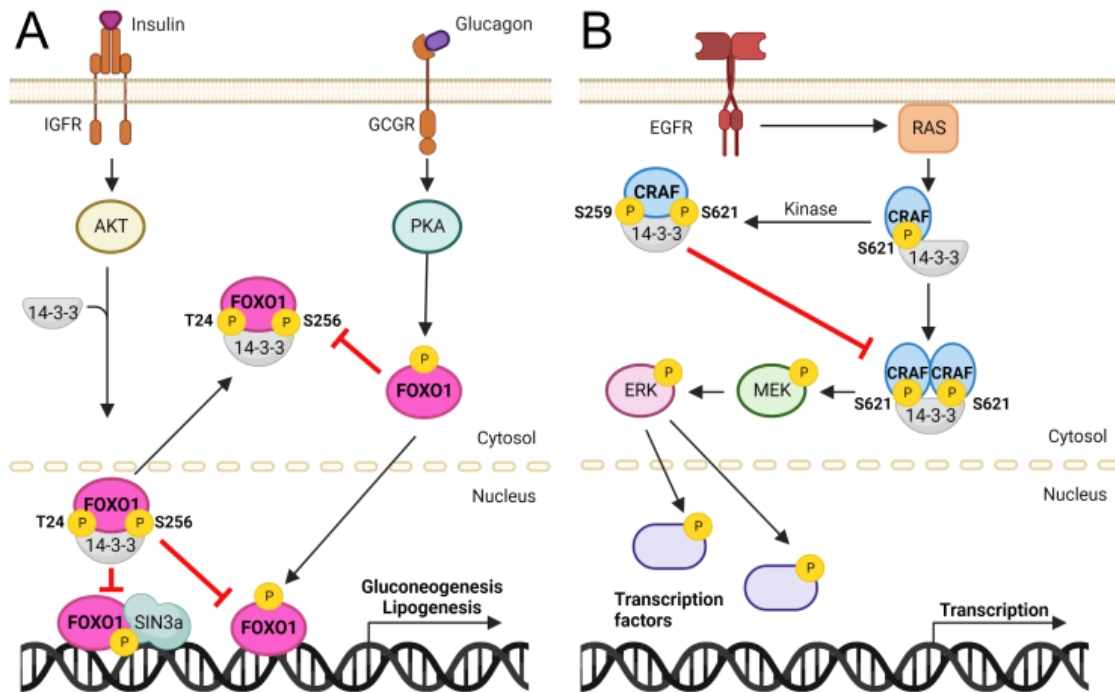
Figure 4.1 Overview of FOXO1 and C-RAF signaling pathways and proposed 14-3-3 regulation. (A) Insulin signaling within the liver, activating AKT and phosphorylating FOXO1 T24 and S256. 14-3-3 binds to FOXO1 at pT24 and pS256, sterically occluding SIN3A binding and exporting FOXO1 out of the nucleus. FOXO1 activation of gluconeogenesis and lipogenesis is halted. Glucagon signals for PKA to activate FOXO1. (B) C-RAF phosphorylation at pS259 results in negative regulation by 14-3-3. However, phosphorylation at S621 without S259 results in dimerization and activation of C-RAF, phosphorylation of MEK and ERK and activation of EGFR pathway.

FOXO1 is an important regulator of cell signaling, apoptosis, and a key mediator of pathways associated with metabolic disease such as gluconeogenesis, adipogenesis, and feeding behavior.[24–27] FOXO1 has been an attractive target for therapeutics as loss-of-function mutations within the liver have led to decreased hepatic gluconeogenesis and improved fasting glycemia; suppression of FOXO1 in adipocytes also decreased body weight and partial inhibition of FOXO1 activity has shown success in decreasing plasma glucose levels in diabetic mice.[26,28,29] However, complete ablation of FOXO1/DNA binding in hepatocytes has produced unintended side effects including increased liver lipogenesis and the development of steatosis.[28,30]

FOXO1 activity is tightly regulated by various posttranslational modifications (PTMs) including phosphorylation at T24 and S256 followed by engagement by 14-3-3.[27,31–33] This results in the disruption of FOXO1/DNA binding and translocation out of the nucleus. However, phosphorylation at S256 results in FOXO1 binding to its corepressor protein, SIN3a. The FOXO1/SIN3a complex has been linked to the unwanted side effects of fatty liver and steatosis.[24–26,34] Phosphorylation of the FOXO1 T24 residue results in dissociation of SIN3a and ablation of these harmful consequences. Therefore, it is possible that 14-3-3 acts as a negative regulator of FOXO1 transcriptional activity and sterically occludes FOXO1/SIN3a binding (**Figure 4.1A**). Protection of the FOXO1 pT24 PTM via selective stabilization of 14-3-3/FOXO1 binding would provide valuable insight into the interplay between different FOXO1 regulatory pathways and a novel, efficacious approach to inhibiting FOXO1 transcriptional activity in metabolic disease whilst mitigating the potential for liver injury.

C-RAF is a kinase in the mitogen-activated protein kinase (MAPK) pathway which, similarly to FOXO1, has multiple complex regulatory pathways involving phosphorylation-mediated 14-3-3 interactions.[35–38] Phosphorylation of the C-terminal residue pS621 results in 14-3-3 binding and induction of C-RAF homodimerization which leads to activation of the kinase and phosphorylation of C-RAF's only known substrate, MEK.[39] When mutated or constitutively activated by the GTPase KRAS, dysregulated C-RAF signaling has been linked to developmental disorders such as Noonan syndrome and Leopard syndrome and cancers such as acute myeloid leukemia and prostate cancer.[40,41] Phosphorylation and 14-3-3 binding to C-RAF residue S259 blocks C-RAF interaction with RAS, prevents both homo- and heterodimerization of C-RAF with the other RAF kinases, and leads to inactivation of kinase activity (**Figure 4.1B**). Selective stabilization of the 14-3-3/pS259 C-RAF inhibitory complex has the potential to produce novel therapeutics for C-RAF driven disorders as well as a range of other Rasopathies given its critical role in the binding and activation of the other RAF isoforms
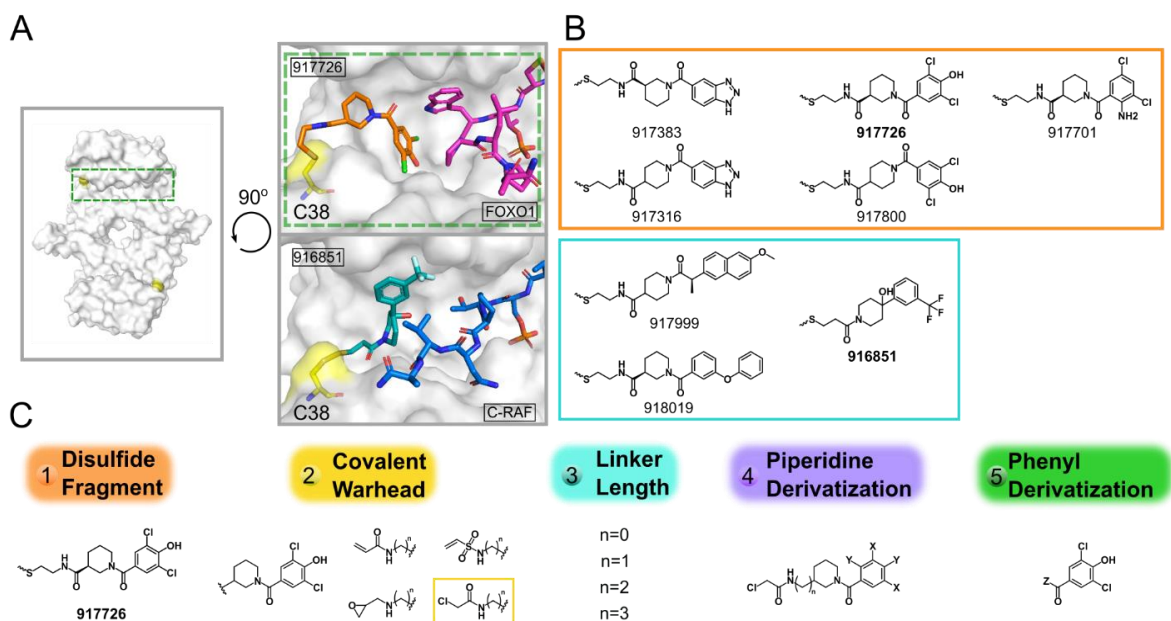
Figure 4.2 Hit-to-lead optimization strategy. (A) Structure of 14-3-3σ dimer (white) highlighting C38 (yellow) and biding groove (green box). X-ray crystal structures of compounds **917726** (orange; top box) and **916851** (cyan; bottom box) bound to C38 (yellow) of 14-3-3σ (white) and FOXO1 (pink) or C-RAF (blue) respectively. (B) Chemical structures of disulfide stabilizers for 14-3-3σ/FOXO1 (orange box) and C-RAF (cyan box). (C) Points of derivatization for compound optimization beginning with the original fragment (orange) as inspiration. Modifications can be made for the covalent warhead (yellow), linker length (cyan), piperidine/14-3-3 contacts (purple), and fragment functional group/peptide contacts (green).

by RAS. This is especially crucial as a measure for overcoming drug resistance observed in the more common B-RAF driven cancers.[42]

The previous chapter outlined the systematic targeting of PPIs via disulfide tethering, a subset of fragment based drug discovery (FBDD), which resulted in selective small molecule scaffolds for stabilizers of the 14-3-3σ/FOXO1 and 14-3-3σ/C-RAF protein/phosphopeptide complexes (**Figure 4.2B**).[43] 14-3-3σ is unique amongst the seven 14-3-3 isoforms expressed in mammalian cells in that it has shown tumor suppressive activity and contains a native cysteine, C38, proximal to the client binding groove. The disulfide fragments engaged C38 in a reversible covalent manner that was amenable to quantification via intact mass spectrometry. Hit fragments were then validated in a series of mass spectrometry and fluorescence anisotropy based dose responses. Structural visualization of specific contacts between stabilizers and the

14-3-3σ/client interface via x-ray crystallography elucidated the key interactions required for selective binding and efficacious stabilization (**Figure 4.2A**). Whilst the compounds show promising activity *in vitro*, the thiol moiety has limited usage in cellular and *in vivo* studies due to its off-target reactivity within biological systems. Utilizing the original disulfide fragment stabilizers as inspiration, we designed and built a structure-activity relationship (SAR) series of covalent compounds sampling various covalent warheads, linker lengths, and substitutions to the original fragment/complex interface in order to develop potent, selective, and bioavailable covalent stabilizers to the 14-3-3σ/FOXO1 and 14-3-3σ/C-RAF PPIs (**Figure 4.2C**). Thorough validation of the resulting compounds showed covalent engagement of 14-3-3σ, however the selectivity and efficacy of the covalent compounds requires further optimization before cell studies can be performed.
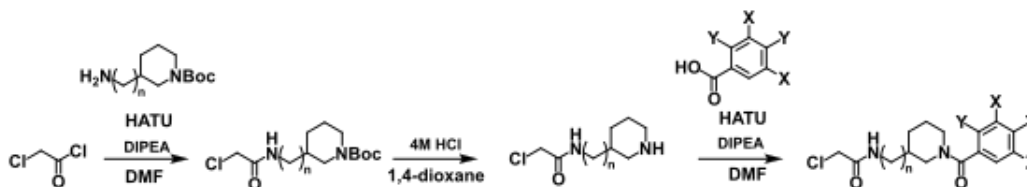
Figure 4.3 Synthetic strategy for chloroacetamide derivatives of disulfide hits with varying linker lengths.

RESULTS AND DISCUSSION

Warhead and Linker Variation. The covalent compound synthesis mirrored that of the disulfide fragment synthesis (**Figure 4.3; Synthetic Procedures**); a large batch of the core piperidine attached to the covalent warhead and various linker lengths was synthesized and purified in bulk, then derivatized by the chemical moieties discovered in the disulfide tethering screen which lent the compounds their selectivity. Cysteine-reactive electrophilic warheads vary in their reactivity, selectivity, and kinetics. A series of small molecules inspired by the chemical structure of compound **917949** sampled five such warheads — acrylamides, chloroacetamides, oxiranes, α-chloroketones, and vinylsulfonamides — and four different linker lengths [med chem paper]. Of the five, there was low or no engagement of 14-3-3σ C38 by the acrylamides, oxiranes, and

78

vinylsulfonamides. The α-chloroketone warhead had the most rapid reactivity, however these compounds showed greatly diminished selectivity for the 14-3-3σ/client interface vs 14-3-3σ alone (termed *apo* 14-3-3σ) in mass spectrometry and fluorescence polarization assays. Although compounds containing the chloroacetamide warhead had slower kinetics, they showcased a much greater selectivity for 14-3-3σ/client over *apo* 14-3-3σ, thus indicating that a moderate reactivity was more amenable to cooperativity, requiring the noncovalent interactions within the 14-3-3σ/client/compound interface for covalent bond formation with 14-3-3σ. Covalent compounds based on the inherently selective thiol stabilizers found in the tethering screen were therefore synthesized with the chloroacetamide warhead as a priority over the other electrophilic moieties.

Linker length was also a key determinant for reactivity, selectivity, and stabilization. Due to the reversal of the amide in the linker portion of the covalent compounds, as compared to their disulfide predecessors, longer linkers positioned the reversed amide farther from the piperidine ring. The contributions of the amide to the stabilization of the 14-3-3σ/client or 14-3-3σ/compound interaction interface was not directly quantified; however, analysis of the structural data indicated that the orientation of the amide faced away from the 14-3-3σ natural product binding pocket, indicating a lack of potential hydrogen bonding and hydrophilic interactions between the amide and 14-3-3σ (Chapter 3). Contacts between the amide and longer, flexible peptides such as C-RAF and USP8 were also not observed. The n=0 and n=1 linker lengths were chosen as a conservative starting point to replicate the disulfide fragment geometry and amide positioning closely, whilst still probing different reactivities and contacts within the 14-3-3σ/client interface and 14-3-3σ natural product binding pocket. The synthesis resulted in 14 compounds which were assessed for their binding to 14-3-3σ C38 and their stabilization of the 14-3-3σ/client protein-phosphopeptide interaction (**Figure S4.1**).
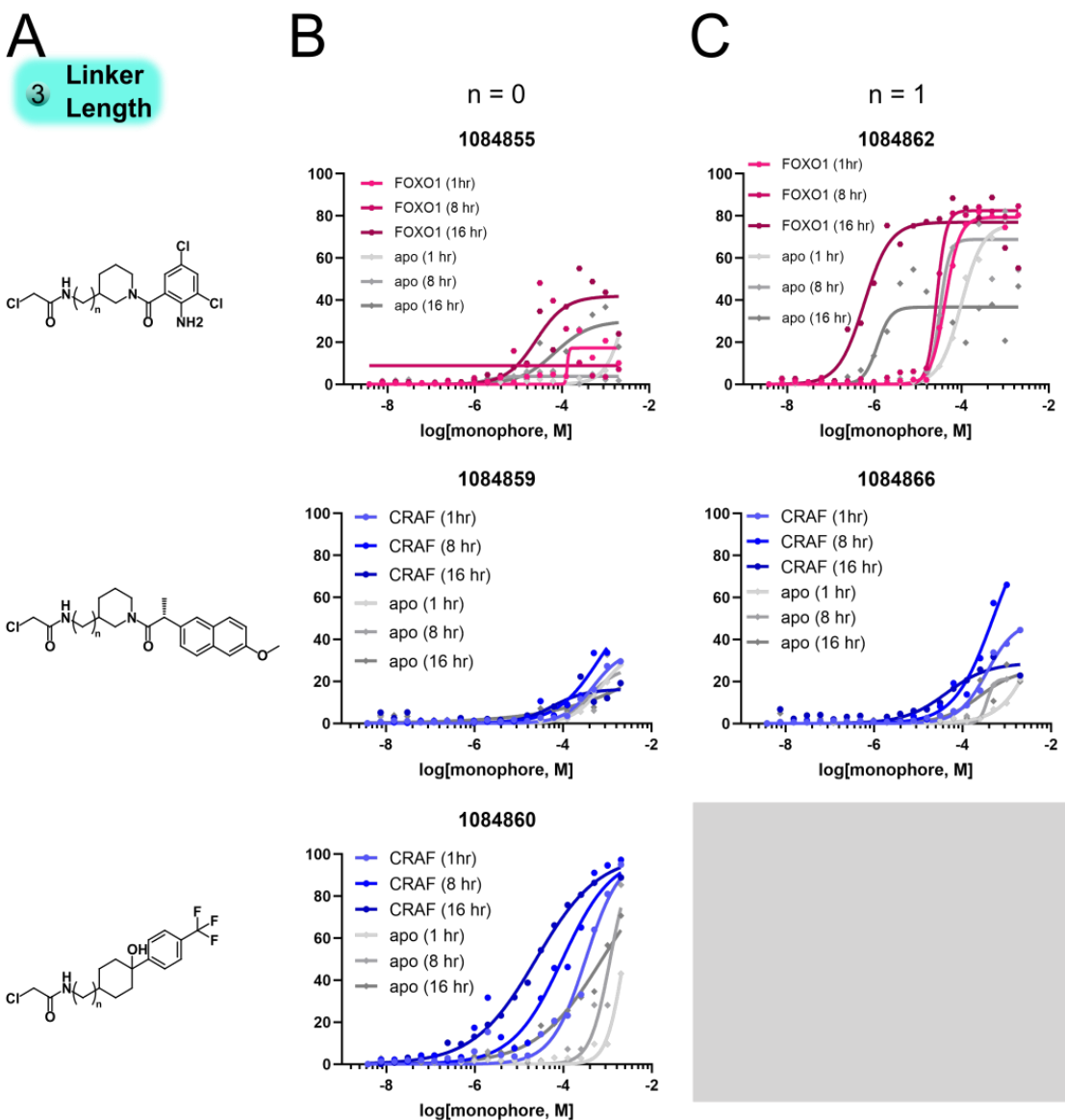
Figure 4.4 MSDR results for 14-3-3/FOXO1 and 14-3-3/C-RAF covalent stabilizers of varying linker lengths. (A) Chemical structures of compounds. (B) MSDR curves showing engagement of n=0 compounds. **1084855** (top), **1084859** (middle), and **1084860** (bottom) had the best DR_{50} values at 16 hours of incubation (2000 µM, >2000 µM, and 88 µM respectively), but showed loss of selectivity. (C) MSDR curves showing engagement of n=1 compounds. **1084862** (top) and **1084866** (middle) had the best DR_{50} values at 16 hours of incubation (35.9 µM and 473 µM respectively) and regained some selectivity for the peptide vs. apo (grey).

FOXO1 Selective Covalent Compound Target Engagement and Stabilization. The efficacy

of the FOXO1 selective compounds was determined utilizing similar validation approaches as

the original disulfide FOXO1 selective stabilizers described above in Chapter 3. Compound

80
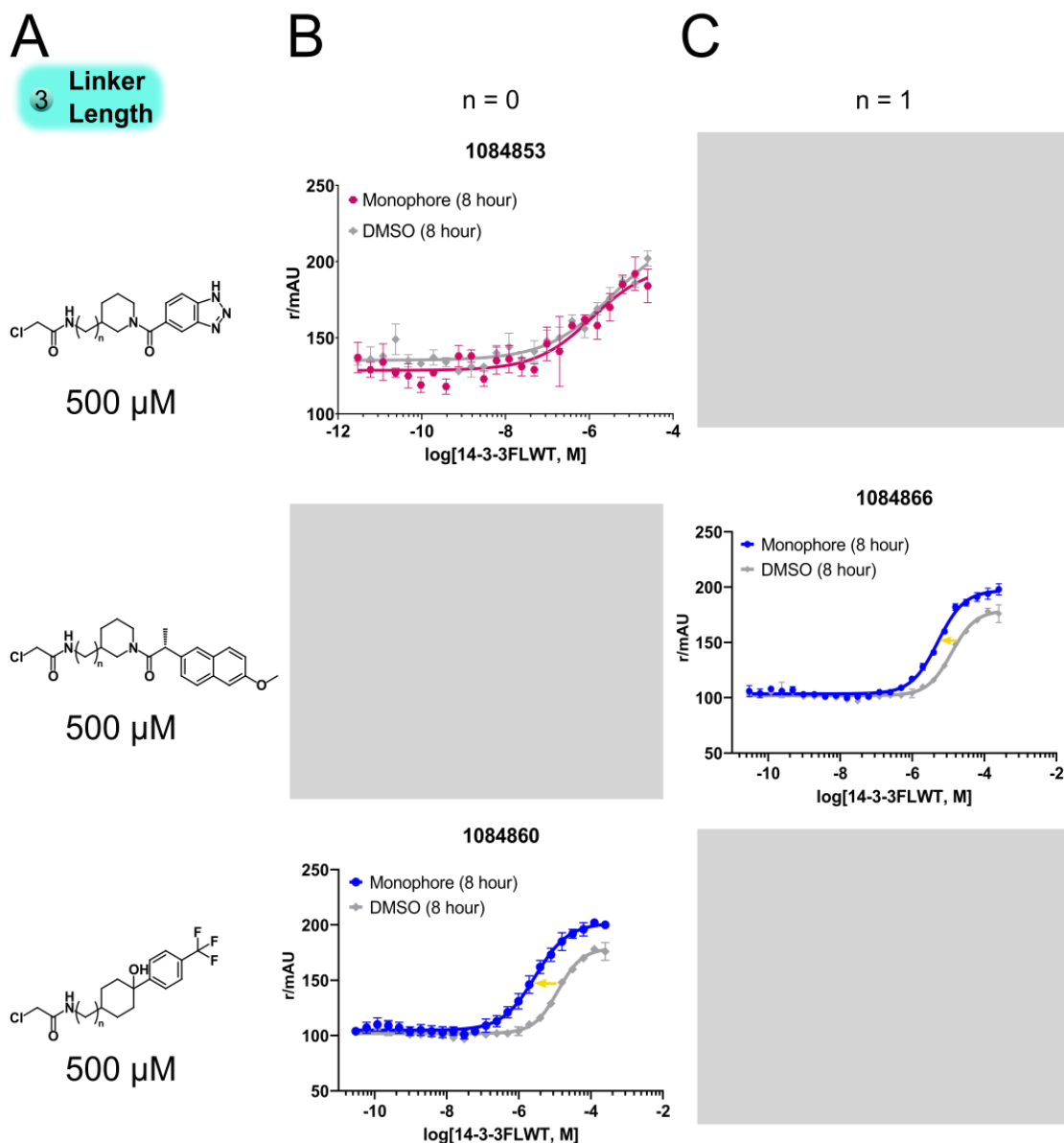
Figure 4.5 Protein titrations for 14-3-3/FOXO1 and 14-3-3/C-RAF covalent stabilizers of varying linker lengths. (A) Chemical structures and concentrations of compounds in assay. (B) Titration curves showing 14-3-3/client stabilization by n=0 compounds. **1084853** (top) and **1084860** (bottom) had the best fold stabilization at 8 hours of incubation (both 4-fold). (C) Titration curves showing 14-3-3/client stabilization by n=1 compounds. **1084866** (middle) had the best fold stabilization at 8 hours of incubation (2-fold).

binding to 14-3-3σ was determined through a modified mass spectrometry dose response

(MSDR; quantified by DR_{50} values). In order to measure compound kinetics, the original 3 hour

incubation was expanded to include four different timepoints (1 hour, 8 hours, 16 hours, and 24

hours; **Figure 4.4 and S4.2**). The effective concentration of the compounds was determined

using a fluorescence anisotropy dose response (FADR, quantified by EC_{50} values; **Figure S4.4**) at the same timepoints as the MSDR. Finally, protein titrations determined the cooperativity of the 14-3-3σ/phosphopeptide/compound complex and the degree of stabilization (quantified via a shift in the K_D; **Figure 4.5**).

Table 4.1 Properties of FOXO1 covalent compounds

SMDC ID	Disul. Frag.	Linker Length	DR_{50} (µM) pep	DR_{50} (µM) apo	EC_{50} (µM)	K_{D_App} (µM)	K_{D_DMSO} (µM)	Fold Stab.
1084853	917316	n=0	1.04	125	--	0.85	3.46	4
1084854	917383	n=0	1000	2000	--	--	--	--
1084861		n=1	2000	2000	--	--	--	--
1084855	917701	n=0	2000	2000	--	701	3.46	0.05
1084862		n=1	35.9	98.13	--	18.0	3.46	0.19
1084856	917726	n=0	2000	2000	--	--	--	--
1084863		n=1	690.4	2000	--	8.88	3.46	0.39
1084857	917800	n=0	78.69	2000	--	32.6	3.46	0.11
1084864		n=1	34.99	2000	--	0.38	0.06	0.17

Within the MSDR assays, compounds **1084853** and **1084857** of the n=0 linker series and compounds **1084862**, **1084863**, and **1084864** from the n=1 linker series showed the greatest 14-3-3σ engagement (**Table 4.1, Table S4.1,** and **Figures S4.2**). **1084853**, **1084857**, and **1084864** had the greatest selectivity in binding to 14-3-3σ in the presence of FOXO1 phosphopeptide vs *apo* 14-3-3σ (120-fold, 25-fold, and 57-fold, respectively; Table xxx). It must be noted that **1084864** had a shorter incubation time at the maximal activity (8 hours vs 16 hours) due to poor signal quality at later timepoints. This might indicate instability or insolubility of the compound. In the protein titrations, compound **1084853** showed the greatest fold-stabilization (4-fold with a K_{D_app} of 0.84 nM) at the 8-hour timepoint. Interestingly, the other compounds failed to produce any stabilization of the 14-3-3σ/FOXO1 complex and a few showed decreased binding affinity (**Table 4.1**, **Table S4.2**, and **Figure S4.5**). This could be due to unfavorable geometry produced by the n=0 and n=1 linkers which are both shorter than the

original disulfide linker length. Modeling and crystallographic structures could lend more visual insight into the discrepancy in 14-3-3σ engagement by the compounds and their stabilization effects on the 14-3-3σ/FOXO1 interaction.

Table 4.2 Properties of C-RAF covalent compounds

SMDC ID	Disulfide Frag.	Linker Length	DR_{50} (µM) pep	DR_{50} (µM) apo	EC_{50} (µM)	K_{D_App} (µM)	K_{D_DMSO} (µM)	Fold Stab.
1084860	916851	n=0	88.0	1000	28.1	2.82	12.2	4
1084859	917999	n=0	2000	2000	--	--	--	--
1084866		n=1	473	2000	136	5.23	12.2	2
1084858	918039	n=0	2000	2000	--	--	--	--
1084865		n=1	2000	2000	--	2.71	12.2	4.5

C-RAF Selective Covalent Compound Target Engagement and Stabilization. 14-3-3σ engagement, effective compound concentration, and compound stabilization of the 14-3-3σ/C-RAF complex were determined through the same validation experiments as 14-3-3σ/FOXO1. In the MSDR, compounds **1084860** and **1084866** showed target engagement and selectivity over the *apo* protein (11-fold and 4-fold respectively; **Figure 4.4**, **Figure S4.3**, **Table 4.2**, and **Table S4.1**). In the FADR, **1084860** had an EC_{50} value of 28 µM and **1084866** had an EC_{50} of 136 µM (**Figure S4.4**). Within the protein titrations, **1084860** produced a 4-fold stabilization of the 14-3-3σ/C-RAF protein-phosphopeptide interaction and **1084866** produced a more modest 2-fold stabilization (**Figure 4.5**, **Figure S4.6**, **Table 4.2**, and **Table S4.2**). These results were more reflective of the MSDR and FADR data than the FOXO1 selective compounds which seemingly bound well to 14-3-3σ in the MSDR but produced low to no stabilization in the protein titrations. However, the shift in stabilization by **1084860** and **1084866** was far less than the disulfides the compounds were based on (4-fold vs 77-fold and 2-fold vs 246-fold; Chapter 3). This might also be a result of insufficient interactions between the compounds and the 14-3-3σ/C-RAF binding interface due to the shortened linker length,

especially with regard to **1084866**. Modeling and crystallographic studies would be useful in illuminating the optimal orientation for warhead engagement of C38 and the appropriate linker length for maximizing contacts between the covalent compounds and the 14-3-3σ/C-RAF 'hotspot.'

CONCLUSIONS

Fragment-based drug discovery and, more specifically, disulfide tethering have great potential as powerful tools for addressing challenging biological problems. The simple chemical building blocks that were found in the prior disulfide tethering screen resulted in inherently selective stabilizers with high ligand efficiency for the 14-3-3σ/FOXO1 and 14-3-3σ/C-RAF interactions. Therefore, the compounds provided a versatile, mutable platform for the development of lead covalent compounds with greater bioavailability and pharmacokinetic properties. The amenability of the compounds to derivatization from all aspects of the molecule — warhead selection, linker length, amide positioning, piperidine ring accessorization, and alterations to the phenyl cores in contact with the phospho-peptide — allow for flexibility that is typically not present in drug discovery campaigns centered around more complex natural products. This flexibility in turn results in a more thorough exploration of the important contacts between the covalent lead compounds and 14-3-3σ, compounds and the phospho-peptide clients, and compounds and the 14-3-3σ/client composite binding interface.

This project embarked on a hit-to-lead optimization campaign in order to design and synthesize biologically active covalent compounds for future use as probes and potential therapeutics in metabolic disease, cancer, and developmental disorders. Linker length had a quantifiable effect on C38 engagement, selectivity over *apo* 14-3-3σ, and stabilization. Although the current compounds that have been synthesized exhibit lower 14-3-3σ C38 engagement in the mass spectrometry assays and decreased stabilization in the activity assays than their disulfide

counterparts, they provide valuable insight into the important facets of the

compound/protein/phospho-peptide trimeric system.

REFERENCES

(1) Rual, J.-F.; Venkatesan, K.; Hao, T.; Hirozane-Kishikawa, T.; Dricot, A.; Li, N.; Berriz, G. F.; Gibbons, F. D.; Dreze, M.; Ayivi-Guedehoussou, N.; Klitgord, N.; Simon, C.; Boxem, M.; Milstein, S.; Rosenberg, J.; Goldberg, D. S.; Zhang, L. V.; Wong, S. L.; Franklin, G.; Li, S.; Albala, J. S.; Lim, J.; Fraughton, C.; Llamosas, E.; Cevik, S.; Bex, C.; Lamesch, P.; Sikorski, R. S.; Vandenhaute, J.; Zoghbi, H. Y.; Smolyar, A.; Bosak, S.; Sequerra, R.; Doucette-Stamm, L.; Cusick, M. E.; Hill, D. E.; Roth, F. P.; Vidal, M. Towards a Proteome-Scale Map of the Human Protein–Protein Interaction Network. *Nature* **2005**, *437* (7062), 1173–1178. https://doi.org/10.1038/nature04209.

(2) Tsai, C.-J.; Ma, B.; Nussinov, R. Protein–Protein Interaction Networks: How Can a Hub Protein Bind so Many Different Partners? *Trends Biochem. Sci.* **2009**, *34* (12), 594–600. https://doi.org/10.1016/j.tibs.2009.07.007.

(3) Stelzl, U.; Worm, U.; Lalowski, M.; Haenig, C.; Brembeck, F. H.; Goehler, H.; Stroedicke, M.; Zenkner, M.; Schoenherr, A.; Koeppen, S.; Timm, J.; Mintzlaff, S.; Abraham, C.; Bock, N.; Kietzmann, S.; Goedde, A.; Toksöz, E.; Droege, A.; Krobitsch, S.; Korn, B.; Birchmeier, W.; Lehrach, H.; Wanker, E. E. A Human Protein-Protein Interaction Network: A Resource for Annotating the Proteome. *Cell* **2005**, *122* (6), 957–968. https://doi.org/10.1016/j.cell.2005.08.029.

(4) Ota, M.; Gonja, H.; Koike, R.; Fukuchi, S. Multiple-Localization and Hub Proteins. *PLOS ONE* **2016**, *11* (6), e0156455. https://doi.org/10.1371/journal.pone.0156455.

(5) Abdrabou, A.; Brandwein, D.; Wang, Z. Differential Subcellular Distribution and Translocation of Seven 14-3-3 Isoforms in Response to EGF and During the Cell Cycle. *Int. J. Mol. Sci.* **2020**, *21* (1). https://doi.org/10.3390/ijms21010318.

(6)   Cornell, B.; Toyo-oka, K. 14-3-3 Proteins in Brain Development: Neurogenesis, Neuronal Migration and Neuromorphogenesis. *Front. Mol. Neurosci.* **2017**, *10*. https://doi.org/10.3389/fnmol.2017.00318.

(7)   Gardino, A. K.; Smerdon, S. J.; Yaffe, M. B. Structural Determinants of 14-3-3 Binding Specificities and Regulation of Subcellular Localization of 14-3-3-Ligand Complexes: A Comparison of the X-Ray Crystal Structures of All Human 14-3-3 Isoforms. *Semin. Cancer Biol.* **2006**, *16* (3), 173–182. https://doi.org/10.1016/j.semcancer.2006.03.007.

(8)   Halskau, Ø.; Ying, M.; Baumann, A.; Kleppe, R.; Rodriguez-Larrea, D.; Almås, B.; Haavik, J.; Martinez, A. Three-Way Interaction between 14-3-3 Proteins, the N-Terminal Region of Tyrosine Hydroxylase, and Negatively Charged Membranes. *J. Biol. Chem.* **2009**, *284* (47), 32758–32769. https://doi.org/10.1074/jbc.M109.027706.

(9)   Iralde-Lorente, L.; Tassone, G.; Clementi, L.; Franci, L.; Munier, C. C.; Cau, Y.; Mori, M.; Chiariello, M.; Angelucci, A.; Perry, M. W. D.; Pozzi, C.; Mangani, S.; Botta, M. Identification of Phosphate-Containing Compounds as New Inhibitors of 14-3-3/c-Abl Protein–Protein Interaction. *ACS Chem. Biol.* **2020**. https://doi.org/10.1021/acschembio.0c00039.

(10)   Liu, C.-C.; Jan, Y.-J.; Ko, B.-S.; Wu, Y.-M.; Liang, S.-M.; Chen, S.-C.; Lee, Y.-M.; Liu, T.-A.; Chang, T.-C.; Wang, J.; Shyue, S.-K.; Sung, L.-Y.; Liou, J.-Y. 14-3-3σ Induces Heat Shock Protein 70 Expression in Hepatocellular Carcinoma. *BMC Cancer* **2014**, *14* (1), 425. https://doi.org/10.1186/1471-2407-14-425.

(11)   Pennington, K. L.; Chan, T. Y.; Torres, M. P.; Andersen, J. L. The Dynamic and Stress-Adaptive Signaling Hub of 14-3-3: Emerging Mechanisms of Regulation and Context-Dependent Protein–Protein Interactions. *Oncogene* **2018**, *37* (42), 5587. https://doi.org/10.1038/s41388-018-0348-3.

(12)   Young, G. M.; Radhakrishnan, V. M.; Centuori, S. M.; Gomes, C. J.; Martinez, J. D. Comparative Analysis of 14-3-3 Isoform Expression and Epigenetic Alterations in Colorectal Cancer. *BMC Cancer* **2015**, *15*. https://doi.org/10.1186/s12885-015-1856-y.

(13)   Ballone, A.; Lau, R. A.; Zweipfenning, F. P. A.; Ottmann, C. A New Soaking Procedure for X-Ray Crystallographic Structural Determination of Protein–Peptide Complexes. *Acta Crystallogr. Sect. F Struct. Biol. Commun.* **2020**, *76* (Pt 10), 501–507. https://doi.org/10.1107/S2053230X2001122X.

(14)   Centorrino, F.; Ballone, A.; Wolter, M.; Ottmann, C. Biophysical and Structural Insight into the USP8/14-3-3 Interaction. *FEBS Lett.* **2018**, *592* (7), 1211–1220. https://doi.org/10.1002/1873-3468.13017.

(15)   De Vries-van Leeuwen, I. J.; da Costa Pereira, D.; Flach, K. D.; Piersma, S. R.; Haase, C.; Bier, D.; Yalcin, Z.; Michalides, R.; Feenstra, K. A.; Jiménez, C. R.; de Greef, T. F. A.; Brunsveld, L.; Ottmann, C.; Zwart, W.; de Boer, A. H. Interaction of 14-3-3 Proteins with the Estrogen Receptor Alpha F Domain Provides a Drug Target Interface. *Proc. Natl. Acad. Sci. U. S. A.* **2013**, *110* (22), 8894–8899. https://doi.org/10.1073/pnas.1220809110.

(16)   Ji, L.; Wang, Q.; Liu, M.; Zhu, C.; Xiao, Y.; Han, J.; Fang, Y.; Ye, J.; Yin, J.; Wei, L. The 14-3-3 Protein YWHAB Inhibits Glucagon-Induced Hepatic Gluconeogenesis through Interacting with the Glucagon Receptor and FOXO1. *FEBS Lett. n/a* (n/a). https://doi.org/10.1002/1873-3468.14063.

(17)   Stevers, L. M.; Sijbesma, E.; Botta, M.; MacKintosh, C.; Obsil, T.; Landrieu, I.; Cau, Y.; Wilson, A. J.; Karawajczyk, A.; Eickhoff, J.; Davis, J.; Hann, M.; O'Mahony, G.; Doveston, R. G.; Brunsveld, L.; Ottmann, C. Modulators of 14-3-3 Protein–Protein Interactions. *J. Med. Chem.* **2018**, *61* (9), 3755–3778. https://doi.org/10.1021/acs.jmedchem.7b00574.

(18)   M. Bustos, D. The Role of Protein Disorder in the 14-3-3 Interaction Network. *Mol. Biosyst.* **2012**, *8* (1), 178–184. https://doi.org/10.1039/C1MB05216K.

(19)   Oldfield, C. J.; Meng, J.; Yang, J. Y.; Yang, M. Q.; Uversky, V. N.; Dunker, A. K. Flexible Nets: Disorder and Induced Fit in the Associations of P53 and 14-3-3 with Their Partners. *BMC Genomics* **2008**, *9* (1), S1. https://doi.org/10.1186/1471-2164-9-S1-S1.

(20)   Sluchanko, N. N.; Bustos, D. M. Chapter Two - Intrinsic Disorder Associated with 14-3-3 Proteins and Their Partners. In *Progress in Molecular Biology and Translational Science*; Uversky, V. N., Ed.; Dancing protein clouds: Intrinsically disordered proteins in health and disease, Part A; Academic Press, 2019; Vol. 166, pp 19–61. https://doi.org/10.1016/bs.pmbts.2019.03.007.

(21)   Zhao, J.; Meyerkord, C. L.; Du, Y.; Khuri, F. R.; Fu, H. 14-3-3 Proteins as Potential Therapeutic Targets. *Semin. Cell Dev. Biol.* **2011**, *22* (7), 705–712. https://doi.org/10.1016/j.semcdb.2011.09.012.

(22)   Diallo, K.; Oppong, A. K.; Lim, G. E. Can 14-3-3 Proteins Serve as Therapeutic Targets for the Treatment of Metabolic Diseases? *Pharmacol. Res.* **2019**, *139*, 199–206. https://doi.org/10.1016/j.phrs.2018.11.021.

(23)   De Vries-van Leeuwen, I. J.; da Costa Pereira, D.; Flach, K. D.; Piersma, S. R.; Haase, C.; Bier, D.; Yalcin, Z.; Michalides, R.; Feenstra, K. A.; Jiménez, C. R.; de Greef, T. F. A.; Brunsveld, L.; Ottmann, C.; Zwart, W.; de Boer, A. H. Interaction of 14-3-3 Proteins with the Estrogen Receptor Alpha F Domain Provides a Drug Target Interface. *Proc. Natl. Acad. Sci.* **2013**, *110* (22), 8894–8899. https://doi.org/10.1073/pnas.1220809110.

(24)   Chen, J.; Lu, Y.; Tian, M.; Huang, Q. Molecular Mechanisms of FOXO1 in Adipocyte Differentiation. *J. Mol. Endocrinol.* **2019**, *62* (3), R239–R253. https://doi.org/10.1530/JME-18-0178.

(25)   Ioannilli, L.; Ciccarone, F.; Ciriolo, M. R. Adipose Tissue and FoxO1: Bridging Physiology and Mechanisms. *Cells* **2020**, *9* (4), 849. https://doi.org/10.3390/cells9040849.

(26)   Kodani, N.; Nakae, J. Tissue-Specific Metabolic Regulation of FOXO-Binding Protein: FOXO Does Not Act Alone. *Cells* **2020**, *9* (3), 702. https://doi.org/10.3390/cells9030702.

(27)   Peng, S.; Li, W.; Hou, N.; Huang, N. A Review of FoxO1-Regulated Metabolic Diseases and Related Drug Discoveries. *Cells* **2020**, *9* (1), 184. https://doi.org/10.3390/cells9010184.

(28)   Zou, P.; Liu, L.; Zheng, L.; Liu, L.; Stoneman, R. E.; Cho, A.; Emery, A.; Gilbert, E. R.; Cheng, Z. Targeting FoxO1 with AS1842856 Suppresses Adipogenesis. *Cell Cycle* **2014**, *13* (23), 3759–3767. https://doi.org/10.4161/15384101.2014.965977.

(29)   *FOXO Transcription Factors: Methods and Protocols*; Link, W., Ed.; Methods in Molecular Biology; Springer New York: New York, NY, 2019; Vol. 1890. https://doi.org/10.1007/978-1-4939-8900-3.

(30)   Nagashima, T.; Shigematsu, N.; Maruki, R.; Urano, Y.; Tanaka, H.; Shimaya, A.; Shimokawa, T.; Shibasaki, M. Discovery of Novel Forkhead Box O1 Inhibitors for Treating Type 2 Diabetes: Improvement of Fasting Glycemia in Diabetic Db/Db Mice. *Mol. Pharmacol.* **2010**, *78* (5), 961–970. https://doi.org/10.1124/mol.110.065714.

(31)   Saline, M.; Badertscher, L.; Wolter, M.; Lau, R.; Gunnarsson, A.; Jacso, T.; Norris, T.; Ottmann, C.; Snijder, A. AMPK and AKT Protein Kinases Hierarchically Phosphorylate the N-Terminus of the FOXO1 Transcription Factor, Modulating Interactions with 14-3-3 Proteins. *J. Biol. Chem.* **2019**, *294* (35), 13106–13116. https://doi.org/10.1074/jbc.RA119.008649.

(32)   Tzivion, G.; Dobson, M.; Ramakrishnan, G. FoxO Transcription Factors; Regulation by AKT and 14-3-3 Proteins. *Biochim. Biophys. Acta BBA - Mol. Cell Res.* **2011**, *1813* (11), 1938–1945. https://doi.org/10.1016/j.bbamcr.2011.06.002.

(33)   Ji, L.; Wang, Q.; Liu, M.; Zhu, C.; Xiao, Y.; Han, J.; Fang, Y.; Ye, J.; Yin, J.; Wei, L. The

14-3-3 Protein YWHAB Inhibits Glucagon-Induced Hepatic Gluconeogenesis through Interacting

with the Glucagon Receptor and FOXO1. *FEBS Lett.* **2021**, *595* (9), 1275–1288.

https://doi.org/10.1002/1873-3468.14063.

(34)   Benchoula, K.; Arya, A.; Parhar, I. S.; Hwa, W. E. FoxO1 Signaling as a Therapeutic

Target for Type 2 Diabetes and Obesity. *Eur. J. Pharmacol.* **2021**, *891*, 173758.

https://doi.org/10.1016/j.ejphar.2020.173758.

(35)   van Veldhuisen, T. W.; Altenburg, W. J.; Verwiel, M. A. M.; Lemmens, L. J. M.; Mason,

A. F.; Merkx, M.; Brunsveld, L.; van Hest, J. C. M. Enzymatic Regulation of Protein-Protein

Interactions in Artificial Cells. *Adv. Mater. n/a* (n/a), 2300947.

https://doi.org/10.1002/adma.202300947.

(36)   Zhang, M.; Jang, H.; Li, Z.; Sacks, D. B.; Nussinov, R. B-Raf Autoinhibition in the

Presence and Absence of 14-3-3. *Structure* **2021**, *29* (7), 768-777.e2.

https://doi.org/10.1016/j.str.2021.02.005.

(37)   Obsilova, V.; Obsil, T. The 14-3-3 Proteins as Important Allosteric Regulators of Protein

Kinases. *Int. J. Mol. Sci.* **2020**, *21* (22), 8824. https://doi.org/10.3390/ijms21228824.

(38)   Park, E.; Rawson, S.; Li, K.; Kim, B.-W.; Ficarro, S. B.; Pino, G. G.-D.; Sharif, H.; Marto,

J. A.; Jeon, H.; Eck, M. J. Architecture of Autoinhibited and Active BRAF–MEK1–14-3-3

Complexes. *Nature* **2019**, *575* (7783), 545–550. https://doi.org/10.1038/s41586-019-1660-y.

(39)   Molzan, M.; Schumacher, B.; Ottmann, C.; Baljuls, A.; Polzien, L.; Weyand, M.; Thiel, P.;

Rose, R.; Rose, M.; Kuhenne, P.; Kaiser, M.; Rapp, U. R.; Kuhlmann, J.; Ottmann, C. Impaired

Binding of 14-3-3 to C-RAF in Noonan Syndrome Suggests New Approaches in Diseases with

Increased Ras Signaling. *Mol. Cell. Biol.* **2010**, *30* (19), 4698–4711.

https://doi.org/10.1128/MCB.01636-09.

(40)   Maurer, G.; Tarkowski, B.; Baccarini, M. Raf Kinases in Cancer–Roles and Therapeutic

Opportunities. *Oncogene* **2011**, *30* (32), 3477–3488. https://doi.org/10.1038/onc.2011.160.

(41)   Holderfield, M.; Deuker, M. M.; McCormick, F.; McMahon, M. Targeting RAF Kinases for

Cancer Therapy: BRAF-Mutated Melanoma and Beyond. *Nat. Rev. Cancer* **2014**, *14* (7), 455–

467. https://doi.org/10.1038/nrc3760.

(42)   Villanueva, J.; Vultur, A.; Herlyn, M. Resistance to BRAF Inhibitors: Unraveling

Mechanisms and Future Treatment Options. *Cancer Res.* **2011**, *71* (23), 7137–7140.

https://doi.org/10.1158/0008-5472.CAN-11-1243.

(43)   Kenanova, D. N.; Visser, E. J.; Virta, J. M.; Sijbesma, E.; Centorrino, F.; Vickery, H. R.;

Zhong, M.; Neitz, R. J.; Brunsveld, L.; Ottmann, C.; Arkin, M. R. A Systematic Approach to the

Discovery of Protein–Protein Interaction Stabilizers. *ACS Cent. Sci.* **2023**.

https://doi.org/10.1021/acscentsci.2c01449.

Chapter 5 Beyond 14-3-3: Application of the Disulfide Tethering Screening Technology to Novel Protein-Protein Interaction Platforms
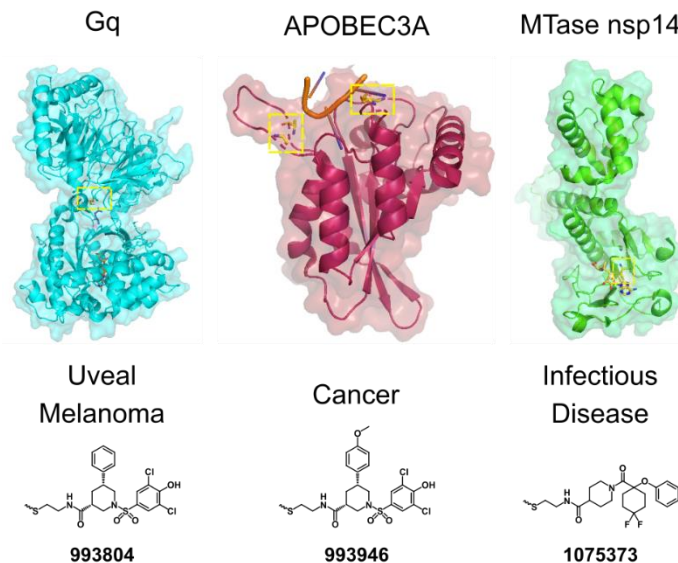
ABSTRACT: The versatility and applicability of the disulfide tethering technology resulted in the discovery and development of selective protein-protein interaction stabilizers for a variety of biologically interesting proteins within the 14-3-3/client stabilization model system. The screen produced multiple scaffolds for hit-to-lead optimization efforts with promising bioavailability and cellular activity. With a greater understanding of the guidelines behind a successful disulfide tethering screening campaign, we set out to expand our technology beyond the realm of 14-3-3 and its clients. Through multiple constructive collaborations, we performed the screen and validation experiments for three target proteins with a broad range of functions and roles in cell signaling: the guanine nucleotide binding protein (Gq) involved in uveal melanoma; apolipoprotein B mRNA editing enzyme, catalytic polypeptide-like 3A (APOBEC3A) involved in cancer and rare disease; SARS-CoV-2 nsp14 (N7-guanine)-methyltransferase (MTase nsp14) involved in infectious disease. These drug discovery efforts resulted in 10 compounds with promising activity for both Gq and APOBEC3A as well as a promising range of small molecule binders to MTase nsp14 awaiting validation. The success of these campaigns underlines the

93

utility of fragment-based drug discovery and disulfide tethering as a starting point for the development of biological probes and potential therapeutics.

INTRODUCTION

Having defined some of the key features of a successful disulfide tethering campaign and hit-to-lead discovery endeavors, we directed our attention to expanding the scope of the technology to diverse systems beyond 14-3-3. In particular, we wanted to probe the ability of the screen to produce interesting chemical scaffolds under three distinct categories – firstly, to selectively target a disease mutant over wildtype protein; secondly, to utilize an engineered, non-native cysteine residue proximal to the binding site of interest;[1–3] lastly, to selectively engage a desired native cysteine proximal to the binding site of interest over other native cysteines in the protein.[4–6] Thus, the screen would be able to address a number of different challenges in drug discovery and provide a robust, precise, and systematic platform for biological probe and therapeutic development. In order to accomplish this goal, we partnered with a number of different labs within and without UCSF.

The guanine nucleotide-binding protein Gq subunit α (Gq) was used to determine selectivity for disease inducing mutant over wildtype. Approximately 90% of all uveal melanomas are a result of mutations in Gq. Q209L and Q209P seemingly account for the majority of the mutations that lead to oncogenesis.[7,8] 50% of the uveal melanoma cases metastasize into the liver, lungs, and bone with poor prognosis for the patient (4-15 month survival).[9–11] As the second most common form of melanoma, this presents a therapeutic window of opportunity to address a vulnerable patient population.[12] The difficulty with targeting the oncogenic mutants of Gq arises from the structural similarity between the mutants and wildtype which is critical and necessary for cellular function.[13–16] A cysteine residue, C219, proximal to the Gq Q209 mutant in the Switch II region of the protein, provides the perfect target for a disulfide tethering campaign evaluating the ability of the screen to produce selective compounds with therapeutic implications (**Figure 5.1A**).[17]
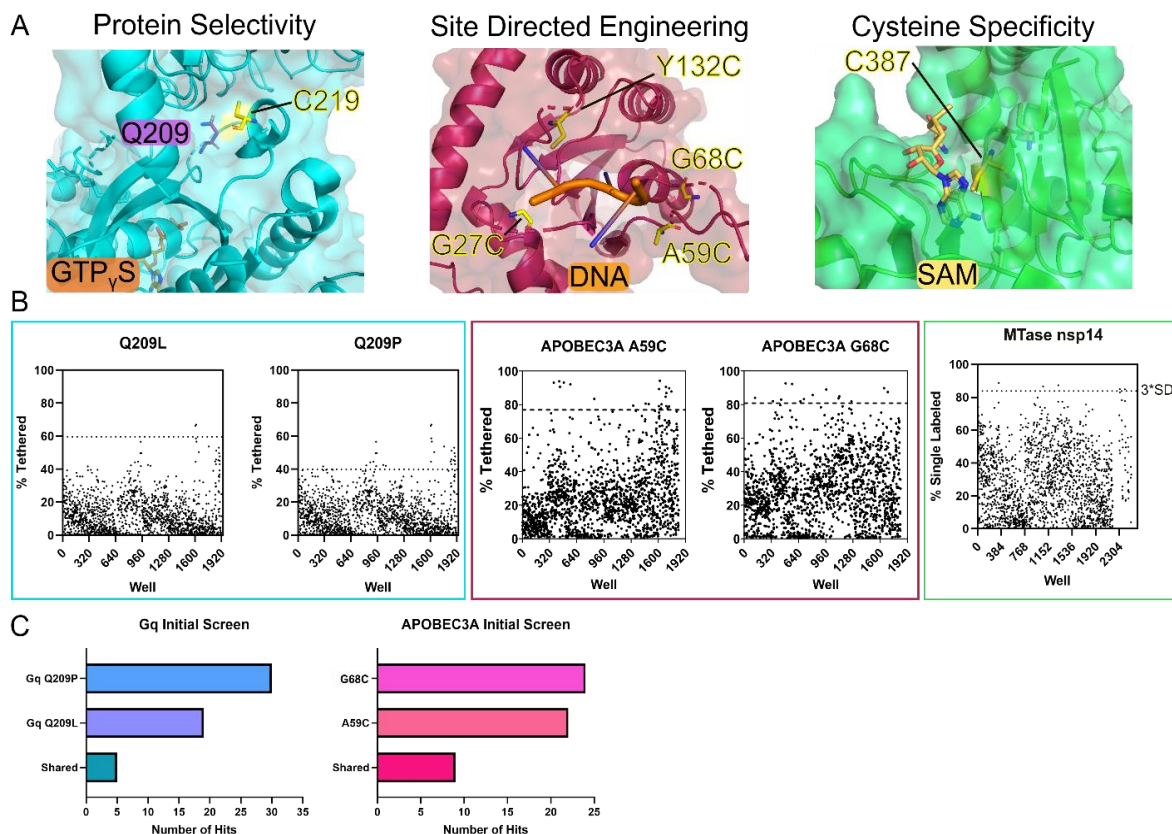
Figure 5.1 Initial screen results and strategies for Gq, APOBEC3A, and SARS-CoV-2 MTase nsp14. (A) Left: x-ray crystal structure for Gq (cyan) bound to GTPγS (orange) highlighting disease relevant residue Q209 (purple) and target cysteine C219 (yellow). Middle: x-ray crystal structure of APOBEC3A (red) bound to DNA (orange) with four mutated target cysteine residues (G27C, A59C, G68C, and Y132C) highlighted in yellow. Right: x-ray crystal structure of MTase nsp14 (green) bound to SAM (yellow) and target cysteine C387 (yellow). PDB IDs from left to right: 3AH8, 5KEG, and 7TW7. (B) Initial screen results for Gq Q209L and Q209P (cyan box), APOBEC3A A59C and G68C (maroon box), and MTase nsp14 (green box). Dotted line shows 3*SD above average and compounds above this line are considered hits. (C) Chart depicting number of selective hits for Gq Q209P vs Q209L (blue) and APOBEC3A G68C vs A59C (pink) as well as overlapping hits.

Apolipoprotein B mRNA editing enzyme, catalytic polypeptide-like 3A (APOBEC3A) functions as

an integral part of the innate immune system and is critical to response against viral infection.

As such, it has implications in SARS-CoV-2 and HPV treatment.[18–23] Additionally, recent

literature suggests that within the family of 7 APOBEC3 DNA cytosine deaminases expressed in

mammalian cells, only APOBEC3A has the profile of an oncogenic driver, inducing C-to-G and

C-to-T mutations in DNA which are characteristic of over half of all cancer types.[24–28]

Site-directed mutagenesis was employed to engineer four cysteine residues within the flexible

regions of the DNA binding groove of APOBEC3A in order to provide site-specific targets for disulfide exchange (**Figure 5.1A**).[29] The goal of this project was to discover whether fragment hits from an engineered system could still produce efficacious inhibitors to APOBEC3A activity that could then be modified to potent, noncovalent inhibitors with biological activity.

The final model system was a joint effort to target the SARS-CoV-2 nsp14 (N7-guanine)-methyltransferase (MTase nsp14) in an effort to determine whether the unique chemical environment of the binding groove is distinct enough to produce selective fragment hits that minimally or do not engage other cysteine residues within the protein and to understand some of the underlying mechanisms of reactivity (solvent exposure, local environment, presence of native ligand, etc.). MTase nsp14 is the enzyme responsible for capping the viral RNA in order to increase stability, increase translation of viral mRNA within mammalian cells, and evade the innate immune system.[30–33] As such, it is a target of paramount interest at the wake of the pandemic and the appearance of viral strains resistant to treatment and vaccination. For the disulfide screen, we utilized an MTase nsp14 TELSAM fusion protein containing 11 cysteines, three which occupied the S-adenosylmethionine (SAM) binding site of the enzyme, and only one of which was optimal for tethering by docking and *in silico* visualization (**Figure 5.1A**).[34]

The three proteins discussed above provide a model for fundamental challenges within drug discovery: off-target engagement of wildtype protein, absence of covalent handle within binding site of interest, and off-target cysteines producing false positives due to nonspecific interactions between fragments and protein of interest. Assessing the efficacy and customizability of the disulfide tethering screen in order to address these challenges provided crucial data on the scope of the screen beyond the 14-3-3 model system. We were successful in obtaining 10 hit compounds which showed efficacy in initial activity assays for the Gq and APOBEC3A systems as well as a successful starting point in the MTase nsp14 system which will be taken into validation and activity assays in the near future. The Gq compounds provided an exciting

conserved chemical motif which led to initial structure-activity relationship (SAR) chemistry for optimized disulfide and irreversible covalent compounds. APOBEC3A produced 4 distinct classes of hit fragment and some interesting overlap in active compounds from two separate tethering points. This could have interesting implications for fragment merging alongside traditional hit-to-lead optimization efforts. Finally, MTase nsp14 produced a wide range of high binding compounds which required triaging against a cysteine-to-serine mutant and provided useful information on whether the % tethering or % single labeling events are the most important metric for a successful screen. With these crucial pieces of data and the information learned from 14-3-3/client protein-protein interaction stabilization discussed in Chapter 3, we have a greater understanding of the capabilities of the disulfide tethering screen and its application as a systematic approach to the modulation of protein-protein, protein-nucleotide, and protein-ligand interactions. Thus, we have produced a powerful tool for addressing challenging and versatile questions in biology and medicine.

RESULTS AND DISCUSSION

Gq, APOBEC3A, and MTase nsp14 Initial Screen. Gq contains a cysteine, C219, proximal to the Switch II region and the oncogenic Q209L and Q209P mutants which was targeted by the disulfide tethering screen. Protein stability, β-mercaptoethanol (BME) optimization, and cysteine reactivity were assessed for optimal screening conditions (Supplemental). The two Gq mutant screens was performed using 200 nM Gq Q209L and Gq Q209P (individually), 200 µM fragment, and 250 µM β-mercaptoethanol (BME). BME acted to facilitate disulfide exchange and as a competitor for nonselective transient interactors of C219. After a 3 hour incubation period, samples were measured via intact-protein LC/MS. In the context of APOBEC3A, four cysteine mutants (G27C, A59C, G68C, and Y132C) were tested for stability, BME engagement, and iodoacetamide labeling. G68C showed the highest stability and lowest double-labeling events in the BME and iodoacetamide samples, however A59C was of a higher priority. Thus, to

maximize the potential hits found in the screen and surveil multiple points of the APOBEC3A

RNA binding site, we decided to perform the screen on both A59C and G68C APOBEC3A

mutants. The screens were performed using the same conditions in order to have a fair

comparison and assess overlapping and selective hits: 500 nM APOBEC3A variant, 200 µM

fragment, and 125 µM BME due to instability of A59C at higher concentrations. MTase nsp14

was screened under the optimized conditions of 250 nM protein, 200 µM fragment, and 500 µM

BME.

The % tethering – defined for all clients as the quotient of the % labeling of fragment to target

protein over the summation of the % labeling of all target moieties then multiplied by 100 –

threshold for hit selection was three standard deviations (3*SD) above average % tethering for

the particular screening condition with the exception of APOBEC3A G68C and MTase nsp14

which had such a high average % tethering that some hit fragments were selected from two

standard deviations (2*SD) above average (**Figure 5.1B**). The Gq Q209P screen yielded 30 hit

compounds with a 40% tethering threshold, Gq Q209L yielded 19 hits with a 60% tethering

threshold, and there were 5 compounds shared between the two mutants. The APOBEC3A

A59C screen yielded 30 selective hits with a 77% tethering threshold and the APOBEC3A G68C

screen yielded 9 selective hits with an 81% tethering threshold, and 5 shared hits (**Figure 5.1C**).

The MTase nsp14 C387 screen yielded 5 hits above 3*SD when analyzing single labeling due

to an exceptionally high average % tethering even under high BME conditions. 89 hits with high

single labeling and total tethering above the 2*SD 80% tethering threshold were selected for

follow-up mass spectrometry dose response validation experiments (**Figure 5.1B**).

Gq Validation, Selectivity, and Activity Assays. The 19 Q209L hits, 30 Q209P hits, and 5

shared hits were taken forward into a mass spectrometry-based compound dose response

(MSDR) in order to quantify dose-dependent fragment engagement of protein (compound DR_{50};

Figure 5.2) and select against false positives or artifacts. The initial screen assay conditions
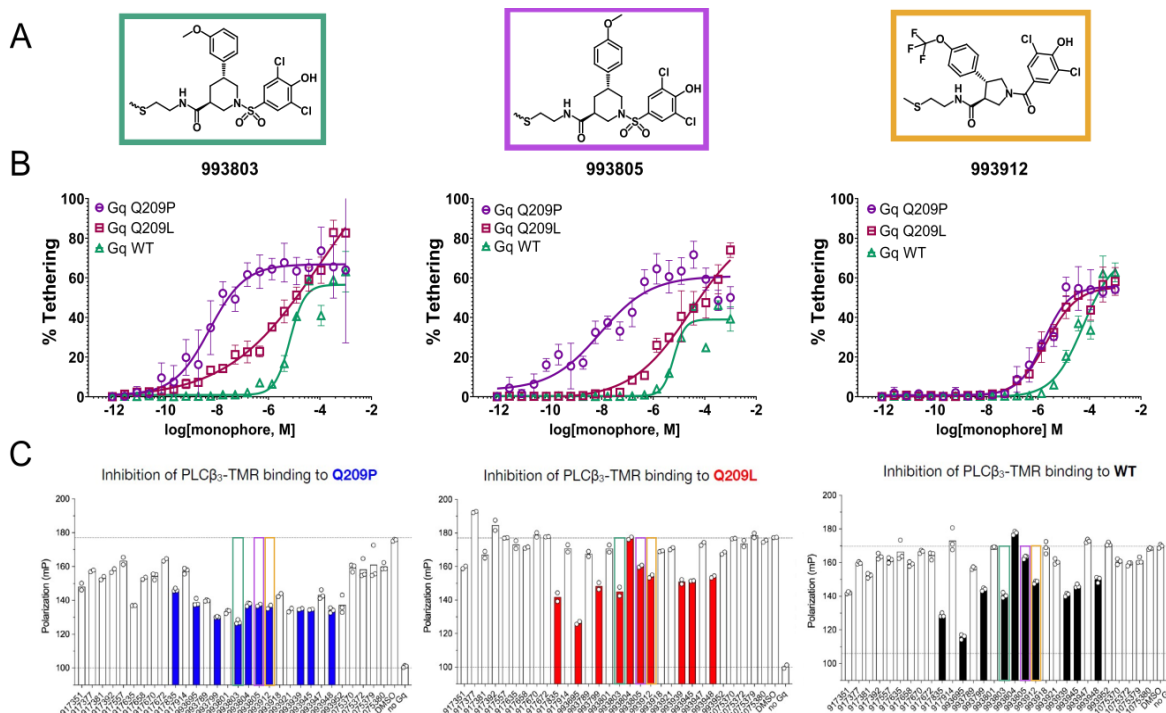
98

Figure 5.2 Gq validation and activity assay results. (A) Chemical structures of best selective inhibitors for Gq Q209P vs WT. (B) Mass spec dose response (MSDR) curves for **993803**, **993805**, and **993912** showing selectivity in binding for Q209P over WT Gq. **993912** showed equivalent engagement of Q209L. (C) Fluorescence anisotropy activity assays for top compounds with Q209P (blue), Q209L (red) and WT (black). **993803**, **993805**, and **993912** are outlined in green, purple, and yellow respectively.

were used apart from a 3-fold fragment titration series from 2 mM to 900 nM. The 54

compounds were also tested against the Gq wildtype protein (Gq WT) in order to discover

selective binders which would only engage the disease mutant targets. Of the compounds

assessed in the MSDR, 32 bound with greater affinity to the Gq mutants than to Gq wildtype

and were taken forward into the fluorescence polarization-based functional assay. The

functional assay measured the fragments' ability to disrupt Gq binding to TAMRA-labeled Gq

client PCLβ3 (PCLβ3-TMR) peptide. The assay was performed at a single concentration of

compound well above the determined DR_{50}. Final assay conditions were 25 nM PCLβ3 peptide,

100 μM fragment, and 100 μM GTPγS. Gq Q209L and Gq WT were at a 1 μM concentration

and Gq Q209P was at 5.25 μM to maximize signal. 10 compounds were determined to be

99

functionally active in disrupting PCLβ₃/Gq binding in one or both of the mutant Gq proteins with a lesser or no effect on Gq WT (**Table 5.1** and **Figure 5.2C**).

Table 5.1 Biophysical properties of Gq hit compounds

SMDC ID	DR$_{50}$ (µM) Q209P	DR$_{50}$ (µM) Q209L	DR$_{50}$ (µM) WT
917835	0.3	48	236
993695	2.0	>2000	31
993799	305	>2000	13
993803	5 nm	102	6.8
993804	>2000	>2000	4.7
993805	9 nm	29	6.3
993912	1.7	2.2	57
993939	14	3.0	29
993945	8.2	1.9	25
993948	5.4	2.6	0.8

APOBEC3A Validation and Activity Assays. 30 of the 35 APOBEC3A A59C hits were available to be taken forward into MSDR validation experiments. 34 compounds were tested in the APOBEC3A G68C MSDR follow-up. Due to the high 3*SD % tethering threshold of the G68C screen, the highest binding compounds from the 2*SD % tethering threshold were also taken into the MSDR in order to provide a broader platform, larger chemical diversity, and increase odds of finding active molecules. 9 of the compounds tested in the MSDR were shared hits between the two screens. The MSDR conditions reflected the initial screening conditions with the exception of the 3-fold dilution of compound. 27 of the 30 compounds tested for APOBEC3A A59C and 28 out of the 34 compounds tested for G68C showed promise in the MSDR with top compounds showing DR$_{50}$ values in the nM range **(Figure 5.3**, **Table 5.2)** and were taken forward into the activity assay. The APOBEC3A activity assay assessed the binding of the APOBEC3A mutants and wildtype control (APOBEC3A WT) to a 5'-TAMRA-labeled DNA tracer via fluorescence polarization. The APOBEC3A A59C and G68C activity assays were

performed as a single point experiment in two replicates using 1 μM protein, 200 μM compound, and 15 nM DNA tracer. The APOBEC3A WT control assay was performed using 10 ng/well protein, 200 μM compound, and 100 nM DNA tracer (**Figure 5.3C**). Of the 55 total compounds tested, 10 showed promising activity with inhibition of APOBEC3A WT and some attenuated activity in the mutants, potentially indicating activity even without covalent engagement of the target. This resulted in a series of promising scaffolds for hit-to-lead optimization efforts.

Table 5.2 Biophysical properties of APOBEC3A hit compounds

SMDC ID	Activity Assay ID	Selectivity	DR_{50} (μM) A59C	DR_{50} (μM) G68C
994471	**42**	**A59C**	**6.79**	**–**
917571	**15**	**G68C**	**–**	**0.01**
993805	**35**	**Both**	**8.25**	**5.44**
993946	**36**	**Both**	**0.82**	**0.002**
967291	32	A59C	3.54	–
917553	14	A59C	13.3	–
994466	40	A59C	30.0	–
967187	29	A59C	34.0	–
917269	5	G68C	–	4.89
916961	1	G68C	–	3.46
917692	16	G68C	–	4.32

MTase nsp14 Initial Screen and Validation. The high % tethering average of the MTase nsp14 screen was unprecedented and potentially indicative of multiple binding events to off-target cysteine residues (**Figure 5.1B**). In the initial iodoacetamide experiments, there was a high abundance of double labeling and a lower instance of a third labeling event. In order to triage the potential for multiple labeling, we counter-screened the 89 hits using a C387S mutant and took the difference between the two as the on-target engagement profile of the compounds. 26 compounds showed dose dependent engagement to MTase nsp14, however, when compared to the C387S mutant, compounds showed either similar or better binding in the case
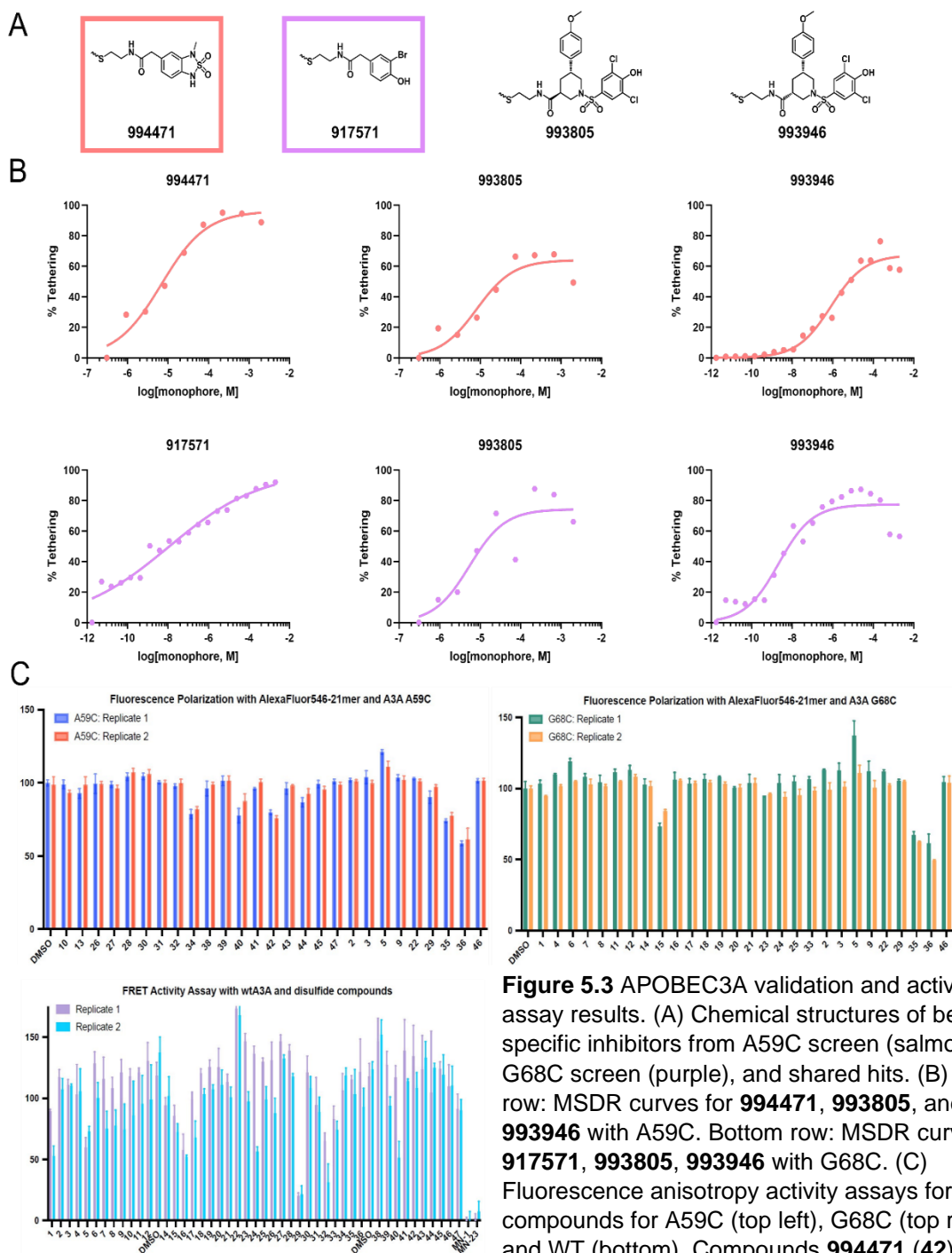
Figure 5.3 APOBEC3A validation and activity assay results. (A) Chemical structures of best specific inhibitors from A59C screen (salmon), G68C screen (purple), and shared hits. (B) Top row: MSDR curves for **994471**, **993805**, and **993946** with A59C. Bottom row: MSDR curves for **917571**, **993805**, **993946** with G68C. (C) Fluorescence anisotropy activity assays for top compounds for A59C (top left), G68C (top right), and WT (bottom). Compounds **994471** (**42**), **993805** (**35**), and **993946** (**36**) showed inhibition of PCLβ₃ in WT assay.

of the mutant (**Figure 5.4A** and **5.4B**). We also tested 20 covalent compounds found from a previous docking campaign in a time course MSDR. Compounds **1124888** and **1124891** showed the greatest similarity in single and total labeling of the protein (**Figure 5.4C** and **5.4D**).
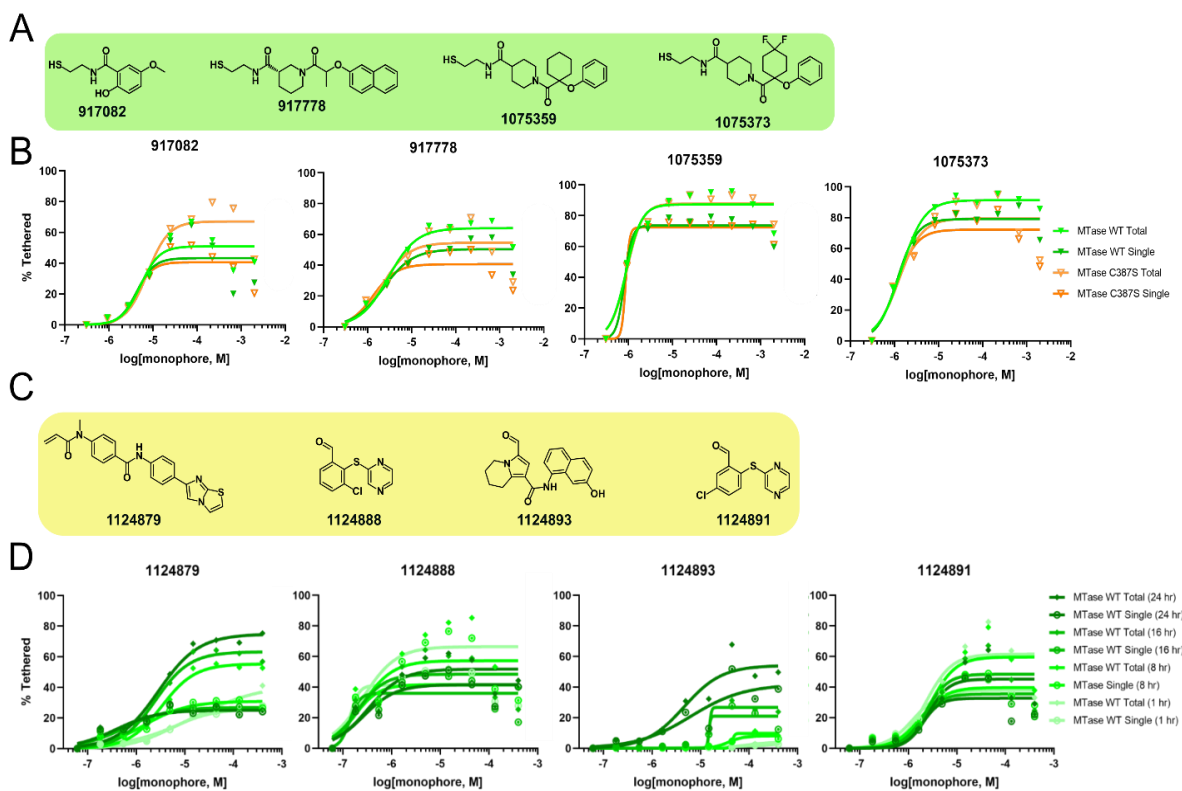
Figure 5.4 MTase MSDR validation assays for disulfide and covalent compounds. (A) Chemical structures of top 4 hits from MTase screen. (B) MSDR curves for top four disulfide compounds showing WT total and single labeling (green) and C387S total and single labeling (orange). (C) Chemical structures of four top covalent compounds from docking campaign. (D) MSDR curves for top four covalent compounds showing single and total labeling over the course of 1hr, 8hr, 16hr, and 24hr incubation time.

When compared to mutant, we saw similar non-specificity for C387 as with the disulfides. This could be due to two other cysteines in the SAM binding pocket (C382 and C399).

CONCLUSIONS

The disulfide tethering technology is a versatile platform for the discovery of small molecule fragments as selective and efficacious platforms for hit-to-lead development. Of the three systems that were tested, we were able to discover approximately 10 scaffolds, often with unique chemical properties, which engaged the target, validated in the MSDR, and showed activity as inhibitors of ligand binding. Further activity assay optimization and compound optimization efforts have the potential to characterize and design novel probes and potential therapeutics for a broad range of protein-protein interactions and diseases, respectively.

The 10 best compounds for the Gq project show moderate selectivity for the Q209P mutant over Q209L and WT. Thus, Q209P appears to have the most viability as a target for compound optimization efforts. Compounds **993805** and **993912** showed the greatest selectivity in inhibition of PCLβ$_3$ binding for Q209P vs WT and shared a similar chemical motif to other hit fragments including the base fragment **992695** (**Table 5.1**). Currently, the focus for the Gq project is to recapitulate the results of the single-point activity assay under optimized conditions and expand the assay to a full fluorescence polarization fragment dose response (FPDR) series utilizing our best compound (**993695**) and a commercially available inhibitor of the Gq/PCLβ$_3$ complex. Protein titrations to determine decrease in cooperativity will follow upon determination of compound EC$_{50}$ values. The results of these assays will inform follow-up chemical optimization, building two libraries: a disulfide SAR series focused on non-covalent interactions between fragment and protein and an SAR series of alternative covalent warheads and linker lengths for greater bioavailability.

The 10 best compounds in the APOBEC3A MSDR could be categorized into distinct chemical moieties, most of which were characterized by large aromatic rings with electron withdrawing accessory groups. The fluorescence polarization assay had an interesting activity profile wherein there was seeming inhibition of the wildtype protein but attenuated response in both of the mutants used in the original tethering screen (**Figures 5.1B** and **5.3C**). Compounds **994471** and **993800** showed the best activity for the A59C specific compounds; compound **917571** showed the best activity for the G68C specific compounds; compounds **993946** and **993805** showed the best activity for the nonselective compounds. However, only compound **917571** had activity when tested against APOBEC3A WT. Instead, compounds **916961**, **917269**, **917692**, **967187**, and **967291** showed the greatest activity (**Figure 5.3C**). This may be the result of the assay conditions under which the compounds were tested. The DNA tracer does not bind tightly to APOBEC3A at pH higher than 7.4. However, the cysteine thiol has a pKa value of 8.3. Thus,

the kinetics of the disulfide reaction between the compound and protein may be unfavorable or slowed under the conditions necessary for APOBEC3A/DNA binding. It is unclear why the WT, which in theory is not covalently targeted by the compounds, shows better compound efficacy. Single-point experiments are limited in scope however, and an extended FPDR at multiple timepoints beyond the 3-hour incubation period may be necessary to understand these results. Another approach would be to develop a small irreversible covalent warhead SAR series of compounds based on the disulfide scaffolds and measure APOBEC3A A59C and G68C engagement and DNA binding inhibition over a series of timepoints. From previous SAR with 14-3-3, α-chloroketones seem to have the most rapid kinetics followed by chloroacetamides and then acrylamides. In this way, even if FPDR conditions facilitate a slower reaction, once fragment is engaged, there is no disulfide exchange and loss of binding. Covalent binders may also be more conducive to structural studies for APOBEC3A/fragment complex visualization.

Comparisons between the MTase nsp14 WT and C387S mutant have shown engagement of both proteins to similar degrees, if not better in the case of the mutant. This indicates off-target binding. Subsequent mutagenesis of proximal cysteines C382 and C399 will give greater insight into which cysteine has the greatest interaction profile with both disulfide and covalent compounds. MTase Glo activity assays will also determine which compounds show inhibition of MTase activity and SAM occlusion from the binding site.

Here, with the collaboration of the Manglik, Harki, Fujimori, and Shoichet labs, I have successfully expanded the reach of the disulfide tethering screen beyond the initial 14-3-3 model system. Although the application delved into the more explored field of inhibitor fragment-based drug discovery, these proteins are representative of a number of diverse and powerful applications of the technology including: selectivity for a specific disease mutant in the case of Gq, site-directed mutagenesis of an engineered cysteine proximal to binding site of interest with APOBEC3A, and selectivity for a specific cysteine residue amidst multiple other

105

native cysteines in the case of MTase nsp14. Even more importantly, all of the targets are central to disease and have the potential for great impact in cancer, rare disease, and infectious disease. The utility of the disulfide tethering screen for rapid, precise, and quantitative discovery of modulators for a plethora of "undruggable," disease-relevant protein-protein interactions exemplifies the power of this tool for basic biology and precision medicine.

REFERENCES

(1)   Sijbesma, E.; Hallenbeck, K. K.; Andrei, S. A.; Rust, R. R.; Adriaans, J. M. C.; Brunsveld, L.; Arkin, M. R.; Ottmann, C. Exploration of a 14-3-3 PPI Pocket by Covalent Fragments as Stabilizers. *ACS Med. Chem. Lett.* **2021**, *12* (6), 976–982. https://doi.org/10.1021/acsmedchemlett.1c00088.

(2)   Sijbesma, E.; Hallenbeck, K. K.; Leysen, S.; de Vink, P. J.; Skóra, L.; Jahnke, W.; Brunsveld, L.; Arkin, M. R.; Ottmann, C. Site-Directed Fragment-Based Screening for the Discovery of Protein–Protein Interaction Stabilizers. *J. Am. Chem. Soc.* **2019**, *141* (8), 3524–3531. https://doi.org/10.1021/jacs.8b11658.

(3)   Sijbesma, E.; Somsen, B. A.; Miley, G. P.; Leijten-van de Gevel, I. A.; Brunsveld, L.; Arkin, M. R.; Ottmann, C. Fluorescence Anisotropy-Based Tethering for Discovery of Protein–Protein Interaction Stabilizers. *ACS Chem. Biol.* **2020**, *15* (12), 3143–3148. https://doi.org/10.1021/acschembio.0c00646.

(4)   Maurais, A. J.; Weerapana, E. Reactive-Cysteine Profiling for Drug Discovery. *Curr. Opin. Chem. Biol.* **2019**, *50*, 29–36. https://doi.org/10.1016/j.cbpa.2019.02.010.

(5)   Van Horn, K. S.; Wang, D.; Medina-Cleghorn, D.; Lee, P. S.; Bryant, C.; Altobelli, C.; Jaishankar, P.; Leung, K. K.; Ng, R. A.; Ambrose, A. J.; Tang, Y.; Arkin, M. R.; Renslo, A. R. Engaging a Non-Catalytic Cysteine Residue Drives Potent and Selective Inhibition of Caspase-6. *J. Am. Chem. Soc.* **2023**. https://doi.org/10.1021/jacs.2c12240.

(6)   Shraga, A.; Resnick, E.; Gabizon, R.; London, N. Chapter Eight - Covalent Fragment Screening. In *Annual Reports in Medicinal Chemistry*; Ward, R. A., Grimster, N. P., Eds.; The Design of Covalent-Based Inhibitors; Academic Press, 2021; Vol. 56, pp 243–265. https://doi.org/10.1016/bs.armc.2021.04.001.

(7)   Terai, M.; Shimada, A.; Chervoneva, I.; Hulse, L.; Danielson, M.; Swensen, J.; Orloff, M.; Wedegaertner, P. B.; Benovic, J. L.; Aplin, A. E.; Sato, T. Prognostic Values of G-Protein Mutations in Metastatic Uveal Melanoma. *Cancers* **2021**, *13* (22), 5749. https://doi.org/10.3390/cancers13225749.

(8)   Silva-Rodríguez, P.; Fernández-Díaz, D.; Bande, M.; Pardo, M.; Loidi, L.; Blanco-Teijeiro, M. J. GNAQ and GNA11 Genes: A Comprehensive Review on Oncogenesis, Prognosis and Therapeutic Opportunities in Uveal Melanoma. *Cancers* **2022**, *14* (13), 3066. https://doi.org/10.3390/cancers14133066.

(9)   Ma, J.; Weng, L.; Bastian, B. C.; Chen, X. Functional Characterization of Uveal Melanoma Oncogenes. *Oncogene* **2021**, *40* (4), 806–820. https://doi.org/10.1038/s41388-020-01569-5.

(10)   Maziarz, M.; Leyme, A.; Marivin, A.; Luebbers, A.; Patel, P. P.; Chen, Z.; Sprang, S. R.; Garcia-Marcos, M. Atypical Activation of the G Protein Gαq by the Oncogenic Mutation Q209P. *J. Biol. Chem.* **2018**, *293* (51), 19586–19599. https://doi.org/10.1074/jbc.RA118.005291.

(11)   Lapadula, D.; Farias, E.; Randolph, C. E.; Purwin, T. J.; McGrath, D.; Charpentier, T. H.; Zhang, L.; Wu, S.; Terai, M.; Sato, T.; Tall, G. G.; Zhou, N.; Wedegaertner, P. B.; Aplin, A. E.; Aguirre-Ghiso, J.; Benovic, J. L. Effects of Oncogenic Gαq and Gα11 Inhibition by FR900359 in Uveal Melanoma. *Mol. Cancer Res.* **2019**, *17* (4), 963–973. https://doi.org/10.1158/1541-7786.MCR-18-0574.

(12)   Andreoli, M. T.; Mieler, W. F.; Leiderman, Y. I. Epidemiological Trends in Uveal Melanoma. *Br. J. Ophthalmol.* **2015**, *99* (11), 1550–1553. https://doi.org/10.1136/bjophthalmol-2015-306810.

(13)   Corson, T. W.; Sishtla, K. Towards a Novel Therapy for Uveal Melanoma: Targeting Oncogenic Gαq. *Invest. Ophthalmol. Vis. Sci.* **2012**, *53* (14), 6877.

(14)   Campbell, A. P.; Smrcka, A. V. Targeting G Protein-Coupled Receptor Signalling by

Blocking G Proteins. *Nat. Rev. Drug Discov.* **2018**, *17* (11), 789–803.

https://doi.org/10.1038/nrd.2018.135.

(15)   Zhang, Q.; Haak, A. J.; Sjögren, B. Regulator of G Protein Signaling 2 Inhibits Gαq-

Dependent Uveal Melanoma Cell Growth. *J. Biol. Chem.* **2022**, *298* (6).

https://doi.org/10.1016/j.jbc.2022.101955.

(16)   Lapadula, D.; Benovic, J. L. Targeting Oncogenic Gαq/11 in Uveal Melanoma. *Cancers*

2021, *13* (24), 6195. https://doi.org/10.3390/cancers13246195.

(17)   Nishimura, A.; Kitano, K.; Takasaki, J.; Taniguchi, M.; Mizuno, N.; Tago, K.; Hakoshima,

T.; Itoh, H. Structural Basis for the Specific Inhibition of Heterotrimeric Gq Protein by a Small

Molecule. *Proc. Natl. Acad. Sci. U. S. A.* **2010**, *107* (31), 13666–13671.

https://doi.org/10.1073/pnas.1003553107.

(18)   Nakata, Y.; Ode, H.; Kubota, M.; Kasahara, T.; Matsuoka, K.; Sugimoto, A.; Imahashi,

M.; Yokomaku, Y.; Iwatani, Y. Cellular APOBEC3A Deaminase Drives Mutations in the SARS-

CoV-2 Genome. *Nucleic Acids Res.* **2023**, *51* (2), 783–795.

https://doi.org/10.1093/nar/gkac1238.

(19)   Kim, K.; Calabrese, P.; Wang, S.; Qin, C.; Rao, Y.; Feng, P.; Chen, X. S. The Roles of

APOBEC-Mediated RNA Editing in SARS-CoV-2 Mutations, Replication and Fitness. *Sci. Rep.*

2022, *12* (1), 14972. https://doi.org/10.1038/s41598-022-19067-x.

(20)   Warren, C. J.; Westrich, J. A.; Doorslaer, K. V.; Pyeon, D. Roles of APOBEC3A and

APOBEC3B in Human Papillomavirus Infection and Disease Progression. *Viruses* **2017**, *9* (8),

233. https://doi.org/10.3390/v9080233.

(21)   Kondo, S.; Wakae, K.; Wakisaka, N.; Nakanishi, Y.; Ishikawa, K.; Komori, T.; Moriyama-Kita, M.; Endo, K.; Murono, S.; Wang, Z.; Kitamura, K.; Nishiyama, T.; Yamaguchi, K.; Shigenobu, S.; Muramatsu, M.; Yoshizaki, T. APOBEC3A Associates with Human Papillomavirus Genome Integration in Oropharyngeal Cancers. *Oncogene* **2017**, *36* (12), 1687–1697. https://doi.org/10.1038/onc.2016.335.

(22)   Papini, C.; Wang, Z.; Kudalkar, S. N.; Schrank, T. P.; Tang, S.; Sasaki, T.; Wu, C.; Tejada, B.; Ziegler, S. J.; Xiong, Y.; Issaeva, N.; Yarbrough, W. G.; Anderson, K. S. Exploring APOBEC3A and APOBEC3B Substrate Specificity and Their Role in HPV Positive Head and Neck Cancer. *iScience* **2022**, *25* (10), 105077. https://doi.org/10.1016/j.isci.2022.105077.

(23)   Ahasan, M. M.; Wakae, K.; Wang, Z.; Kitamura, K.; Liu, G.; Koura, M.; Imayasu, M.; Sakamoto, N.; Hanaoka, K.; Nakamura, M.; Kyo, S.; Kondo, S.; Fujiwara, H.; Yoshizaki, T.; Mori, S.; Kukimoto, I.; Muramatsu, M. APOBEC3A and 3C Decrease Human Papillomavirus 16 Pseudovirion Infectivity. *Biochem. Biophys. Res. Commun.* **2015**, *457* (3), 295–299. https://doi.org/10.1016/j.bbrc.2014.12.103.

(24)   Law, E. K.; Levin-Klein, R.; Jarvis, M. C.; Kim, H.; Argyris, P. P.; Carpenter, M. A.; Starrett, G. J.; Temiz, N. A.; Larson, L. K.; Durfee, C.; Burns, M. B.; Vogel, R. I.; Stavrou, S.; Aguilera, A. N.; Wagner, S.; Largaespada, D. A.; Starr, T. K.; Ross, S. R.; Harris, R. S. APOBEC3A Catalyzes Mutation and Drives Carcinogenesis in Vivo. *J. Exp. Med.* **2020**, *217* (12), e20200261. https://doi.org/10.1084/jem.20200261.

(25)   Lopez-Bigas, N.; Gonzalez-Perez, A. Are Carcinogens Direct Mutagens? *Nat. Genet.* **2020**, *52* (11), 1137–1138. https://doi.org/10.1038/s41588-020-00730-w.

(26)   Langenbucher, A.; Bowen, D.; Sakhtemani, R.; Bournique, E.; Wise, J. F.; Zou, L.; Bhagwat, A. S.; Buisson, R.; Lawrence, M. S. An Extended APOBEC3A Mutation Signature in Cancer. *Nat. Commun.* **2021**, *12* (1), 1602. https://doi.org/10.1038/s41467-021-21891-0.

(27)   Landry, S.; Narvaiza, I.; Linfesty, D. C.; Weitzman, M. D. APOBEC3A Can Activate the DNA Damage Response and Cause Cell-Cycle Arrest. *EMBO Rep.* **2011**, *12* (5), 444–450. https://doi.org/10.1038/embor.2011.46.

(28)   Law, E. K.; Levin-Klein, R.; Jarvis, M. C.; Kim, H.; Argyris, P. P.; Carpenter, M. A.; Starrett, G. J.; Temiz, N. A.; Larson, L. K.; Durfee, C.; Burns, M. B.; Vogel, R. I.; Stavrou, S.; Aguilera, A. N.; Wagner, S.; Largaespada, D. A.; Starr, T. K.; Ross, S. R.; Harris, R. S. APOBEC3A Catalyzes Mutation and Drives Carcinogenesis in Vivo. *J. Exp. Med.* **2020**, *217* (12), e20200261. https://doi.org/10.1084/jem.20200261.

(29)   Kouno, T.; Silvas, T. V.; Hilbert, B. J.; Shandilya, S. M. D.; Bohn, M. F.; Kelch, B. A.; Royer, W. E.; Somasundaran, M.; Kurt Yilmaz, N.; Matsuo, H.; Schiffer, C. A. Crystal Structure of APOBEC3A Bound to Single-Stranded DNA Reveals Structural Basis for Cytidine Deamination and Specificity. *Nat. Commun.* **2017**, *8* (1), 15024. https://doi.org/10.1038/ncomms15024.

(30)   Lin, S.; Chen, H.; Chen, Z.; Yang, F.; Ye, F.; Zheng, Y.; Yang, J.; Lin, X.; Sun, H.; Wang, L.; Wen, A.; Dong, H.; Xiao, Q.; Deng, D.; Cao, Y.; Lu, G. Crystal Structure of SARS-CoV-2 Nsp10 Bound to Nsp14-ExoN Domain Reveals an Exoribonuclease with Both Structural and Functional Integrity. *Nucleic Acids Res.* **2021**, *49* (9), 5382–5392. https://doi.org/10.1093/nar/gkab320.

(31)   Hsu, J. C.-C.; Laurent-Rolle, M.; Pawlak, J. B.; Wilen, C. B.; Cresswell, P. Translational Shutdown and Evasion of the Innate Immune Response by SARS-CoV-2 NSP14 Protein. *Proc. Natl. Acad. Sci.* **2021**, *118* (24), e2101161118. https://doi.org/10.1073/pnas.2101161118.

(32)   Walter, M.; Chen, I. P.; Vallejo-Gracia, A.; Kim, I.-J.; Bielska, O.; Lam, V. L.; Hayashi, J. M.; Cruz, A.; Shah, S.; Soveg, F. W.; Gross, J. D.; Krogan, N. J.; Jerome, K. R.; Schilling, B.;

Ott, M.; Verdin, E. SIRT5 Is a Proviral Factor That Interacts with SARS-CoV-2 Nsp14 Protein. *PLOS Pathog.* **2022**, *18* (9), e1010811. https://doi.org/10.1371/journal.ppat.1010811.

(33)   Otava, T.; Šála, M.; Li, F.; Fanfrlík, J.; Devkota, K.; Perveen, S.; Chau, I.; Pakarian, P.; Hobza, P.; Vedadi, M.; Boura, E.; Nencka, R. The Structure-Based Design of SARS-CoV-2 Nsp14 Methyltransferase Ligands Yields Nanomolar Inhibitors. *ACS Infect. Dis.* **2021**, *7* (8), 2214–2220. https://doi.org/10.1021/acsinfecdis.1c00131.

(34)   Kottur, J.; Rechkoblit, O.; Quintana-Feliciano, R.; Sciaky, D.; Aggarwal, A. K. High-Resolution Structures of the SARS-CoV-2 N7-Methyltransferase Inform Therapeutic Development. *Nat. Struct. Mol. Biol.* **2022**, *29* (9), 850–853. https://doi.org/10.1038/s41594-022-00828-1.

Publishing Agreement

It is the policy of the University to encourage open access and broad distribution of all theses, dissertations, and manuscripts. The Graduate Division will facilitate the distribution of UCSF theses, dissertations, and manuscripts to the UCSF Library for open access and distribution. UCSF will make such theses, dissertations, and manuscripts accessible to the public and will take reasonable steps to preserve these works in perpetuity.

I hereby grant the non-exclusive, perpetual right to The Regents of the University of California to reproduce, publicly display, distribute, preserve, and publish copies of my thesis, dissertation, or manuscript in any form or media, now existing or later derived, including access online for teaching, research, and public service purposes.

Author Signature

5/17/2023

Date